Barker, P.F., Camerlenghi, A., Acton, G.D., et al., 1999
Proceedings of the Ocean Drilling Program, Initial Reports Volume 178

3. EXPLANATORY NOTES[1]

Shipboard Scientific Party[2]

INTRODUCTION

In this chapter, we have assembled information that documents our scientific methods. This information concerns only shipboard methods described in the site reports in the Leg 178 *Initial Reports* volume of the Leg 178 *Proceedings of the Ocean Drilling Program* (ODP). Methods for shore-based analysis of Leg 178 data will be described in the individual scientific contributions to be published in scientific journals and in the *Scientific Results* volume. Coring techniques and core handling, including the numbering of sites, holes, cores, sections, and samples, were the same as those reported in previous *Initial Reports* volumes of the *Proceedings of the Ocean Drilling Program* (e.g., Shipboard Scientific Party, 1998b).

Authorship of Site Chapters

Site chapters should be treated as a publication contributed by all the scientists listed at the front of this volume. Each scientist, however, had one or more areas in which he or she was one of the primary contributors. These are listed below (authors are listed in alphabetical order; no seniority is necessarily implied):

Principal Results: Barker, Camerlenghi
Background and Scientific Objectives: Barker, Camerlenghi
Operations: Acton, Grout
Lithostratigraphy: Cowan, Daniels, Escutia, Eyles, Maldonado, Pudsey, Wolf-Welling
Biostratigraphy: Iwai, Osterman, Weinheimer, Winter
Paleomagnetism: Acton, Brachfeld, Guyodo
Organic Geochemistry: Sjunneskog
Inorganic Geochemistry: Kyte, Schuffert

[1]Examples of how to reference the whole or part of this volume.
[2]Shipboard Scientific Party addresses.

Ms 178IR-104

Physical Properties: Barker (heat flow), Evans, Moerz, Vigar
Composite Depths: Iorio
Sedimentation Rates: Brachfeld, Iwai, Weinheimer, Winter
Seismic Stratigraphy: Escutia, Moerz
Downhole Measurements: Lauer, Moerz, Williams

Shipboard Scientific Procedures

Numbering of Sites, Holes, Cores, and Samples

For all ODP drill sites, a letter suffix distinguishes each hole drilled at the same site. The first hole drilled is assigned the site number modified by the suffix "A," the second hole takes the site number and suffix "B," and so forth. The cored interval is measured in meters below seafloor (mbsf). The depth below seafloor is determined by subtracting the water depth estimated from the initial drill-pipe measurement, which gives the length of pipe from the rig floor to the seafloor (measured in meters below rig floor [mbrf]), from the total drill-pipe measurement. Each cored interval is generally 9.5 m long, which is the length of a core barrel. Coring intervals may be shorter and may not necessarily be adjacent if separated by drilled intervals.

A recovered core is divided into 1.5-m sections that are numbered serially from the top. When full recovery is obtained, the sections are numbered from 1 to 7; the last section may be <1.5 m (rarely, an unusually long core may require >7 sections). When less than full recovery is obtained, there will be as many sections as needed to accommodate the length of the core recovered. By convention, material recovered from the core catcher of a sedimentary core is placed in a separate section during the core description, labeled core catcher (CC), and placed below the last section recovered in the liner. The core catcher is placed at the top of the cored interval in cases where material is only recovered in the core catcher.

When the recovered core is shorter than the cored interval, the top of the core is equated with the top of the cored interval by convention, to achieve consistency in handling analytical data derived from the cores. Samples removed from the cores are designated by distance measured in centimeters from the top of the section to the top and bottom of each sample removed from that section. A full identification number for a sample consists of the following information: leg, site, hole, core number, core type, section number, and interval in centimeters measured from the top of section. For example, a sample identification of "178-1096A-3H-1, 10–12 cm" would be interpreted as representing a sample removed from the interval between 10 and 12 cm below the top of Section 1, Core 3 (H designates that this core was taken during hydraulic piston coring) of Hole 1096A from Leg 178.

All ODP core identifiers indicate core type. The following abbreviations are used: H = hydraulic piston core (HPC; also referred to as APC, or advanced hydraulic piston core); X = extended core barrel (XCB); R = rotary core barrel (RCB); and M = miscellaneous material.

Core Handling

Sediments

As soon as a core is retrieved on deck, it goes through a sequence of processing steps. First, a sample is taken from the core catcher and

given to the paleontological laboratory for an initial age assessment. The core is then placed on a long horizontal rack, and gas samples may be taken by piercing the core liner and withdrawing gas into a vacuum tube ("Vacutainer"). Voids within the core are sought as sites for gas sampling. Next, the core is marked into section lengths, each section is labeled, and the core is cut into sections. Interstitial water (IW) whole-round samples are then taken as a matter of ODP policy (typically on every third core); whole-round samples for organic geochemistry may also be taken at this stage if they have been requested. After initial IW and gas samples had been collected during Leg 178, small holes were drilled into the core liners for some of the cores to allow gas to escape.

Each section is then sealed at the top and bottom by attaching color-coded plastic caps, blue to identify the top of a section and clear for the bottom. A yellow cap is placed on the section ends from which a whole-round sample has been removed, and the sample code (e.g., IW) is written on the yellow cap. The caps are usually attached to the liner by coating the end liner and the inside rim of the cap with acetone (or a mixture of acetone and propanol), and then the caps are taped to the liners. The core sections are then carried into the laboratory, where the individual sections are again labeled using an engraver to mark permanently the full designation of the section. The length of the core in each section and the core-catcher sample are measured to the nearest centimeter; this information is logged into the shipboard JANUS database.

Cores of soft material are split lengthwise into working and archive halves. The softer cores are split using a wire or saw, depending on the degree of induration. Harder cores are split using a band or diamond saw. The wire-cut cores are split from bottom to top; thus, investigators should be aware that older material could have been transported up the core on the split face of each section. Following the initial scientific measurements, both halves of the core are put into labeled plastic tubes, sealed, and transferred to cold-storage space aboard the drilling vessel. At the end of Leg 178, the cores were transferred from the ship in refrigerated containers to cold storage at the ODP Core Repository in Bremen, Federal Republic of Germany.

LITHOSTRATIGRAPHY

Sediment Classification

Leg 178 sediment classification is based on visual core description, smear-slide analysis, and spectrophotometer reflectance data. Data are condensed to ODP standard barrel sheet format and presented using the program AppleCore. Shipboard sedimentologists chose to follow a modified version of the ODP Leg 105 sediment classification (Shipboard Scientific Party, 1987), which is suited to describing glaciomarine sediment in that it distinguishes several categories of siliciclastic sediments (gravel, sand, silt, and clay) facies. The Leg 178 classification shown in Figure F1 is a simplification of the classification shown in figure 7 of the Leg 105 "Explanatory Notes" chapter of Shipboard Scientific Party (1987). Existing ODP classifications, however, do not adequately address nonsorted or poorly sorted admixtures of siliciclastic sediments, such as tills, ice-rafted and ice-turbated deposits, and debris flows. For these types of clastic sediment, we use the descriptive terms *diamict* (unlithified) or *diamictite* (lithified).

F1. Lithologic classification scheme with sediments of >70% terrigenous components, p. 37.

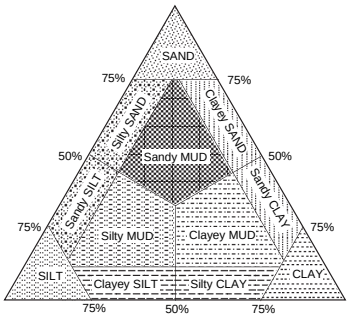

Major sediment types are distinguished on the basis of the dominant component (>50%), which provides the principal lithologic name (e.g., diatom ooze and silty sand). When a component comprises 25%–50% of the sediment, it is mentioned as a major modifier preceding the principal name (e.g., diatomaceous clay and nannofossil silty sand). Minor constituents (10%–25%) are included using the term *-bearing* (e.g., diatom-bearing clay; nannofossil-bearing silty sand). The sediment modifiers are ordered so that the minor modifier(s) precede the major modifier(s). Specific nomenclature for each major compositional group is given below.

Terrigenous Sediments

The terrigenous category refers to sediments having >50% terrigenous component, which are classified on the basis of grain size as shown in Figure **F1.** This classification differs from that of Leg 105 in that sediments having >75% of a single component are given that name (e.g., 23% silt, 77% sand = SAND; or 24% clay, 76% silt = SILT). The term *diamict* is employed for the coarse terrigenous sediments recovered during Leg 178 that comprises gravel and granule clasts (>2 mm), matrix-supported by admixtures of sand and mud (see below).

When the biogenic component is between 25% and 50%, a biogenic modifier is used as shown in Figure **F2**. In this case, the size designation for the terrigenous sediments is based on the composition of the terrigenous components (e.g., 40% diatoms, 40% clay, 20% silt = DIATOM SILTY CLAY). When both siliceous and carbonate biogenic components are present, and one type of biogenic material has more than one component (e.g., silica composed of diatoms, radiolarians, and sponge spicules), the entire biogenic fraction is treated as a single entity (e.g., 11% foraminifers, 15% radiolarians, 20% diatoms, 30% clay, 17% silt, 7% sand = FORAMINIFER-BEARING SILICEOUS MUD), showing the importance of that type of biogenic material rather than the individual components.

F2. Compositional classification for biogenic and siliciclastic marine sediments, **p. 38.**

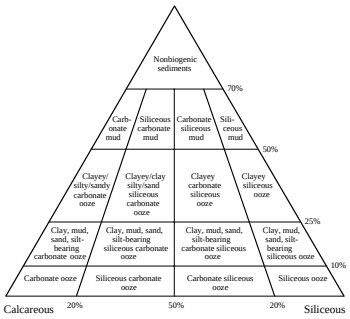

Biogenic Sediments

When the biogenic component exceeds 50%, the sediment is an ooze (or lithified equivalent), following Figure **F2.** As with the biogenic modifiers for the terrigenous sediments, the designation as siliceous or carbonate sediment depends upon grouping all of the biogenic components with that composition, and the terrigenous size fraction is determined only on the basis of the terrigenous components (e.g., 30% clay, 25% foraminifers, 15% nannofossils, 30% radiolarians = CLAYEY FORAMINIFERAL SILICEOUS OOZE).

When the terrigenous component is between 10% and 25%, it is followed by the word *-bearing*. If the terrigenous component is <10%, it is not included in the description.

Turbidites and Contourites

A common component of the sediments recovered at deep-water sites of Leg 178 are thin-bedded, fine-grained silts and clays showing a consistent succession of sedimentary structures. These were deposited from turbidity currents. Other fine-grained laminated facies were deposited from bottom currents (contourites). What follows is a brief discussion of the criteria used to separate these two facies.

Turbidites are recognized by reference to the classic descriptive scheme of Bouma (1962) (divisions T_A–T_E). Fine-grained turbidites recovered during Leg 178 show most commonly the T_C–T_E divisions corresponding to cross-laminated silt, parallel-laminated silt, and mud components. Bouma's original scheme has been found, however, to be too generalized for application to muddy turbidites. To facilitate detailed descriptions, Piper (1978) further subdivided the T_D and T_E divisions of Bouma into laminated silt (D), laminated mud (E_1), graded mud (E_2), ungraded mud (E_3), and pelagic and hemipelagic (H) intervals (Fig. F3). The presence of multiple silt laminations in division T_D results from repeated cycles of shear sorting of silt grains and clay flocs in the bottom boundary layer. The overlying T_E division records suspension deposition from the tail of the turbidity current, followed by hemipelagic deposition, and reworking by bottom (contour) currents (see Pickering et al., 1989; see below). Later workers have erected more detailed classifications of structures within muddy turbidites (e.g., Stow and Piper, 1984), but discrimination of the different divisions is dependent upon quantitative grain-size measurements and X-radiographs, which were not possible during Leg 178. The interpretation of fine-grained deposits was based, in consequence, upon visual and hand-lens examination using Piper's (1978) scheme. During Leg 178 three distinct facies, L_1, L_2, and L_3, are recognized (Fig. F3) on the basis of the presence or absence of silt laminae. These typically form a depositional continuum in which individual facies are related to distance from source (Fig. F4; Stow and Piper, 1984). Each facies provides important information regarding depositional energy.

F3. Representation of internal structure of facies within turbidites, p. 39.

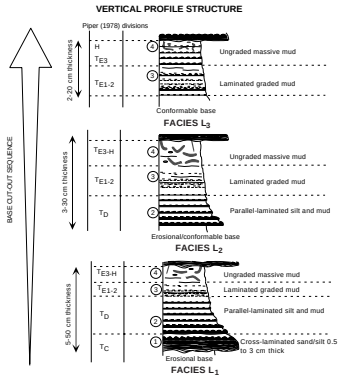

Contourites

Hill (1984) showed that fine-grained turbidites and contourites represent end-members of a continuum of deep-sea sediments that accumulate in very low energy settings; in some cases, distinction may be difficult. This is particularly the case where the tail of a muddy low-energy turbidity current discharges any remaining suspended fine-grained sediment into the water column where it is then affected by bottom currents. Such processes are well described by Stow and Wetzel (1990).

End-member muddy turbidites show sharp bases, a well-defined internal structure, and grain-size sorting (e.g., silt to mud) and, as shown above, are categorized using the descriptive schemes of Bouma (1962) and Piper (1978). In contrast, end-member muddy contourites generally lack any consistent internal structure, although they may reveal the presence of diffuse laminae and isolated ripples, with transitions from silt to mud reflecting the variation in strength of a relatively slow-moving, near-continuous bottom current (e.g., Gonthier et al., 1984; Stow et al., 1986; Nelson et al., 1993; see Facies C, Fig. F5). Such facies typically show complete, pervasive bioturbation (e.g., Gonthier et al., 1984). The differences outlined above are essentially the result of high deposition rates and the short recurrence interval between successive turbidity currents, compared to contourite drifts deposited from bottom currents. The internal structure of a turbidite bed reflects deposition from a discrete, decelerating turbidity current; deposition is relatively rapid (e.g., hours to a few days), and a comparatively thick sediment layer can accumulate in a short interval (Nelson et al., 1991).

F4. Typical downslope and across-slope relationship between turbidite Facies L_1, L_2, and L_3, p. 40.

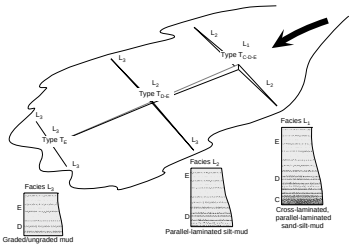

F5. Schematic representation of Facies C, p. 41.

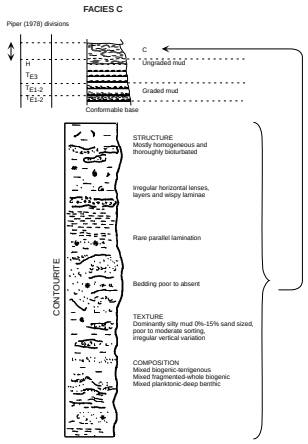

A repetitive internal structure (the "Bouma" sequence) and a tendency to form thick and repetitively bedded stratigraphic successions are considered the most important characteristics for distinguishing turbidites from contourites. Bottom (contour) currents are characterized by nonsystematic changes in flow velocity resulting in much poorer overall sorting and a lack of any consistent and repetitive characteristic internal structure (Stow and Piper, 1984). Contourites can be associated with lag surfaces that record increased bottom current velocities; in addition, contourites are extensively mixed and burrowed by ichnofauna (Wetzel, 1984), which reflect comparatively low deposition rates. Very similar criteria for distinguishing turbidites from contourites were employed by Leg 105 scientists (Hiscott et al., 1989).

Glaciogenic Sediments

The objectives of Leg 178 are to examine depositional processes and the history of climate change along the glacially influenced continental margin of the Antarctic Peninsula. In such settings, an important sediment type is poorly sorted diamict facies.

Diamict is used here as a nongenetic term for sediment consisting of admixtures of clasts (defined here as fragments larger than 2 mm in diameter), sand, and mud where clasts are matrix supported (Flint et al., 1960). Matrix support distinguishes diamicts from other poorly sorted sediments such as muddy gravels, which are clast supported. Matrix grain size in diamicts can be described using the scheme outlined in Figure **F1.** The term *diamict* is synonymous with diamicton (both are used in the literature for unlithified sediment), whereas the term *diamictite* is employed for lithified sediments. Diamicts are characteristic of depositional environments receiving poorly sorted glacial or volcaniclastic sediment. Universal descriptive schemes for diamict(ite) have been developed regardless of depositional environment or setting and emphasize the presence or absence of internal structure and organization. Diamict facies are either massive or variably stratified.

Massive diamict facies have no internal organization or structure and consist of scattered clasts supported by fine-grained matrix. In glacial and glacially influenced marine settings, such facies are not diagnostic of any one subenvironment and are produced by a wide range of sedimentary processes. Massive diamicts can be deposited subglacially (till), or by postdepositional downslope resedimentation as massive debris flows (debrites); the same debrite facies, however, can be generated in nonglacial settings from the mixing of different sediment populations during downslope mass flow, most commonly by mixing gravelly debris flows or turbidites with fine-grained slope sediments. Massive diamict facies also accumulate in deeper water below wave base, by ice rafting of sand and larger clasts into muddy basinal deposits (rainout facies). In many cases, the internal distribution of clasts within massive diamict may provide diagnostic information (e.g., normal or inverse grading). Another useful descriptor is clast abundance (e.g., clast poor or clast rich), which relies on visual classification of number of clasts/area on the surface of the split core. We adopted the comparison chart for visual percentage estimation presented by Mazzullo et al. (1988; fig. 16). A visual percentage estimate of 20% gravel clasts is taken as the boundary between clast-poor and clast-rich facies.

Stratified diamict facies encompass a range of subfacies from well-stratified through weakly stratified to chaotic. Again, no particular subfacies is diagnostic of any specific environment although a dominance

of stratified diamict facies usually indicates a slope setting. Stratified facies can originate by repeated sediment gravity flow, variation in the flux of sediment delivered from suspension settling or rainout from floating ice, or reworking by currents. Chaotic facies can be produced by incomplete mixing of different sediment populations during downslope mass flow and may indicate an ice-proximal location (Eyles, 1993). The same facies, however, may be associated with strata deformed either below glacier ice (glaciotectonism) or by grounding keels of floating icebergs and pack ice (ice turbation).

Bioturbated diamict facies arise from bioturbation of existing diamicts (thereby providing important data regarding the physical properties of the diamict at the time of bioturbation) but also from the disruption of interbedded muddy/sand facies containing ice-rafted debris.

Regardless of type, diamict facies must be interpreted with care, using criteria such as vertical and lateral facies associations (i.e., sequence context), any paleontological data, overall basinal setting and geometry, and acoustic signature as identified from seismic records. For example, on glaciated continental margins, the intimate association of diamict facies with turbidite facies is usually a good indicator of a setting dominated by sediment gravity flows and suggests a debrite origin for diamicts. A channeled geometry and hummocky upper surface is typical of, but not exclusive to, this sedimentary setting. Paleontological data provide critical contextual information. Thus, downslope sediment flow and mixing may be identified by the presence of displaced shallow-water microfauna, the presence of rainout facies, or by an in situ microbiota. As with interpretation of massive diamict facies, the examination of the sequence context of facies, in addition to paleontological information and ichnofacies types, will provide important clues as to depositional environment.

Confusion can arise where ice-rafted debris is present in muddy strata. A massive or laminated mud with ice-rafted clasts is not regarded as a diamict in the absence of a poorly sorted matrix. The general rule of thumb is that a mud with >10% of gravel clasts by volume should be described as a diamict. This number varies from worker to worker and is subjective, but it can be estimated from the comparison chart for visual percentage estimation presented as figure 16 in Mazzullo et al. (1988).

To avoid usage of genetic terms such as till, Eyles et al. (1983) proposed a simple lithofacies scheme for description of diamict facies (Fig. F6). This scheme is now widely employed for sediment description in volcanogenic and glaciogenic environments where large volumes of poorly sorted sediment are produced (e.g., Miall, 1984).

F6. Schematic representation of diamict and other facies and physical structures, p. 42.

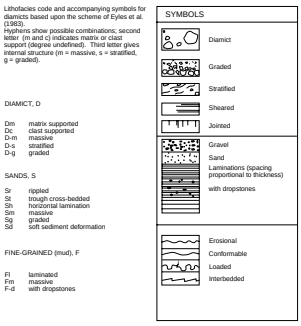

Till-Forming Processes

Till(ite) is a specific genetic term employed for a diamict(ite) deposited directly by glacier ice (Eyles and Eyles, 1992). Tills are deposited subglacially by a variety of processes and are correspondingly lumped together as basal tills. Lodgement/melt-out tills are deposited where debris in the ice base is plastered over a stiff substrate (a hard bed). Such tills are predominantly massive diamict facies (with secondary stratified facies) and tend to be thin (<10 m) in a basinal context. In contrast, much thicker basal till strata, up to 50 m or more, accumulate by repeated deposition from debris being transported as a "deforming layer" (referred to as a "soft bed"). Current models assume that resultant deformation tills are deposited by successive "freezing" of debris at the base of the deforming layer. These conditions apply where ice over-

rides soft sediments that undergo pervasive deformation, mechanical mixing, and homogenization analogous to processes in a cement mixer. These tills consist of stacked beds of massive diamict facies, but rafts of pre-existing sediment can commonly be identified where homogenization was incomplete. "Soft bed" conditions have now been identified across much of the outer margins of the large continental ice sheets in the Northern Hemisphere. These outer margins were highly lobate, and probably fast-flowing ice streams lubricated by soft beds developed over wet sediment or poorly lithified bedrock. Similar conditions probably applied as expanded Antarctic ice sheets moved across shelf sediments during successive glacial maxima. At the shelf edge, such subglacial debris was probably discharged downslope and redeposited as a variety of sediment gravity flows. The term *waterlain till* has been used in the past to refer to such sediments, but the term is not preferred here because the debris has undergone redeposition by nonglacial processes.

Other Diamict-Forming Processes on Continental Shelves

The role of "ice turbation" is now increasingly recognized. At ice-sheet margins, seafloor sediments in water depths perhaps as deep as 500 m are subject to mechanical deformation and sorting by the repeated grounding of iceberg keels (or, in shallower water, by grounding keels of pressure-ice ridges). Seismic data and direct observation of ice scours (on modern shelves and from Pleistocene examples) show deformed ice-turbated sediment akin to diamict.

Sedimentary and Biogenic Structures

Nomenclature is that of Miall (1984), Mazzullo et al. (1988), and Pemberton et al. (1992). Key symbols used on ODP visual description forms and barrel sheets are standard (Fig. F7).

F7. Key symbols used in core description forms and barrel sheets, p. 43.

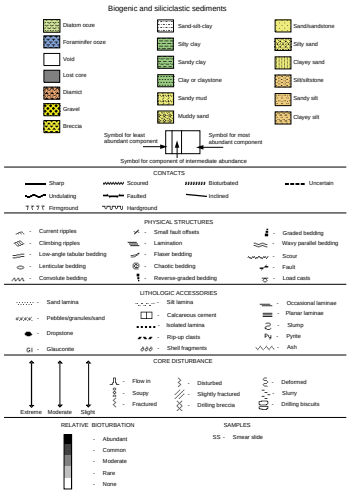

Bed/Lamination Thickness

Nomenclature remains unchanged from Mazzullo et al. (1988) and uses terms such as thinly laminated (1–3 mm thick), laminated (3 mm–1 cm thick), very thin bedded (1–3 cm thick), thin bedded (3–10 cm), medium bedded (10–30 cm), thick bedded (30–100 cm), and very thick bedded (>100 cm).

Induration

These terms follow standard ODP nomenclature (Mazzullo et al., 1988) and that used during Leg 105 (Shipboard Scientific Party, 1987).

Spectrophotometer

Reflectance from cores was routinely measured at evenly spaced intervals of 5 cm downhole using a Minolta Spectrophotometer CM-2002, except for Site 1098, where the measurements were taken at 1- or 2-cm intervals. Measurements were taken as soon as possible after the cores were split to minimize redox-associated color changes that occur when deep-sea sediments are exposed to the atmosphere. We followed the procedure described in the Leg 174A "Explanatory Notes" chapter of Shipboard Scientific Party (1998a). The spectrophotometer records

the percentage of reflected light in 10-nm wavelength steps, from 400 to 700 nm. The hue and chroma attributes were used to determine the standard Munsell notation. A tristimulus system is used to describe color; the measured reflectance of a specific spectral energy distribution under standardized conditions is compared with the three primary colors, red, green, and blue. The result of the comparison is expressed as X, Y, and Z, respectively, and called the tristimulus values. The tristimulus values X, Y, and Z can be converted to the CIELAB system, with derived values called L*, a*, and b*, where L* is the lightness parameter, and a* and b* represent the chromaticity parameters. As an aid to defining lithostratigraphic units, we used one of the parameters (L*, a*, b*) of the CIELAB system because these give a maximum response to changes of lithology in the sediments cored during Leg 178 (see also Blum, 1997, Chap. 7).

BIOSTRATIGRAPHY

Time Scale/Chronological Framework

The biostratigraphy of high-latitude regions in the Southern Hemisphere was vastly improved by ODP Legs 113, 114, 119, 120, and 177 (e.g., Gersonde et al., 1990; Thomas et al., 1990; Barron et al., 1991; Harwood et al., 1992; Gersonde and Bárcena, 1998; Shipboard Scientific Party, 1999a). An important outcome of these studies was the direct correlation of species-stratigraphic ranges to the geomagnetic polarity time scale (GPTS). The biochronological framework used during Leg 178 basically follows that established during Legs 119 (Barron et al., 1991) and 120 (Harwood et al., 1992; Harwood and Maruyama, 1992). We tie the biochronology to the GPTS of Berggren et al. (1995; BKSA95), which uses the magnetic polarity chrons of Cande and Kent (1995; CK95) for correlation between the magnetostratigraphy and the chronologic time scale (Table T1; Fig. F8). BKSA95 also follows the astronomical time scale values of polarity boundaries from Chron 1n to 3n.4n (Thvera) (0–5.23 Ma) (Shackleton et al., 1990; Hilgen, 1991a, 1991b), which results in coherent and congruent magnetostratigraphic and astronomic chronologies back to 5.23 Ma. Extension of the astronomical time scale into the Miocene Epoch (Shackleton et al., 1995; Shipboard Scientific Party, 1995) and fine tuning of the chronology of the astronomical time scale (e.g., Langereis et al., 1994) are an ongoing process, and differences between astronomical and geomagnetic time scales still exist (Table T2).

Figure F9 illustrates the magnetic calibration and estimated ages of biostratigraphic zones used during Leg 178. Absolute radiolarian and diatom datum ages were converted from published age estimates based on Berggren et al. (1985a, 1985b) to the time scale of Berggren et al. (1995) through linear interpolation between the nearest geomagnetic reversal boundaries (Fig. F8).

Age assignments of the standard epoch/stage boundaries are shown in Table T3. Throughout this volume, "m.y." denotes duration in millions of years, whereas "Ma" denotes an absolute age in millions of years.

T1. Neogene geomagnetic polarity time scale and magnetostratigraphic nomenclature, Leg 178, p. 53.

F8. Geomagnetic polarity time scale of Berggren et al., p. 44.

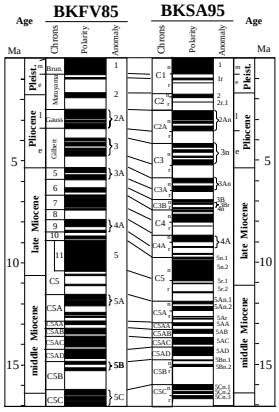

T2. Correlation among published Neogene geomagnetic polarity time scales and magnetostratigraphic nomenclature, p. 55.

F9. Combined geomagnetic polarity time scales of Berggren et al. with Leg 178 biostratigraphic zones, p. 45.

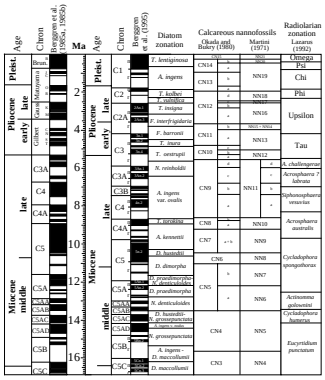

T3. Age assignments of epoch/stage boundaries, p. 57.

Biostratigraphy

The preliminary biostratigraphic age assessments for Leg 178 are determined on the basis of analysis of calcareous nannofossils, foraminifers, radiolarians, and diatoms from core-catcher samples. Stratigraphic constraint of calcareous nannofossil and diatom datums is generally determined on board ship by examining one sample per stratigraphic section (1.5 m). Foraminifers and radiolarian datums are placed on the basis of core-catcher material. Improved dating of Neogene biostratigraphic ranges can be accomplished by correlation with orbitally tuned isotopic signals or other data sets with high temporal resolution, such as color reflectance, magnetic susceptibility, and gamma-ray attenuation porosity evaluator (GRAPE) density.

Diatoms

Numerous diatom biostratigraphic studies have been completed for the Southern Ocean (Gersonde and Burckle, 1990; Baldauf and Barron, 1991; Harwood and Maruyama, 1992; Gersonde and Bárcena, 1998; Shipboard Scientific Party, 1999a). The Neogene and Quaternary diatom zonal scheme used during Leg 178 was primarily that proposed by Harwood and Maruyama (1992, Leg 120) (Figs. **F9, F10**). Some zone names have been revised following the taxonomic conversion of genus *Nitzschia* to *Fragilariopsis* (Round et al., 1990; Hasle, 1993; Gersonde and Bárcena, 1998). The *Fragilariopsis kerguelensis* Zone was removed, and the *Fragilariopsis barronii* datum was retained as a subzonal marker because early forms of *F. kerguelensis* are not distinctive and can be mistaken for *F. barronii* or *Fragilariopsis ritscherii*. This change follows the scheme used by Leg 177; thus, some continuity between the legs has been attempted.

All absolute ages for the marker species datums were recalculated to Berggren et al. (1995) (Table **T4**). The change in ages repositioned some of the boundaries but did not necessitate any major revisions. A new marker species, *Thalassiosira oliverana,* was adopted for the base of the *Nitzschia reinholdii* Zone. This species is more structurally distinctive than *Thalassiosira miocenica,* the species used originally for this datum. The lower boundary age of this zone was not changed by this substitution. Several new zones for the Pleistocene were established in a recent paper (Gersonde and Bárcena, 1998), and the *Proboscia barboi* Zone of Leg 177 (Shipboard Scientific Party, 1999a) is included. The detailed diatom biostratigraphy of Gersonde and Bárcena (1998) was considered during this cruise, but as its data were drawn from sediment recovered farther north, we chose not to incorporate these zones into our initial biostratigraphic scheme. Note that Gersonde, Hodell, Blum, et al. (Shipboard Scientific Party, 1999a) indicated that the first occurrence (FO) of *Thalassiosira vulnifica,* which marks the base of the *Thalassiosira insigna–T. vulnifica* Zone of Harwood and Maruyama (1992), is a diachronous event. They tentatively replaced this zone with the *T. insigna* Zone and divided it into Subzones a–c. This new zone was defined wholly by the FO and last occurrence (LO) of *T. insigna,* which was observed in lower abundances at sites closer to the Antarctic continent. Thus, the older zone definition was retained for this study.

Figure **F10** illustrates the zonal scheme, paleomagnetic calibration, and marker species datums used during this leg. However, this zonation scheme was not fully applicable to the diatom flora in all the sediments recovered during Leg 178 because of the absence or low abundance of

F10. Diatom zones and datums used during Leg 178, **p. 46.**

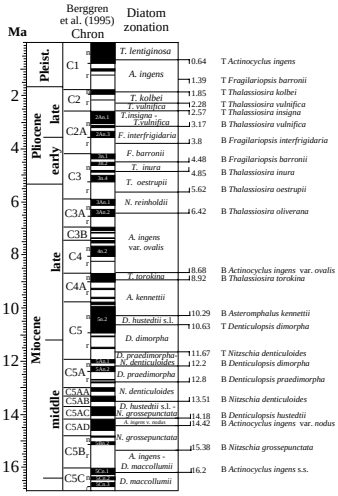

T4. Combined published ages referenced for Leg 178, **p. 58.**

several marker species. Additional investigation will be necessary when examining material with reworked specimens, especially for LO datums.

Methods

Smear slides from core-catcher samples were examined routinely for stratigraphic marker species. When required (in material with few specimens), selected samples were processed using hydrogen peroxide and 10% hydrochloric acid. Strewn slides and sieved slides (>20 µm) were also prepared from the acid-cleaned samples, when necessary, to remove excess quantities of clays. Slides were routinely examined using a Zeiss compound microscope at of 630× and 1000×, with the higher power being reserved mainly for taxonomic identification.

Abundance of diatoms was determined by the number of specimens observed per field of view at a magnification of 630×. These abundance estimates were recorded as follows:

A = abundant (>10 valves per field of view);
C = common (>1 valve per field of view);
F = few (>1 valve per 10 fields of view and <1 valve per field of view);
R = rare (>3 valves per traverse of coverslip and <1 valve per 10 fields of view);
\+ = present (<3 valves per traverse of coverslip, including an appearance as fragments); and
B = barren (no valves observed in slide).

Preservation of diatoms was determined qualitatively and recorded as follows:

G = good (slight to no fragmentation and dissolution);
M = moderate (moderate fragmentation and dissolution); and
P = poor (severe effects of fragmentation and dissolution).

Radiolarians

The radiolarian biostratigraphic scheme proposed by Lazarus (1990, 1992) was applied to Leg 178 material. This zonation is based on the earlier schemes of Hays (1965), Chen (1975), Weaver (1976), Keany (1979), and Caulet (1991) and refined by Lazarus (1992) using sediments recovered during Legs 119 and 120. Species concepts follow those used by Keany (1979), Lazarus (1990, 1992), and references therein. The species events and their respective zones are illustrated with the magnetostratigraphy of Berggren et al. (1995) in Figure **F11**. Stratigraphic constraint of radiolarian events is determined on the basis of an examination of one sample per core (core catcher).

Methods

Sample preparation for radiolarian analysis followed the procedure of Sanfilippo et al. (1985). Samples were sieved at 63 µm. Only samples with significant carbonate fraction were treated with hydrochloric acid. Strewn slides of the residue were made and mounted in Picolyte.

Abundance of total radiolarians is defined as follows:

F11. Radiolarian zonation used for Leg 178, **p. 47.**

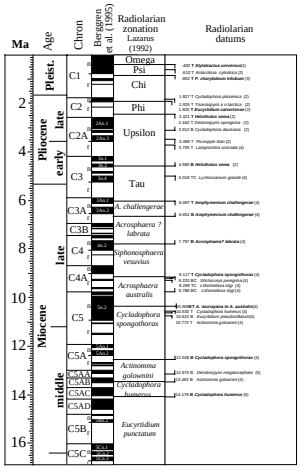

A = abundant (>100 per traverse);
C = common (50–100 per traverse);
F = few (10–50 per traverse);
R = rare (<10 per traverse);
+ = present (<10 per slide); and
B = barren (no skeletons observed).

Species abundances were recorded as follows:

A = abundant (> 20 per slide);
C = common (10–20 per slide);
F = few (5–10 per slide);
R = rare (<5 per slide); and
X = present (1 per slide).

Preservation is defined as follows:

E = excellent (nearly pristine);
G = good (most specimens complete, minor breakage and dissolution);
M = moderate (dissolution and small amount of breakage evident); and
P = poor (extensive breakage, dissolution, or recrystallization).

Calcareous Nannofossils

During Leg 178, the zonal schemes referred to were those of Martini (1971) and Bukry (1973, 1975, 1978), code numbered by Okada and Bukry (1980) (Figs. **F9, F12**). These zonations provide the framework for the biostratigraphic subdivision of low-latitude Cenozoic marine sediments on the basis of calcareous nannofossils. In addition to the traditional use of first/last occurrences of index species, ranges of taxa were used to improve the stratigraphic resolution of the Pleistocene interval. These include the commonly used *Emiliania huxleyi* acme Zone, which roughly covers the last 90 k.y. (Thierstein et al., 1977), and the "small *Gephyrocapsa* Zone" of Gartner (1977), an interval that defines the last 300 k.y. of Okada and Bukry's CN13b biozone. According to the Leg 175 Shipboard Scientific Party (1998c), this interval ranges from marine isotope Stage 30 to 44. The top of the *Gephyrocapsa caribbeanica* acme Zone, dated at 260 ka, is synchronous with the FO of *E. huxleyi* (Pujos, 1988) and thus provides a useful alternative to identify the base of Martini's NN21 zone. Ages of most calcareous nannofossil data employed to construct the Leg 178 age model for the Pliocene–Pleistocene interval come from the work of Raffi et al. (1993) and Wei (1993).

F12. Geomagnetic polarity time scale of Berggren et al.; correlation of biostratigraphic zonations, **p. 48.**

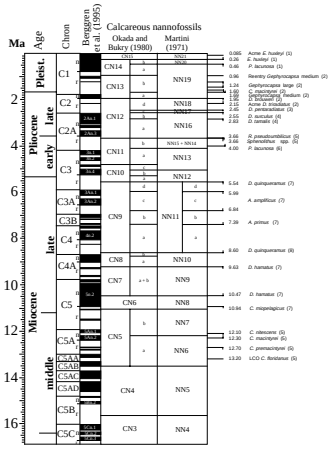

Methods

Smear slides were prepared using Norland Optical Adhesive as a mounting medium. Calcareous nannofossils were examined using a polarizing microscope at a magnification of 1000×. Unless otherwise noted, the taxonomic concepts summarized by Perch-Nielsen (1985) were followed. For morphometric concepts concerning the *Gephyrocapsa* group, the Raffi et al. (1993) proposal was utilized.

Etching and overgrowth are the most important features of nannofossil preservation. To establish a ranking of preservation, the code sys-

tem adopted by the Leg 172 Shipboard Scientific Party (1998b) was used:

G = good (little or no evidence of dissolution and/or secondary overgrowth of calcite; diagnostic characters fully preserved);
M = moderate (dissolution and/or secondary overgrowth; partially altered primary morphological characteristics [however, nearly all specimens can be identified at the species level]); and
P = poor (severe dissolution, fragmentation, and/or secondary overgrowth with primary features largely destroyed; many specimens cannot be identified at the species level and/or generic level).

Total abundance of calcareous nannofossil for each sample was estimated as follows:

VA = very abundant (>100 nannoliths per field of view);
A = abundant (10–100 nannoliths per field of view);
C = common (1–10 nannoliths per field of view);
R = rare (<1 nannolith per 10 fields of view); and
B = barren.

Planktonic and Benthic Foraminifers

Several zonal schemes have been developed for the mid- and high latitudes of the Southern Hemisphere (e.g., Jenkins and Srinivasan, 1986; Berggren et al., 1995). However, these schemes are not fully applicable to the planktonic foraminiferal fauna in all the sediments recovered during Leg 178 because of the absence or low abundance of foraminiferal species. In general, high-latitude foraminiferal assemblages contain low-diversity and long-ranging species that are of limited biostratigraphic use. Planktonic foraminiferal zonation and classification follow Berggren (1992).

Benthic foraminifers provide limited biostratigraphic age control as currently applied to Leg 178 samples, and all zones recognized are local assemblage zones. Individual benthic foraminiferal datums are recognized and discussed for each site.

Methods

Core-catcher sediment samples were soaked in tap water, disaggregated, wet sieved over a 63-µm sieve, and dried in an oven at temperatures <60°C. Several different methods were used for disaggregation, including ultrasonic treatment, heating on a hot plate, Calgon solution, and hydrogen peroxide for consolidated sediments. Well-indurated samples were subjected to drying and wetting to break up the sample. The sieves were soaked in water containing methylene blue between successive samples to stain specimens left in the sieves from previous samples. Foraminifers were separated and identified under the microscope. A 20-cm^3 wet sample was used for shipboard studies and in calculating abundances. The abundance of planktonic foraminifers as a group relative to the total sieved residue was categorized as follows:

A = abundant (>50%);
C = common (25%–50%);
F = few (10%–25%);

R = rare (<5% of the residue); and
B = barren (no specimens in sample).

Benthic foraminifer species abundances were recorded as follows:

D = dominant (>50% of total assemblage);
A = abundant (10%–50% of total assemblage);
C = common (1%–10% of total assemblage);
F = few (0.1%–1% of total assemblage);
R = rare (<0.1% of total assemblage); and
B = barren (no specimens observed).

Foraminifer preservation was categorized as follows:

G = good (dissolution effects are rare);
M = moderate (dissolution damage, including etched and partially broken tests or fragments, is common); and
P = poor (a high degree of fragmentation is common and specimens are small, encrusted, and possibly reworked).

Bolboforma

Bolboforma are an extinct group of calcareous plankton that lived in temperate to cold conditions that have characterized subantarctic water masses, and may provide useful biostratigraphy in southern high-latitude sites. Thirteen zones have been established for the Eocene–upper Pliocene (Spiegler and von Daniels, 1991). The work of Spiegler (1991) on Leg 114 material from the South Atlantic Ocean and that of Mackensen and Spiegler (1992) on Leg 120 material from the Kerguelen Plateau, Southern Indian Ocean, suggest that the biostratigraphic utility of this group in the Southern Ocean may be improved further. In addition, *Bolboforma* were identified at Site 1092 of Leg 177 (Shipboard Scientific Party, 1999b). The preparation methods used to obtain *Bolboforma* were the standard techniques used to obtain foraminifers described above. The occurrences of *Bolboforma* are designated as follows:

A = abundant (>25 specimens per 20 cm^3);
C = common (11–25 specimens per 20 cm^3); and
R = rare (1–10 specimens per 20 cm^3).

PALEOMAGNETISM

Paleomagnetic work during Leg 178 consisted of long-core measurements of the natural remanent magnetization (NRM) of archive-half core sections before and after alternating field (AF) demagnetization, and magnetic remanence measurements on discrete samples collected from the working half of core sections.

Long-core remanence measurements and AF demagnetization were performed using a long-core cryogenic magnetometer (2-G Model 760-R) with an in-line AF demagnetizer capable of reaching peak fields of 80 mT. Archive halves of all core sections were measured, unless precluded by drilling-related deformation. The number of demagnetization steps applied to each core section was controlled by time constraints. A four-step demagnetization scheme taking ~15 min per section was applied

initially and consisted of stepwise demagnetization at 0 (NRM), 10, 20, and 30 mT. This scheme was revised to a three-step demagnetization at 0, 20, and 30 mT to speed core flow through the laboratory. The decision to commence at the 20-mT demagnetization level was justified by the high coercivity of the drill-string overprint. The low maximum peak demagnetization fields ensured that the archive halves remain useful for shore-based high-resolution (U-channel) studies of magnetic remanence. At Site 1095, we used a 4-cm interval for long-core remanence measurements, starting 12 cm above the core section top (leader) and ending 12 cm below the core section base (trailer). At all subsequent sites, we used a 5-cm measurement interval with 15-cm-long headers and trailers. The large leader and trailer distance was used to allow future deconvolution of the long-core data. For the shipboard analysis, we did not use measurements within 8–10 cm of the ends of each section, which are compromised by an edge effect, the false apparent low intensities and inaccurate directions occurring where the wide response function of the SQUID sensors averages empty space with the core signal. Core images were examined to delete data from disturbed or missing intervals. For each site, we produced a set of CD-ROM tables that contain these cleaned data (see **TABLES** directory). The raw data are available in the JANUS database.

Discrete samples were collected from working halves in standard 8-cm³ plastic cubes with an arrow on the bottom of the sampling box pointing upcore. The sampling frequency was generally two samples per core section at one hole per site. Intervals of drilling-related core deformation were avoided. Discrete samples were collected by two different sampling methods. Very soft intervals were sampled by pushing the plastic cube directly into the sediment. Stiffer intervals were sampled using an extruder. These two sampling methods yield a 180° difference in the orientations of both the +X and +Y axes, relative to the standard up arrow (the –Z direction) drawn on the bottom of the sample box (Fig. **F13**). The shipboard long-core cryogenic magnetometer was used to measure the NRM of the discrete samples. Samples were measured in a tray designed for seven samples. All discrete measurements were done using the "NORMAL X & Y" option in the cryogenic magnetometer control program, and the samples were placed into the tray such that they had the normal working-half orientation. Magnetic susceptibility was measured on the discrete samples using a Bartington MS2 Susceptibility Meter with a dual frequency M.S.1.B Sensor. The discrete samples will be further analyzed on shore to study the magnetic properties of the sediments and the mineralogy of remanence carriers.

All cores were affected to some extent by a vertically downward overprint attributed to the drill string. Cores with higher clay and water content also had a radial overprint, manifested as declinations of 0° along the entire length of a section. Shallow cores from Hole 1095A required demagnetization at 30 mT to remove the radial overprint.

Where magnetic cleaning successfully isolated the characteristic component of remanence, paleomagnetic inclinations were used to define polarity zones. The revised time scale of Cande and Kent (1995), as presented in Berggren et al. (1995), was used as a reference for the ages of Cenozoic polarity chrons (Fig. **F12;** Table **T1**).

F13. Paleomagnetic coordinate system for archive halves, discrete samples, and push-in samples, **p. 49.**

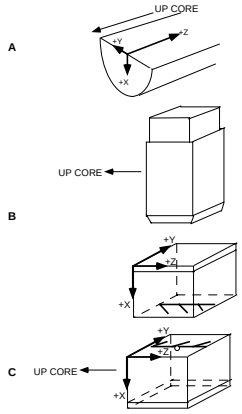

ORGANIC GEOCHEMISTRY

The shipboard organic geochemistry program for Leg 178 included (1) real-time monitoring of volatile hydrocarbons as required by ODP safety regulations, (2) measurement of inorganic carbon content of the sediments, and (3) elemental analyses of total carbon, nitrogen, and sulfur.

Volatile Hydrocarbons

For safety and pollution prevention, concentrations and distribution of light hydrocarbon gases, mainly methane (C_1), ethane (C_2), and propane (C_3), were monitored upon retrieval of each core. The standard method used was headspace sampling as described by Kvenvolden and McDonald (1986). While the core was still on deck, a 5-cm^3 sediment sample was collected using a calibrated cork borer. The sample was placed in a 21.5-cm^3 glass serum vial that was sealed with a septum and metal crimp cap. When consolidated or lithified samples were found, chips of material were placed in the vial and sealed. Before gas analyses, the vial was heated to 60°C for 30 min. A 5-cm^3 volume of the headspace gas was extracted from each vial using a standard glass syringe. Vacutainer samples were collected from gas pockets by penetrating the liner using a syringe connected to a penetration tool. The constituents of the gas were analyzed using a Hewlett Packard (HP) 5890 II gas chromatograph equipped with a flame ionization detector (FID) and a stainless-steel column (2.4 m × 3.2 mm) packed with HayeSep S (80–100 mesh). When heavier hydrocarbons (C_{3+}) were detected, the sample was analyzed using a natural gas analyzer (NGA). The NGA is used to quantify C_1–C_6 and also nitrogen, oxygen, and carbon dioxide. The NGA system is connected to an HP 5890 II gas chromatograph equipped with an FID, a thermal conductivity detector (TCD), and a DB-1 capillary column (60 m × 0.32 mm). Helium was used as the carrier gas, and HP Chemstation software was used for data acquisition and processing. Chromatographic response was calibrated against standards, and the result is reported as parts per million (ppm).

Inorganic Carbon

Inorganic carbon was determined using a Coulometrics 5011 Carbon Dioxide Coulometer equipped with a System 140 carbonate carbon analyzer. A 10- to 20-mg aliquot of freeze-dried ground sediment was weighed and reacted with 2 M HCl to liberate CO_2. The CO_2 was titrated electrochemically, and the change in light transmittance monitored by a photodetection cell. Calcium carbonate content (wt%) was calculated from the inorganic carbon content using the following equation and assuming that all the CO_2 evolved was derived from dissolution of calcium carbonate:

$$\%CaCO_3 = \%IC \text{ (inorganic carbon)} \times 8.33.$$

Elemental Analyses

Total carbon, nitrogen, and sulfur were analyzed using a Carlo Erba 1500 CNS Analyzer. A 10- to 20-mg aliquot of dried ground sediment was combusted at 1000°C in a stream of oxygen. Nitrogen oxides were

reduced to N_2, and the mixture of N_2, CO_2, and SO_2 gases was separated by gas chromatography and measured using a TCD. All measurements were calibrated against standards. The amount of total organic carbon (TOC) is calculated as the difference between total carbon (TC) and inorganic carbon (IC):

$$\%TOC = \%TC - \%IC.$$

Organic Matter Characterization and Maturity Determination

The type of organic matter in a selected group of samples was characterized by pyrolysis using a Delsi Rock-Eval II system. This method is based on a whole-rock pyrolysis technique designed to identify the type and maturity of organic matter and to detect the petroleum potential of sediments (Espitalié et al., 1986). The Rock-Eval system is controlled by a temperature program that first releases volatile hydrocarbons (S_1) at 300°C for 3 min. Hydrocarbons are then released via thermal cracking of kerogen (S_2) as the temperature steadily increases to 550°C at 25°C/min. S_1 and S_2 hydrocarbons are measured by FID and reported in milligrams per gram of dry sediment. The temperature at which the kerogen yields the maximum amount of hydrocarbons during the S_2 program provides T_{max}, a parameter used to assess the maturity of the organic matter. Between 300°C and 390°C of the stepped pyrolysis, CO_2 released from the thermal degradation of organic matter (S_3) is trapped and measured by a TCD in milligrams per gram dry sediment. Rock-Eval II parameters help to characterize organic matter through the following indices: hydrogen index (HI; $S_2/TOC \times 100$), oxygen index (OI; $S_3/TOC \times 100$), S_2/S_3 ratio, and production index (PI; $S_1/(S_1+S_2)$). Interpretation of Rock-Eval data is questionable for samples containing <0.5% TOC.

Extraction of Long-Chain Hydrocarbons

Freeze-dried sediment samples (~2 g) were extracted ultrasonically in hexane for 20 min to extract long-chain hydrocarbons. The sediment-solvent mixture was filtered through a 0.45-µm filter using a Millipore filter flask connected to a vacuum pump. Three replicate extracts were combined and evaporated under a stream of helium. The combined extract was redissolved in a few drops of hexane and analyzed using an HP 5890 II Plus gas chromatograph equipped with an HP Ultra 1 capillary column (50 m × 0.2 mm). The temperature program was 50°C (1 min), 10°C/min to 200°C, 4°C/min to 320°C (20 min); the injector temperature was 290°C, and the detector temperature was 300°C. Chromatograms were evaluated on the basis of alkane standards available on board.

INORGANIC GEOCHEMISTRY

Interstitial Water Sampling and Chemistry

Interstitial water samples for Leg 178 were obtained from 5- to 10-cm, whole-round core samples cut immediately after the core arrived on deck. Specific sampling strategies varied among sites, as described in

each site chapter, with allowance for the recovery of suitable core material. In general, we took at least one sample per core within the upper 50 mbsf and one every third core thereafter, typically from the bottom of the third section, adjacent to the headspace sample taken from the top of the fourth section. At Site 1098, however, we took one sample per section for a high-resolution, shore-based study of carbon and oxygen isotopes.

Interstitial water was collected using titanium squeezers modified after the standard ODP stainless-steel squeezer of Manheim and Sayles (1974). Each whole-round sample was carefully scraped using a stainless-steel spatula to remove the outer rind, squeezed through two Whatman No. 1 filters pre-rinsed in high-purity water, and then passed through a 0.45-µm Gelman polysulfone disposable filter into a 50-mL plastic syringe. Interstitial water was extruded by applying pressures up to 40,000 lb using a Carver Laboratory Press (Model 2702). After collection of 40–50 mL of interstitial water, the syringe was removed, a fresh 0.45-µm Gelman filter was attached, and aliquots were dispensed into plastic vials for shipboard analyses and into acid-washed plastic vials and 5-mL glass ampules (heat sealed) for future shore-based work.

Interstitial water was routinely analyzed for salinity as total dissolved solids with a Goldberg optical handheld refractometer (Reichart). Alkalinity and pH were measured immediately after squeezing by Gran titration using a Metrohm autotitrator and Brinkmann pH electrode, respectively. Chloride was measured by manual titration with $AgNO_3$. Calcium, Mg, K, and SO_4 were measured to within 3% and 5% on 1/200 diluted aliquots in nanopure water using a Dionex DX-100 ion chromatograph. In general, this instrument yields less accurate results than other methods; however, the relative trends are usually similar and can serve as a second check of results generated by the other methods. Silica, ammonium, phosphate, and fluoride were determined by colorimetric methods using a Milton Roy Spectronic spectrophotometer with a 1-cm cell and sample introduction by Mister Sipper. The chemical methods employed follow those of Gieskes et al. (1991) and Grasshoff et al. (1983). For most of these analyses, the International Association of Physical Sciences Organizations seawater was used for standardization.

Strontium, iron, and manganese were determined using a Varian Spectra AA-20 atomic absorption spectrophotometer. Samples for Fe and Mn were acidified immediately after collection with concentrated HCl (50 µL/5 mL) and analyzed using an air-acetylene flame, whereas Sr was analyzed using a N_2O-acetylene flame. Standards were matched in matrix composition to the samples, and lanthanum chloride was used as an ionization suppressant for Sr and Mn analyses. Manganese was determined on 1/5 diluted aliquots, Sr was determined on 1/10 diluted aliquots, and Fe was determined without dilution. The precision of these techniques is ~<4%, except for Fe and Mn concentrations <10 µM, for which the precision can be significantly lower.

The Fe data should be interpreted with caution for two reasons: (1) it was not possible to squeeze sediment samples under oxygen-free conditions and maintain timely processing of samples through the chemistry laboratory; thus, some dissolved Fe^{+2} may have been oxidized, trapped on filters, or adsorbed on the walls of the syringe, and (2) some colloidal iron oxides can pass through 0.45-µm filters. The first effect would cause Fe^{+2} concentrations to be underestimated, whereas the second could result in an overestimate. Despite these potential problems, the

Fe data reported here probably represent at least qualitatively the true in situ Fe concentrations.

X-Ray Fluorescence and X-Ray Diffraction

X-ray fluorescence (XRF) analyses of trace elements (Nb, Zr, Y, Sr, Rb, Zn, Cu, Ni, Cr, V, and Ba) were performed on sediments from Sites 1095, 1096, and 1097 in an attempt to detect a change in provenance of detrital sediments related to uplift and unroofing of the Antarctic Peninsula or to glacial–interglacial climate variability. Samples of ~10 g were freeze-dried, ground gently in an agate mortar, washed with 150 mL of nanopure water to remove excess salts, sonicated for 30–40 min, and centrifuged. This washing probably also removed weakly adsorbed ions on sediment grain surfaces. Some discoloration of the supernatant solution was observed in most samples, probably reflecting loss of some fraction of colloidal phases, and possibly traces of the finest clays; however, this should not significantly affect the bulk composition of the primary terrigenous phases. Centrifuged sediments were dried for at least 12 hr at 120°C and powdered in a tungsten carbide mixer mill. A ~1-g aliquot was ignited for 10 hr at 950°C to determine loss on ignition and to oxidize all iron to the trivalent state. This sample was retained for postcruise major-element analysis. Pressed pellets for trace-element analyses were made from ~6.5 g of dried powder mixed with ~50 drops of Chemplex liquid binder and pressed to ~6 t pressure.

Trace-element abundances were determined using an automated ARL 8420 wavelength-dispersive spectrograph, equipped with an end-window, Rh-target X-ray tube and operated under the conditions outlined in Table T5. The actual analyses were performed on board ship during the early part of Leg 179. Trace-element analyses were corrected for nonlinear backgrounds, spectral interferences, and matrix absorption effects using the ARL software package and a range of geologic standards. Precision and accuracy were assessed by multiple analysis of Standard Reference Material MAG-1 (Table T6), a marine mud prepared by the U.S. Geological Survey (Govindaraju, 1989).

T5. XRF operating conditions for sediment trace elements, p. 61.

T6. Precision and accuracy of replicate trace-element analyses, MAG-1, p. 62.

X-ray diffraction (XRD) analyses were performed using a Philips APD 3720 diffractometer, operated by Philips software PC-APC, version 3.6. The diffractometer was operated using Cu-K_α radiation at 35 mA and 40 keV, a focusing graphite monochromator, and a 12.5-mm theta compensating slit. Bulk mineralogy by XRD was determined on a split of the final powder from each XRF sample and on other freeze-dried samples that were powdered in an agate mortar, without washing. These samples were scanned from 2° to 70° 2θ. Clay mineralogy was examined by XRD on separate 3-g samples that were freeze-dried, placed in a 50-mL centrifuge tube with distilled water, and sonicated for 15 min. After flocculation, samples were centrifuged, and washing was repeated until the clays dispersed. Some samples required treatment with a buffered solution (pH 5) of sodium acetate and acetic acid to remove carbonates. Sodium pyrophosphate was added to reach a 1.5% solution. These samples were sonicated for 15 min and centrifuged at 1000 for 5 min; a sample was taken off the top 1 cm of the suspension. This clay-sized fraction was collected by vacuum filtration on a 0.45-µm Millipore filter. The clay was transferred to a glass slide by placing the filter on the slide and gently rolling the back of the filter with a small roller. Two slides were prepared for each sample: one slide was air dried and scanned, heated to 550°C to collapse kaolinite and smectite, and scanned again. The second slide was solvated with ethylene glycol for at

least 8 hr at 60°C to determine the presence of expandable clays. Clay samples were scanned from 2° to 35° 2θ. Mineral identification followed standard procedures as outlined in Brown (1980), Brown and Brindley (1980), and Moore and Reynolds (1989).

PHYSICAL PROPERTIES

Introduction

The purposes of physical properties measurements during Leg 178 were (1) to provide near-continuous records for hole-to-hole correlation, the construction of complete stratigraphic sequences, and core-to-downhole log ties; and (2) to provide estimates of sediment properties, which can be used to reconstruct glacial and interglacial/proglacial depositional processes.

The physical properties measurements were made only after the cores had equilibrated to ambient temperature, 3–4 hr after recovery. The first measurement station was the multisensor track (MST), which combines four sensors on an automated track to measure magnetic susceptibility, bulk density (by gamma-ray attenuation), *P*-wave velocity, and natural gamma-ray emission, on whole-core sections. The maximum run time for a section was 11 min, 24 s. Next, thermal conductivity was measured on whole-core sections at sites where downhole temperature measurements were taken.

The cores were then split, and *P*-wave velocity and shear strength were measured on the working half. Moisture content and density measurements were made on samples taken either one per section or three per core. Most of the methods are described in detail in the *Physical Properties Handbook* (Blum, 1997), and a summary of procedures and details of the resolution of these measurements is given below.

MST Measurements

Magnetic Susceptibility

Magnetic susceptibility was usually measured with a Bartington meter MS1 using an 8-cm loop and the low-sensitivity setting (1.0 Hz). Sample periods were 2 s, and sample intervals were set at 2 cm. The raw mean value of the measurements was calculated and stored automatically. These values can be converted to volume-normalized magnetic susceptibilities by multiplying by ~0.7×10^{-5} (Blum, 1997).

In addition, magnetic susceptibility measurements were taken at 1-cm intervals using the Bartington magnetic sensor probe on several split cores from Sites 1095 and 1096 with the aim of obtaining a more detailed susceptibility record to correlate with previously studied piston cores from the same sediments (Pudsey and Camerlenghi, 1998).

Bulk Density and Porosity (Gamma-Ray Attenuation)

Bulk density was estimated for whole-round core sections using a sampling period of 2 s every 2 cm on the MST. The gamma-ray source was ^{137}Ce. The calibration was based on aluminum standards of different thickness mounted in a water-filled core liner (Blum, 1997). The calibration takes into consideration (1) the higher Compton scattering in water, (2) the changes in GRAPE densities resulting from different count

rates for calibrations using uncombined pure standards, compared with sediments in which the solid and liquid components are mixed pervasively (Weber et al., 1997), and (3) correction for the core liner. For each site, the GRAPE bulk densities and the bulk densities measured on separate samples were compared.

P-wave Velocity

P-wave velocity was measured over 2 s in steps of 2 cm on whole-round core sections, orthogonal to the core axis, with the *P*-wave logger (PWL) mounted on the MST.

Natural Gamma-Ray Emission

Natural gamma-ray emissions were measured over 15 s for every 15 cm length of the core. Calibration was performed at the beginning of the leg, and sample standards were measured at the end of every site. Background radiation, determined with a water core, was ~3 counts per second (cps). Background radiation has not been subtracted from data presented in the site chapters. The total counts were useful for definition of some lithologic trends.

Thermal Conductivity

Thermal conductivity was measured during Leg 178 when required for geothermal heat flow determination, using the TK04 system described by Blum (1997) and available on board ship since ODP Leg 168. It employs a single-needle probe (Von Herzen and Maxwell, 1959) heated continuously, in full-space configuration for soft sediments (via a hole in the liner of an unsplit core), and in half-space configuration (embedded in clear plastic in good thermal contact with a flat surface) for hard rock. Thermal contact for the half-space method is made using Type 120 Thermal Joint Compound (Wakefield Engineering, Wakefield MA); the measured sections are marked with a yellow caution label.

Data are reported in W/(m·K), with a stated error of ~5%. Choice of measurement interval and assessment of thermal stability are automatic with the TK04. In contrast with the system it replaced, it requires no calibration beyond a simple check against a Macor standard.

Downhole Temperature

The *JOIDES Resolution* carries three tools for downhole temperature measurements, two of which were used during Leg 178. The Adara temperature tool, a thermistor and its associated control, measurement, and memory circuitry, is built into an APC cutting shoe and may be used provided the formation is not too hard. Normally its use requires that, after the APC has fired, it remains motionless in the sediment for at least 8 min to record the temperature decline toward ambient values after frictional heating during corer penetration has dissipated. The thermal decay curve is modeled to determine in situ temperature. It is inadvisable to use this tool within the top 30 m of a hole because the sediment at shallow depth may be insufficiently consolidated to prevent bit movement over this 8-min period, causing additional frictional heating and disturbing the thermal decay. During Leg 178, the Adara temperature tool was also used to obtain a bottom-water temperature by pausing for 10 min above the mudline before firing the first core. In

this mode, the core cutter is slightly recessed within the outer bit for the measurement period, but it equilibrates rapidly with seawater.

The second tool is the Davis-Villinger probe (Davis et al., 1997), considerably more rugged than the Adara temperature tool and capable of use in more indurated sediments. It latches into the base of the bottomhole assembly (BHA) so that a narrow cone, which contains two thermistors and projects 1.4 m ahead of an XCB or RCB bit, may be pushed into the underlying sediments. It needs a separate wireline trip between cores for its operation, which also includes a 5- to 10-min period in the sediments. It is therefore more time consuming to use than the Adara temperature tool. Temperature determination is as for Adara temperature tool data.

Moisture and Density

Moisture and density (MAD) measurements were made on ~8-cm^3 samples taken from the working half of cores as required for ODP shipboard procedures (gravimetric/volumetric determinations of water content, bulk density, grain (solid) density, and related properties such as porosity, void ratio, and dry density). The measured parameters are initial wet bulk mass, then dry mass and volume after drying the samples in a convection oven for 24 hr at 105°C. Masses were measured with an electronic balance (precision = ±0.01 g), and volumes with a helium-displacement pycnometer (precision = ~±0.02 cm^3).

Samples for MAD measurements were taken at either one per core section or three per core. All significant lithologies throughout the cores were sampled. In XCB cores, which commonly showed a biscuiting type of disturbance, particular care was taken to sample undisturbed parts of the core and to avoid the drilling slurry.

P-wave Velocities on Split Cores

The choice of method for compressional wave velocity measurements (V_p) depended upon the degree of consolidation of the sediments. Two *P*-wave transducer pairs (PWS1 and PWS2), located so as to examine the same sediment interval, were inserted along and orthogonal to the core axis in sections of soft sediment, to examine sediment anisotropy. Transducer spacings were 69.5 (PWS1) and 34.8 mm (PWS2). In harder sediments, transverse *P*-wave velocity was measured using the PWS3 contact probe system (a modified Hamilton Frame). Measurements were made across the split-core section, through transducer contact with the sediment on top and the core liner on bottom. All signals were digitized by an oscilloscope, and the raw waveform was saved to a computer using either 500 or 1000 points.

The PWS1 and PWS2 split-core velocimeter calculates velocity based on a fixed distance and measured traveltime. Anisotropy is then calculated by the difference between these horizontal and vertical velocities using the following equation:

$$\text{anisotropy} = 2\,(V_{Pt} - V_{Pl})/(V_{Pt} + V_{Pl}),$$

where V_{Pt} is the transverse compressional wave velocity and V_{Pl} is the longitudinal velocity. The velocity meter was calibrated by measuring V_p in water.

In addition to traveltime, the PWS3 system measures variable sample thickness using a digital micrometer that is zeroed periodically. The calibration procedures for both the PWL and PWS3 followed Blum (1997). Measurements were taken once per section and at lithologic changes.

Shear and Compressional Strength

Undrained shear strength (S_u) was estimated using a vane that is inserted into soft sediment and rotated until the sediment fails. The apparatus is a motorized miniature vane shear, following the ASTM D 4648-87 procedure (ASTM, 1987). The difference in rotational strain between the top and bottom of a spring is measured digitally.

Because there are potential sources of error using the motorized vane shear device at S_u >100–150 kPa, the pocket penetrometer was used when S_u values were >100 kPa. The pocket penetrometer is a flat-footed, cylindrical probe that is pushed 6.4 mm deep into the split-core surface. The resulting resistance is the unconfined compressive strength, or 2 S_u. The maximum S_u that can be measured with the pocket penetrometer is 220 kPa.

COMPOSITE DEPTHS

The recovery of continuous sections from APC-cored intervals of the sedimentary sequence was crucial to the high-resolution, paleoceanographic objectives of Leg 178. Drilling multiple APC holes offset in depth at each site has traditionally helped to ensure that intervals of no recovery in a single APC hole were recovered in an adjacent hole. During Leg 178, as on several previous ODP legs, the continuity of recovery was tested by the development of composite depth sections and splices at the multiple-cored sites (Sites 1095, 1096, 1098, and 1099). The method used during Leg 178, and briefly summarized below, was similar to that used to construct composite depth sections during Leg 138 (Hagelberg et al., 1992), Leg 154 (Shipboard Scientific Party, 1995), Leg 162 (Shipboard Scientific Party, 1996), and Leg 167 (Shipboard Scientific Party, 1997b). At each site, high-resolution (2 cm) measurements of magnetic susceptibility, GRAPE wet bulk density, *P*-wave velocity, and standard measurements (15 cm) of natural gamma ray were made on whole-core sections using the MST soon after the core had equilibrated to laboratory temperature. These measurements were entered into the shipboard database. Additionally, measurements of color reflectance in the 0- to 700-nm band were made at 5- and 2-cm resolution on the split cores (see **"Lithostratigraphy,"** p. 3) using a Minolta color scanner. These parameters were used to correlate between the different holes at each site and to construct a composite section and spliced record.

Adjustments to the shipboard mbsf depth scale are required for several reasons (cf. Ruddiman et al., 1987; Farrell and Janecek, 1991; and Hagelberg et al., 1995). Elastic response of the sediment to reduced pressure accompanying core recovery causes the cored sediment sequence to be expanded relative to the drilled interval. In addition, other factors, including tides, random variations in ship motion, and heave, can affect the true in situ depth of each core by introducing errors. Even between successive cores having nominally 100% recovery or greater, portions of the sediment sequence are usually missing. As a result, the composite depth scale increases downhole relative to the mbsf scale, typically on the order of 10%. To span the gaps between cores, multiple

holes are required, and the core breaks must be staggered so that material missing at one core break is available in another hole.

Hole-to-hole correlation was made using interactive Unix platform software (Splicer) developed by the Borehole Research Group of Lamont-Doherty Earth Observatory (LDEO) and patterned after the Leg 138 correlation software. Initially, all data sets listed above for each hole were visually examined to check the consistency of data. One near-continuous data set, with visually distinctive and high-amplitude variations, was chosen for primary use in correlation. This data set, typically magnetic susceptibility or reflectance, was plotted on the screen for all holes at the site simultaneously. Subsequently, the core that appeared to have the best recovery at the sediment/water interface was chosen as the top core of the composite section.

By visually comparing the data of the working core to data of the uppermost fixed core in one of the other holes, distinctive patterns could be observed in both cores. Recognized features were tied and correlated using a cross-correlation function. The depth of the working core was then adjusted upward or downward relative to the depth of the fixed core. This process was repeated for the uppermost core from other holes. Moving back and forth between all holes (commonly three), the sedimentary sections were correlated between holes and the depth scale was adjusted. The resulting composite depth scale (meters composite depth [mcd]) was then added as an additional column to the original data files. Depths are not adjusted within each core, thus no stretching or compression is allowed by the available software in any individual cores.

After creating a preliminary composite depth, this composite depth scale was applied to other parameters. The process as described above was then repeated. The position of each core was examined, and minor adjustments were made where necessary.

The composite depths for each site are presented in tabular form in the composite depth section of each site chapter (see, for example, Table **T36,** p. 166, in the "Site 1095" chapter). The mcd tables include the original (mbsf) depth of the top of each core, the composite depths (mcd), and the offset between the two depth scales, which had to be used to convert from the mbsf to the mcd scale. The current version of the scale is considered to be preliminary owing to time limitations on the ship and to the evolving nature of age data (magnetostratigraphy and biostratigraphy), which were not incorporated into the current scale. Therefore, the mcd scale has not been incorporated into the JANUS database. Instead, we intend to produce a revised mcd scale, incorporating also the use of the proposed "Sagan" software, for publication in the Leg 178 *Scientific Results* volume, with the goal of incorporating a revised scale into JANUS. The offset tables are presented within the "Composite Depths" sections of the site chapters, should the current scale need to be used.

Finally, a single spliced record of each parameter from all holes was assembled using the best-correlated tie points, to select segments of the composite section to be inserted into the final spliced section. The splice was extended downward by moving from hole to hole and bridging the gaps in the sedimentary sequence at the core breaks. Each splice was designed to provide a continuous record of sedimentary sequence for a site. The tie points used to splice cores are always given as a table in each site chapter (e.g., Table **T37,** p. 168, in the "Site 1095" chapter). An example of a composite section is illustrated in Figure **F14**. In column A, the magnetic susceptibility from two holes at Site 1096 is

F14. Example of the magnetic susceptibility records from Site 1096, **p. 50.**

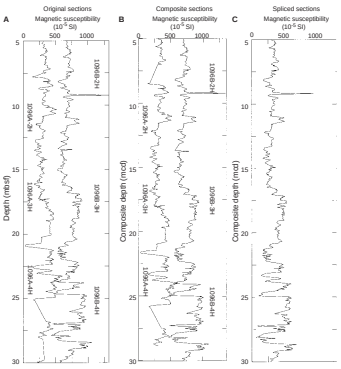

shown on the mbsf depth scale. In column B, the same record is shown after composition to mcd scale, so that correlative features are aligned. Where the amount of offset necessary to align features was ambiguous or imprecise for all lithologic parameters, or where multiple-hole data were unavailable, no composite depth adjustments were made. In these cases, the total amount of offset between mbsf depth and mcd equals the cumulative offset from the overlying core parts. The composite depth section extends only to the base of multiple-cored intervals. Below the multiple-cored intervals, core depths were appended using the offset of the last core in the composite domain.

DOWNHOLE MEASUREMENTS

Introduction

Downhole logs are used to determine physical, chemical, and structural properties of formations penetrated by drilling. The data are rapidly collected, are continuous with depth, and measure in situ properties; they can be interpreted in terms of the formation's stratigraphy, lithology, and mineralogy. Where there is no core recovery, logs provide the only means to describe the formation; where the XCB recovers biscuited core, logs will often provide physical and chemical measurements superior to those from the core; where core recovery is good, log data complement core data. Logs also provide a link between core and seismic section: sonic velocity logs improve depth to traveltime conversion, and synthetic seismograms may be compared directly to the seismic section.

Logging tools are joined together in "tool strings" and are run sequentially into the hole on wireline cable. During Leg 178, we used the triple combination, Formation MicroScanner (FMS)–sonic, geological high-sensitivity magnetic tool (GHMT), and the well seismic tool (WST) (Table T7). Examples of the use of downhole logs for paleoceanographic objectives are given in the Leg 167 *Initial Reports* volume (Shipboard Scientific Party, 1997b), the GHMT is described in the Leg 162 *Initial Reports* volume (Shipboard Scientific Party, 1996), and the integrated porosity-lithology tool (IPLT) and WST are described in the Leg 166 *Initial Reports* volume (Shipboard Scientific Party, 1997a).

T7. Specifications of downhole tools deployed during Leg 178, p. 63.

About the Acronyms

Every Schlumberger tool and tool measurement has a three- or four-letter acronym associated with it. Table T8 lists those used by ODP, tool by tool. Often, there is no convenient translation of the acronym; the acronym itself becomes the name of the tool or measurement. This has the disadvantage of making the meaning of many of the acronyms completely opaque to the uninitiated. In the site chapters, we have tried to combat this by referring to, for example, "density" as well as "RHOM" (the corrected density measurement). The GHMT is always called the GHMT, and the FMS is always called the FMS. The advantage of using the acronyms is that the tool, units, and measurement method are completely specified by the three- or four-letter acronym.

T8. Schlumberger tool and measurement acronyms, p. 64.

Principles and Uses of the Tools

The principle of operation and uses of the tools are described in detail in Serra (1984, 1986), Timur and Toksöz (1985), Ellis (1987), and Rider (1996), and briefly below.

The hostile environment natural gamma-ray sonde (HNGS) and natural gamma-ray tool (NGT) measure the natural gamma radiation from isotopes of potassium, thorium, and uranium in the sediment surrounding the tool.

The accelerator porosity sonde (APS) emits fast neutrons, which are slowed by hydrogen in the formation, and the energy of the rebounded neutrons is measured at detectors spaced along the tool. Most hydrogen is in the pore water, hence porosity may be derived. Hydrogen bound in minerals such as clays also contributes to the measurement, however, so that the raw porosity value is often an overestimate. The neutrons slowed to thermal energies are captured by nuclei, especially those of chlorine and the heavier elements; this effect is measured by the APS as the neutron capture cross section, Σ_f.

The hostile environment lithodensity sonde (HLDS) emits high-energy gamma rays, which are scattered by the electrons in the formation. The electron density, and hence the bulk density, is derived from the energy of the returning gamma rays. Porosity may also be derived from this bulk density, if the matrix density is known. In addition, the HLDS measures the photoelectric effect (PEF, absorption of low-energy gamma rays), which varies according to the chemical composition of the sediment (e.g., PEF of pure calcite = 5.08, illite = 3.03, quartz = 1.81, and kaolinite = 1.49 barns/e^-). The HNGS, APS, and HLDS together comprise the IPLT.

The dual induction tool measures the formation resistivity at three different penetration depths, by electromagnetic induction for deep and medium resistivity, and by current balancing for shallow resistivity. Porosity, fluid salinity, clay content, and gas hydrate content all contribute to the resistivity.

The digital sonic tool measures the traveltime of sound waves through the formation between two transmitters and two receivers, over distances of 2.4, 3.0, and 3.6 m. The sonic velocity increases with compaction and lithification. An impedance log (density × velocity) can be used to generate synthetic seismograms for comparison with the seismic survey sections.

The FMS produces high-resolution images of the microresistivity of the borehole wall. The tool has four orthogonally oriented pads, each having 16 button electrodes that are pressed against the borehole wall (Serra, 1989). Approximately 30% of a 25-cm-diameter borehole is imaged. The vertical resolution is ~5 mm, which allows features such as clasts, thin beds, fractures, and veins to be imaged. The images are oriented; thus, both strike and dip can be obtained for the sediment fabric.

The susceptibility magnetic sonde (SUMS) measures magnetic susceptibility using low-frequency induction in the surrounding sediment. The tool responds to magnetic minerals (mainly magnetites, hematite, and iron sulfides), which are often contained in the detrital sediment fraction and can be a proxy for paleoenvironmental change.

The nuclear magnetic resonance sonde (NMRS) measures the total magnetic field using a proton precession magnetometer. A polarity stratigraphy can usually be determined by comparing the variations in total field and susceptibility downhole, after removal of the background geomagnetic reference field and the effect of the pipe (also see

"Magnetic Polarity," p. 28). The SUMS and NMRS together comprise the GHMT.

The WST contains a geophone that records the traveltime of sonic waves from an air gun or similar source fired next to the ship. The tool provides the best available conversion from depth to traveltime. Additionally, reflectors below the geophone can be located, if the recorded waveform is of good quality. The WST differs from the other tools in that it remains in a fixed position (clamped against the borehole wall) during measurement at each station. Station separation was ~33 m at Site 1095.

Logging Operations

After the hole is cored, it is usually filled with viscous drilling fluid. The base of the drill string is raised to ~90 mbsf, run back to the full depth, and returned to ~90 mbsf to clean the hole and stabilize the walls. Two to four tool strings are run sequentially down each hole on wireline cable, and the hole is logged on the upward pass, typically at speeds of 300 m/hr for the triple combination and FMS-sonic, and at 400 m/hr for the GHMT. The wireline heave compensator is used to minimize the effect of the ship's motion on the tool position.

Incoming data for each logging run were recorded and monitored in real time on the Schlumberger Maxis 500 logging computer. Schlumberger's GeoFrame software was used to process the FMS images. All logging data except FMS and WST were transferred by satellite high-speed data link (Inmarsat B) to LDEO, where the logging runs were shifted to a common depth scale and the NGT logs were recomputed. These processed logs were returned to the ship ~1 week after logging and are displayed in the logging summary figures (Figs. **F40,** p. 88, **F41,** p. 89, both in the "Site 1095" chapter; Figs. **F43,** p. 82, **F45,** p. 84, both in the "Site 1096" chapter; Figs. **F27,** p. 66, **F28,** p. 67, both in the "Shelf Transect" chapter). The processed logs can be obtained from this World Wide Web address: **http://www.ldeo.columbia.edu/BRG/ODP/DATABASE/DATA/search.html.**

Data Quality

The principal influence on data quality is the state of the borehole wall. If the borehole width varies much over short intervals, or is >15 in wide, results from those tools (density, porosity, and FMS) that require good contact with the wall may be degraded. Very narrow ("bridged") sections will also cause irregular log results. The quality of the borehole is helped by minimizing the circulation of fluid during drilling and by logging a young hole. The RCB bit (10-in diameter) is narrower than the APC/XCB bit (11.75-in diameter) and thus will ordinarily create a narrower hole.

Measurements that penetrate deeply into the formation, such as resistivity and susceptibility, are least sensitive to borehole conditions. Sonic velocity is more reliable in more compacted sediment. The maximum extent of the FMS pads is 15 in; boreholes wider than this cannot be well imaged. Of the two natural gamma tools, the HNGS has the more sensitive detector, and the data are corrected for borehole width in the tool itself; the NGT data require shore-based reprocessing.

Log Depth Scales

The depth of the logged measurements is calculated from the length of cable, minus the cable length to the seafloor (seafloor is identified by the step reduction in gamma-ray activity at the sediment/water boundary). Differences between the drill-pipe depth and the log depth occur for a number of reasons. Drill-pipe depth may be inaccurate owing to core expansion, incomplete core recovery, and nonrecovery of the mudline. The log depth may be inaccurate because of incomplete heave compensation, cable stretch (~1 m/1 km), and cable slip. Other differences may reflect tidal effects, which may differ between when the drill-pipe measurement and logging measurement are made. Hence, there can be small but significant offsets between the drill-pipe and log depths, which should be considered when using the logs.

Derivations from the Logs

Porosity

APS porosities often overestimate the actual porosities, because of water in, and bound to, the clays. An alternative porosity (Φ) was derived from the bulk density log (RHOM), assuming a constant grain density:

$$\Phi = (\rho_{gr} - \rho_b)/(\rho_{gr} - \rho_w),$$

where ρ_{gr} (mean grain density) is given by the index physical properties measurements (e.g., 2.76 g/cm^3 for Hole 1095B), ρ_w (pore-water density) is taken to be 1.03 g/cm^3, and ρ_b (bulk density) is provided by the density log. This typically gives an improved estimate of porosity, except where tool contact with the borehole wall is poor.

Pseudosonic Velocity

Where the sonic velocity tool was not run, for example at Hole 1095B, an alternative method estimates the velocity of the formation (v_{pseudo}), using the porosity (Φ):

$$1/v_{pseudo} = F \cdot (1/v_{fluid}) + (1 - F) \cdot (1/v_{grain}).$$

Magnetic Polarity

The total magnetic field (B) measured in the borehole depends on position p and time t (Pozzi et al., 1988):

$$B(p,t) = Br(p) + Ba(p) + Bt(p,t) + Bf(p),$$

where $Bf(p) = Bfi(p) \pm Bfr(p)$. $Br(p)$ is the Earth's magnetic field, generated in the Earth's core (39,000 to 45,000 nT for Leg 178 sites); $Ba(p)$ is the magnetic field resulting from the bottom-hole assembly (BHA) (up to ~2000 nT, decaying away from the BHA) and crustal heterogeneities; and $Bt(p, t)$ is the time-varying field. We run two passes of the GHMT to check that $Bt(p,t)$ is negligible. $Bfi(p)$ is the field produced in the borehole by the induced magnetization (J_i) of the sediment, which is parallel to $B(p,t)$ and proportional to the magnetic susceptibility (χ):

$$J_i = B(p,t) \cdot \chi,$$

and *Bfi(p)* is given by

$$Bfi(p) = (J_i/2) \cdot (1 - 3\sin^2 I),$$

where *I* is the inclination of the Earth's field at the site. *Bfr(p)* is the field produced in the borehole by the remanent magnetization (J_r) of the sediment, whose polarity we aim to determine. J_r is either approximately parallel (normal polarity) or antiparallel (reversed polarity) to *B(p,t),* if the site has not moved significantly (relative to the magnetic poles) since sediment deposition.

We find *Bfr(p)* by subtracting *Br(p), Ba(p),* and *Bfi(p)* from the total field measurement, *B(p,t).* Then, for preliminary interpretation of the Leg 178 data, if *Bfr(p)* is negative, the polarity is normal, and if *Bfr(p)* is positive, the polarity is reversed. Often, the assumptions involved in modeling *Ba(p)* and calculating *Bfi(p)* are not accurate enough to allow reliable determination of polarity directly from the sign of *Bfr(p).* An extra step can then be performed to calculate a linear regression between *Bfr(p)* and *Bfi(p)* within a sliding depth window: correlation indicates normal polarity; anticorrelation indicates reversed polarity.

The LDEO Borehole Research Group, Leicester University Borehole Research, United Kingdom, and the Laboratoire de Mesures en Forage, Aix-en-Provence, France, in conjunction with Schlumberger Well Logging Services, provided the wireline logging services aboard the *JOIDES Resolution*.

SEISMIC STRATIGRAPHY

Precruise Seismic Surveys

Site selection for Leg 178 was based on multichannel and single-channel seismic reflection profiles, collected in recent years either as dedicated site surveys or as part of large-scale regional reconnaissance surveys (data compilation took place within the ANTOSTRAT Antarctic Peninsula Regional Working Group: see Cunningham et al., 1995). The data were collected with a variety of configurations and have variable vertical and horizontal resolution. The principal multichannel, single-channel, and deep-tow boomer data sets and their acquisition parameters are summarized in Tables T9 and T10.

Multichannel (MCS) seismic data sets were processed to common-midpoint stack using standard procedures, which include spherical divergence compensation, predictive deconvolution, common midpoint gather, and normal move-out correction before stacking. Migration was applied to selected lines (e.g., IT92-109: see "Seismic Stratigraphy," p. 31, in the "Site 1096" chapter). Attenuation of the seafloor multiple reflection on profiles from the continental shelf was achieved by application of f–k filter before stack (British Antarctic Survey profiles) or application of a median filter on common shot gathers after move-out with water velocity (Osservatorio Geofisico Sperimentale profiles). Further details of the seismic data recorded at each site are given in the "Seismic Stratigraphy" sections of site chapters.

During the interpretation procedure, seismic units are defined between reflectors that either are unconformities or mark distinct changes in seismic character or both, following procedures described,

T9. MCS surveys associated with the continental shelf and rise sites, p. 65.

T10. Single-channel and deep-tow boomer surveys across the continental shelf, p. 66.

for instance, in Vail et al. (1977) and Posamentier et al. (1988). Boundaries on seismic reflection profiles are correlated at each site with logging data and physical properties measurements through the production of synthetic seismograms (see "Synthetic Seismograms," p. 30). A detailed seismic stratigraphic background for each of the Leg 178 sites can be found in the individual site chapters.

Synthetic Seismograms

Synthetic seismograms were computed for most of the sites using density and compressional wave velocity from all available sources. These included MST whole-core and individual sample measurements, and downhole logging data. Density (D) and P-wave velocity (v) together define the acoustic impedance (Z):

$$Z = D \times v.$$

The acoustic impedance contrast (reflectivity, $R_{1/2}$) determines how much of the wave energy is reflected and how much is transmitted at a boundary between layers of impedance Z_1 and Z_2:

$$R_{1/2} = (Z_1 - Z_2)/(Z_1 + Z_2).$$

Here, we assume that the travel path of the wave is perfectly vertical, we do not consider multiple reflections between layers, and we ignore attenuation and dispersion.

A wavelet representative of the seismic data is derived either from a far-field signature in water or from the seafloor reflection next to the drill site (see "Seismic Stratigraphy" sections in site chapters for details). The synthetic seismogram is calculated by convolving the source wavelet with a reflectivity model (Kearey and Brooks, 1984; Bender, 1985).

An example (Fig. F15) shows a simplified earth model with four reflectors. To convolve a source signal (with a wavelength of several meters) with a reflectivity profile in length units (for the MST data, 2-cm spacing), the reflectivity profile is transformed into a time-dependent profile with the same time resolution as the source wavelet (Mayer, 1994).

Data Evaluation and Correction

Before creating a synthetic seismogram, the raw data are edited and corrected for artifacts that could have a dominant effect on the results. Impedance values that are larger or smaller than a defined percentage above or below a multiple polynomial regression curve are removed and replaced by interpolated values. The correction is done in two steps. During the first step, lower order polynomials and wider thresholds are used. In a second step, more restrictive correction terms can be applied. Special care is taken for values at the beginning and end of the series. An example of an application of the method to a 20-m-long data section is shown in Figure F16. After calculation of the synthetic trace, appropriate band-pass filtering is applied to make the synthetic seismogram comparable to the site-survey profiles (see "Seismic Stratigraphy" sections in site chapters).

F15. Example of a synthetic seismogram, p. 51.

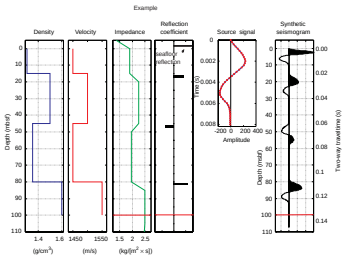

F16. Example of the data "cleaning" process to remove extreme values and artifacts from raw data sets, p. 52.

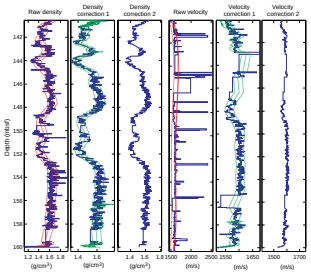

REFERENCES

Abelmann, A., 1992. Early to Middle Miocene radiolarian stratigraphy of the Kerguelen Plateau, Leg 120. *In* Wise, S.W., Jr., Schlich, R., et al., *Proc. ODP, Sci. Results,* 120: College Station, TX (Ocean Drilling Program), 757–783.

ASTM, 1987. Standard test method for laboratory miniature vane shear test for saturated fine-grained clayey soil. In *Annual Book of ASTM Standards* (Vol. 04.08): Philadelphia (Am. Soc. Testing and Mater.).

Backman, J., and Raffi, I., 1997. Calibration of Miocene nannofossil events to orbitally tuned cyclostratigraphies from Ceara Rise. *In* Shackleton, N.J., Curry, W.B., Richter, C., and Bralower, T.J. (Eds.), *Proc. ODP, Sci. Results*, 154: College Station, TX (Ocean Drilling Program), 83–99.

Baldauf, J.G., and Barron, J.A., 1991. Diatom biostratigraphy: Kerguelen Plateau and Prydz Bay regions of the Southern Ocean. *In* Barron, J., Larsen, B., et al., *Proc. ODP, Sci. Results,* 119: College Station, TX (Ocean Drilling Program), 547–598.

Barron, J.A., Baldauf, J.G., Barrera, E., Caulet, J.-P., Huber, B.T., Keating, B.H., Lazarus, D., Sakai, H., Thierstein, H.R., and Wei, W., 1991. Biochronologic and magnetochronologic synthesis of Leg 119 sediments from the Kerguelen Plateau and Prydz Bay, Antarctica. *In* Barron, J., Larsen, B., et al., *Proc. ODP, Sci. Results,* 119: College Station, TX (Ocean Drilling Program), 813–847.

Bender, F. (Ed.), 1985. *Angewandte Geowissenschaften, Band II, Methoden der Angewandten Geophysik und mathematische Verfahren in den Geowissenschaften:* Stuttgart (Ferdinand Enke Verlag), 156–171.

Berggren, W.A., 1992. Neogene planktonic foraminifer magnetobiostratigraphy of the southern Kerguelen Plateau (Sites 747, 748, and 751). *In* Wise, S.W., Jr., Schlich, R., et al., *Proc. ODP, Sci. Results,* 120 (Pt. 2): College Station, TX (Ocean Drilling Program), 631–647.

Berggren, W.A., Kent, D.V., Flynn, J.J., and van Couvering, J.A., 1985a. Cenozoic geochronology. *Geol. Soc. Am. Bull.,* 96:1407–1418.

Berggren, W.A., Kent, D.V., Swisher, C.C., III, and Aubry, M.-P., 1995. A revised Cenozoic geochronology and chronostratigraphy. *In* Berggren, W.A., Kent, D.V., Aubry, M.-P., and Hardenbol, J. (Eds.), *Geochronology, Time Scales and Global Stratigraphic Correlation*. Spec. Publ.—Soc. Econ. Paleontol. Mineral. (Soc. Sediment. Geol.), 54:129–212.

Berggren, W.A., Kent, D.V., and van Couvering, J.A., 1985b. The Neogene, Part 2. Neogene geochronology and chronostratigraphy. *In* Snelling, N.J. (Ed.), *The Chronology of the Geological Record.* Geol. Soc. London Mem., 10:211–260.

Blum, P., 1997. Physical Properties Handbook: a Guide to the Shipboard Measurements of Physical Properties of Deep-Sea Cores. *ODP Tech. Note,* 26.

Bouma, A.H., 1962. *Sedimentology of Some Flysch Deposits: A Graphic Approach to Facies Interpretation:* Amsterdam (Elsevier).

Brown, G., 1980. Associated minerals. *In* Brindley, G.W., and Brown, G. (Eds.), *Crystal Structures of Clay Minerals and Their X-ray Identification.* Mineral. Soc. Monogr. London, 5:361–410.

Brown, G., and Brindley, G.W., 1980. X-ray diffraction procedures for clay mineral identification. *In* Brindley, G.W., and Brown, G. (Eds.), *Crystal Structures of Clay Minerals and Their X-ray Identification.* Mineral. Soc. Monogr. London, 5:305–359.

Bukry, D., 1973. Low-latitude coccolith biostratigraphic zonation. *In* Edgar, N.T., Saunders, J.B., et al., *Init. Repts. DSDP,* 15: Washington (U.S. Govt. Printing Office), 685–703.

Bukry, D., 1975. Coccolith and silicoflagellate stratigraphy near Antarctica, Deep Sea Drilling Project, Leg 28. *In* Hayes, D.E., Frakes, L.A., et al., *Init. Repts. DSDP,* 28: Washington (U.S. Govt. Printing Office), 709–723.

Bukry, D., 1978. Biostratigraphy of Cenozoic marine sediment by calcareous nannofossils. *Micropaleontology,* 24:44–60.

Cande, S.C., and Kent, D.V., 1992. A new geomagnetic polarity time scale for the Late Cretaceous and Cenozoic. *J. Geophys. Res.,* 97:13917–13951.

Cande, S.C., and Kent, D.V., 1995. Revised calibration of the geomagnetic polarity timescale for the Late Cretaceous and Cenozoic. *J. Geophys. Res.,* 100:6093–6095.

Caulet, J.-P., 1991. Radiolarians from the Kerguelen Plateau, Leg 119. *In* Barron, J., Larsen, B., et al., *Proc. ODP, Sci. Results,* 119: College Station, TX (Ocean Drilling Program), 513–546.

Chen, P.-H., 1975. Antarctic radiolaria. *In* Hayes, D.E., Frakes, L.A., et al., *Init. Repts. DSDP,* 28: Washington (U.S. Govt. Printing Office), 437–513.

Cunningham, A.P., Vanneste, L.E., and ANTOSTRAT Antarctic Peninsula RWG, 1995. The ANTOSTRAT Antarctic Peninsula Regional Working Group digital navigation compilation. *In* Cooper, A.K., Barker, P.F., and Brancolini, G. (Eds.), *Geology and Seismic Stratigraphy of the Antarctic Margin,* Antarct. Res. Ser., 68.

Davis, E.E., Villinger, H., Macdonald, R.D., Meldrum, R.D., and Grigel, J. 1997. A robust, rapid-response probe for measuring bottom-hole temperatures in deep-ocean boreholes. *Mar. Geophys. Res.,* 19:267–281.

Ellis, D.V., 1987. *Well Logging for Earth Scientists:* Amsterdam (Elsevier).

Espitalié, J., Deroo, G., and Marquis, F., 1986. La pyrolyse Rock-Eval et ses applications, Partie III. *Rev. Inst. Fr. Pet.,* 41:73–89.

Eyles, N., 1993. Earth's glacial record and its tectonic setting. *Earth-Sci. Rev.,* 35:1–248.

Eyles, N., and Eyles, C.H., 1992. Glacial depositional systems. *In* Walker, R.G., and James, N.P. (Eds.), *Facies Models: Response to Sea level Change:* St. Johns, Newfoundland (Geol. Assoc. Canada), 73–100.

Eyles, N., Eyles, C.H., and Miall, A.D., 1983. Lithofacies types and vertical profile models: an alternative approach to the description and environmental interpretation of glacial diamict sequences. *Sedimentology,* 30:393–410.

Farrell, J.W., and Janecek, T.R., 1991. Late Neogene paleoceanography and paleoclimatology of the northeast Indian Ocean (Site 758). *In* Weissel, J., Peirce, J., Taylor, E., Alt, J., et al., *Proc. ODP, Sci. Results,* 121: College Station, TX (Ocean Drilling Program), 297–355.

Flint, R.F., Sanders, J.E., and Rodgers, J., 1960. Diamictite, a substitute term for symmictite. *Geol. Soc. Am. Bull.,* 71:1809.

Gartner, S., 1977. Calcareous nannofossil biostratigraphy and revised zonation of the Pleistocene. *Mar. Micropaleontol.,* 2:1–25.

Gartner, S., 1990. Neogene calcareous nannofossil biostratigraphy, Leg 116 (Central Indian Ocean). *In* Cochran, J.R., Stow, D.A.V., et al., *Proc. ODP, Sci. Results,* 116: College Station, TX (Ocean Drilling Program), 165–187.

Gersonde, R., Abelmann, A., Burckle, L.H., Hamilton, N., Lazarus, D., McCartney, K., O'Brien, P., Spieß, V., and Wise, S.W., Jr., 1990. Biostratigraphic synthesis of Neogene siliceous microfossils from the Antarctic Ocean, ODP Leg 113 (Weddell Sea). *In* Barker, P.F., Kennett, J.P., et al., *Proc. ODP, Sci. Results,* 113: College Station, TX (Ocean Drilling Program), 915–936.

Gersonde, R., and Bárcena, M.A., 1998. Revision of the late Pliocene–Pleistocene diatom biostratigraphy for the northern belt of the Southern Ocean. *Micropaleontology,* 44:84–98.

Gersonde, R., and Burckle, L.H., 1990. Neogene diatom biostratigraphy of ODP Leg 113, Weddell Sea (Antarctic Ocean). *In* Barker, P.F., Kennett, J.P., et al., *Proc. ODP, Sci. Results,* 113: College Station, TX (Ocean Drilling Program), 761–789.

Gieskes, J.M., Gamo, T., and Brumsack, H., 1991. Chemical methods for interstitial water analysis aboard the *JOIDES Resolution. ODP Tech. Note,* 15.

Gonthier, E.G., Faugeres, J.C., and Stow, D.A.V. 1984. Contourite facies of the Faro Drift, Gulf of Cadiz. *In* Stow, D.A.V. and Piper, D.J.W. (Eds.), Fine-Grained Sediments: Deep Water Processes and Facies: Geol. Soc. Spec. Publ., 15:275–292.

Govindaraju, K., 1989. 1989 compilation of working values and sample description for 272 geostandards. *Geostand. Newsl.,* 13 (spec. iss.).

Grasshoff, K., Ehrhardt, M., and Kemling, K., 1983. *The Methods of Seawater Analysis:* Weinheim, F.R.G. (Verlag Chemie).

Hagelberg, T.K., Pisias, N.G., Shackleton, N.J., Mix, A.C., and Harris, S., 1995. Refinement of a high-resolution, continuous sedimentary section for studying equatorial Pacific Ocean paleoceanography, Leg 138. *In* Pisias, N.G., Mayer, L.A., Janecek, T.R., Palmer-Julson, A., and van Andel, T.H. (Eds.), *Proc. ODP, Sci Results,* 138: College Station, TX (Ocean Drilling Program), 31–46.

Hagelberg, T., Shackleton, N., Pisias, N., and Shipboard Scientific Party, 1992. Development of composite depth sections for Sites 844 through 854. *In* Mayer, L., Pisias, N., Janecek, T., et al., *Proc. ODP, Init. Repts.,* 138: College Station, TX (Ocean Drilling Program), 79–85.

Harwood, D.M., Lazarus, D.B., Abelmann, A., Aubry, M.-P., Berggren, W.A., Heider, F., Inokuchi, H., Maruyama, T., McCartney, K., Wei, W., and Wise, S.W., Jr., 1992. Neogene integrated magnetobiostratigraphy of the central Kerguelen Plateau, Leg 120. *In* Wise, S.W., Jr., Schlich, R., et al., *Proc. ODP, Sci. Results,* 120: College Station, TX (Ocean Drilling Program), 1031–1052.

Harwood, D.M., and Maruyama, T., 1992. Middle Eocene to Pleistocene diatom biostratigraphy of Southern Ocean sediments from the Kerguelen Plateau, Leg 120. *In* Wise, S.W., Jr., Schlich, R., et al., *Proc. ODP, Sci. Results,* 120: College Station, TX (Ocean Drilling Program), 683–733.

Hasle, G.R., 1993. Nomenclatural notes on marine planktonic diatoms. The family Bacillariaceae. *Nova Hedwigia. Beih.,* 106:315–321.

Hays, J.D., 1965. Radiolaria and late Tertiary and Quaternary history of Antarctic seas. *In* Llano, G.A. (Ed.), *Biology of the Antarctic Seas II*. Antarct. Res. Ser., 5:125–184.

Hays, J.D., and Opdyke, N.D., 1967. Antarctic radiolaria, magnetic reversals, and climate change. *Science,* 158:1001–1011.

Hilgen, F.J., 1991a. Extension of the astronomically calibrated (polarity) ß time scale to the Miocene/Pliocene boundary, *Earth Planet. Sci. Lett.,* 107:349–368.

Hilgen, F.J., 1991b. Astronomical calibration of Gauss to Matuyama sapropels in the Mediterranean and implication for the geomagnetic polarity time scale. *Earth Planet. Sci. Lett.,* 104:226–244.

Hill, P.R., 1984. Facies and sequence analysis of Nova Scotian slope muds: turbidite vs 'hemipelagic' deposition. *In* Stow, D.A.V. and Piper, D.J.W. (Eds.), *Fine-Grained Sediments: Deep-Water Processes and Facies.* Geol. Soc. Spec. Publ., 15:311–318.

Hiscott, R.N., Cremer, M., and Aksu, A.E., 1989. Evidence from sedimentary structures for processes of sediment transport and deposition during post-Miocene time at Sites 645, 646, and 647, Baffin Bay and the Labrador Sea. *In* Srivastava, S.P., Arthur, M.A., Clement, B., et al., *Proc. ODP, Sci. Results,* 105: College Station, TX (Ocean Drilling Program), 53–63.

Jenkins, D.G., and Srinivasan, M.S., 1986. Cenozoic planktonic foraminifers from the equator to the sub-antarctic of the Southwest Pacific. *In* Kennett, J.P, von der Borch, C.C., et al., *Init. Repts. DSDP,* 90: Washington (U.S. Govt. Printing Office), 795–834.

Keany, J., 1979. Early Pliocene radiolarian taxonomy and biostratigraphy in the Antarctic region. *Micropaleontology,* 25:50–74.

Kearey, P., and Brooks, M., 1984. *An Introduction to Geophysical Exploration:* Oxford (Blackwell Scientific).

Kvenvolden, K.A., and McDonald, T.J., 1986. Organic geochemistry on the *JOIDES Resolution*—an assay. *ODP Tech. Note,* 6.

Langereis, G.G., Van Hoof, A.M., and Hilgen, F.J., 1994. Steadying the rates. *Nature,* 369:615.

Lazarus, D., 1990. Middle Miocene to Recent radiolarians from the Weddell Sea, Antarctica, ODP Leg 113. *In* Barker, P.F., Kennett, J.P., et al., *Proc. ODP, Sci. Results,* 113: College Station, TX (Ocean Drilling Program), 709–727.

Lazarus, D., 1992. Antarctic Neogene radiolarians from the Kerguelen Plateau, Legs 119 and 120. *In* Wise, S.W., Jr., Schlich, R. et al., *Proc. ODP, Sci. Results,* 120: College Station, TX (Ocean Drilling Program), 785–809.

Lourens, L.J., Antonarakou, A., Hilgen, F.J., Van Hoof, A.A.M., Vergnaud-Grazzini, C., and Zachariasse, W.J.,1996. Evaluation of the Pliocene–Pleistocene astronomical timescale. *Paleoceanography,* 11:391–413.

Lyle, M., Koizumi, I., Richter, C., et al., 1997. *Proc. ODP, Init. Repts.,* 167: College Station, TX (Ocean Drilling Program).

Mackensen, A., and Spiegler, D., 1992. Middle Eocene to early Pliocene *Bolboforma* (algae?) from the Kerguelen Plateau, southern Indian Ocean. *In* Wise, S.W., Jr., Schlich, R., et al., *Proc. ODP, Sci. Results,* 120: College Station, TX (Ocean Drilling Program), 675–682.

Manheim, F.T., and Sayles, F.L., 1974. Composition and origin of interstitial waters of marine sediments, based on deep sea drill cores. *In* Goldberg, E.D. (Ed.), *The Sea* (Vol. 5): *Marine Chemistry: The Sedimentary Cycle:* New York (Wiley), 527–568.

Martini, E., 1971. Standard Tertiary and Quaternary calcareous nannoplankton zonation. *In* Farinacci, A. (Ed.), *Proc. 2nd Int. Conf. Planktonic Microfossils Roma:* Rome (Ed. Tecnosci.), 2:739–777.

Mayer, L.A., 1994. Paleoceanography from a single hole to the ocean basins. *Oceanus,* 36:40–44.

Mazzullo, J.M., Meyer, A., and Kidd, R.B., 1988. New sediment classification scheme for the Ocean Drilling Program. *In* Mazzullo, J., and Graham, A.G. (Eds.), *Handbook for Shipboard Sedimentologists. ODP Tech. Note,* 8:45–67.

Miall, A.D., 1984. *Principles of Sedimentary Basin Analysis* (2nd Ed.): New York (Springer-Verlag).

Moore, D.M., and Reynolds, R.C., Jr., 1989. *X-ray Diffraction and the Identification and Analysis of Clay Minerals:* Oxford (Oxford Univ. Press).

Nelson, C.H., Baraza, J., and Maldonado, A., 1993. Mediterranean undercurrent sandy contourites, Gulf of Cadiz, Spain. *Sediment. Geol.* 82:103–131.

Nelson, C.H., Maldonado, A., Barber, J.H., Jr., and Alonso, B., 1991. Modern sand-rich and mud-rich siliciclastic aprons, alternative base-of-slope turbidite systems to submarine fans. *In* Weimer, P., and Link, M. (Eds.), *Seismic facies and sedimentary processes of modern and ancient submarine fans:* New York (Springer-Verlag), 171–190.

Okada, H., and Bukry, D., 1980. Supplementary modification and introduction of code numbers to the low-latitude coccolith biostratigraphic zonation (Bukry, 1973; 1975). *Mar. Micropaleontol.,* 5:321–325.

Pemberton, S.G., McEachern, J.A., and Frey, R.W., 1992. Trace fossil facies models: environmental and allostratigraphic significance. *In* Walker, R.G., and James, N. (Eds.), *Facies Models: Response to Sea Level Change.* Geol. Assoc. Canada, 42–72.

Perch-Nielsen, K., 1985. Mesozoic calcareous nannofossils. *In* Bolli, H.M., Saunders, J.B., and Perch-Nielsen, K. (Eds.), *Plankton Stratigraphy:* Cambridge (Cambridge Univ. Press), 329–426.

Pickering, K.T., Hiscott, R., and Hein, F.J., 1989. *Deep-marine Environments: Clastic Sedimentation and Tectonics:* London (Unwin Hyman).

Piper, D.J.W., 1978. Turbidite muds and silts on deepsea fans and abyssal plains. *In* Stanley, D.J., and Kelling, G. (Eds.), *Sedimentation in Submarine Canyons, Fans and Trenches:* Stroudsburg, PA (Dowden, Hutchinson and Ross), 163–175.

Posamentier, H.W., Jervey, M.T., and Vail, P.R., 1988. Eustatic controls on clastic deposition, I. Conceptual framework. *In* Wilgus, C.K., Hastings, B.S., Kendall, C.G.St.C., Posamentier, H.W., Ross, C.A., and Van Wagoner, J. (Eds.), *Sea-Level Changes: An Integrated Approach.* Spec. Publ.—Soc. Econ. Paleontol. Mineral., 42:109–124.

Pozzi, J.-P., Martin, J.P., Pocachard, J., Feinberg, H., and Galdeano, A., 1988. In situ magnetostratigraphy: interpretation of magnetic logging in sediments. *Earth Planet. Sci. Lett.,* 88:357–373.

Pudsey, C.J., and Camerlenghi, A., 1998. Glacial-interglacial deposition on a sediment drift on the Pacific Margin of the Antarctic Peninsula. *Antarct. Sci.*, 10:286–308.

Pujos, A., 1988. Spatio-temporal distribution of some Quaternary coccoliths. *Oceanol. Acta*, 11:65–77.

Raffi, I., Backman, J., Rio, D., and Shackleton, N.J., 1993. Plio-Pleistocene nannofossil biostratigraphy and calibration to oxygen isotopes stratigraphies from Deep Sea Drilling Project Site 607 and Ocean Drilling Program Site 677. *Paleoceanography,* 8:387–408.

Raffi, I., and Flores, J.-A., 1995. Pleistocene through Miocene calcareous nannofossils from eastern equatorial Pacific Ocean (Leg 138). *In* Pisias, N.G., Mayer, L.A., Janecek, T.R., Palmer-Julson, A., and van Andel, T.H. (Eds.), *Proc. ODP, Sci. Results,* 138: College Station, TX (Ocean Drilling Program), 233–286.

Rider, M., 1996. *The Geological Interpretation of Well Logs:* Caithness (Whittles Publishing).

Round, F.E., Crawford, R.M., and Mann, D.G., 1990. *The Diatoms: Biology and Morphology of the Genera:* Cambridge (Cambridge Univ. Press).

Ruddiman, W.F., Cameron, D., and Clement, B.M., 1987. Sediment disturbance and correlation of offset holes drilled with the hydraulic piston corer: Leg 94. *In* Ruddiman, W.F., Kidd, R.B., Thomas, E., et al., *Init. Repts. DSDP,* 94 (Pt. 2): Washington (U.S. Govt. Printing Office), 615–634.

Sanfilippo, A., Westberg-Smith, M.J., and Riedel, W.R., 1985. Cenozoic radiolaria. *In* Bolli, H.M., Saunders, J.B., and Perch-Nielsen, K. (Eds.), *Plankton Stratigraphy:* Cambridge (Cambridge Univ. Press), 631–712.

Serra, O., 1984. *Fundamentals of Well-Log Interpretation* (Vol. 1): *The Acquisition of Logging Data:* Dev. Pet. Sci., 15A: Amsterdam (Elsevier).

Serra, O., 1986. *Fundamentals of Well-Log Interpretation* (Vol. 2): *The Interpretation of Logging Data.* Dev. Pet. Sci., 15B.

Serra, O., 1989. *Formation MicroScanner Image Interpretation:* Houston (Schlumberger Educ. Services), SMP-7028.

Shackleton, N.J., Berger, A., and Peltier, W.A., 1990. An alternative astronomical calibration of the lower Pleistocene timescale based on ODP Site 677. *Trans. R. Soc. Edinburgh: Earth Sci.,* 81:251–261.

Shackleton, N.J., Crowhurst, S., Hagelberg, T., Pisias, N.G., and Schneider, D.A., 1995. A new late Neogene time scale: application to Leg 138 sites. *In* Pisias, N.G., Mayer, L.A., Janecek, T.R., Palmer-Julson, A., and van Andel, T.H. (Eds.), *Proc. ODP, Sci. Results,* 138: College Station, TX (Ocean Drilling Program), 73–101.

Shipboard Scientific Party, 1987. Explanatory notes: ODP Leg 105, Baffin Bay and Labrador Sea. *In* Srivastava, S.P., Arthur, M., et al., *Proc. ODP, Init. Repts.,* 105: College Station, TX (Ocean Drilling Program), 21–42.

Shipboard Scientific Party, 1995. Explanatory notes. *In* Curry, W.B., Shackleton, N.J., Richter, C., et al., *Proc. ODP, Init. Repts.,* 154: College Station, TX (Ocean Drilling Program), 11–38.

Shipboard Scientific Party, 1996. Explanatory notes. *In* Jansen, E., Raymo, M.E., Blum, P., et al., *Proc. ODP, Init. Repts.,* 162: College Station, TX (Ocean Drilling Program), 21–45.

Shipboard Scientific Party, 1997a. Explanatory notes. *In* Eberli, G.P., Swart, P.K., Malone, M.J., et al., *Proc. ODP, Init. Repts.,* 166: College Station, TX (Ocean Drilling Program), 43–65.

Shipboard Scientific Party, 1997b. Explanatory notes. *In* Lyle, M., Koizumi, I., Richter, C., et al., *Proc. ODP, Init. Repts.,*167: College Station, TX (Ocean Drilling Program), 15–39.

Shipboard Scientific Party, 1998a. Explanatory notes. *In* Austin, J.A., Christie-Blick, N., Malone, M.J., et al., *Proc. ODP, Init. Repts.,* 174A: College Station, TX (Ocean Drilling Program).

Shipboard Scientific Party, 1998b. Explanatory notes. *In* Keigwin, L.D., Rio, D., Acton, G.D., et al., *Proc. ODP, Init. Repts.,* 172: College Station, TX (Ocean Drilling Program), 13–29.

Shipboard Scientific Party, 1998c. Explanatory notes. *In* Wefer, G., Berger, W.H., Richter, C., et al., *Proc. ODP, Init. Repts.,* 175: College Station, TX (Ocean Drilling Program).

Shipboard Scientific Party, 1999a. Explanatory notes. *In* Gersonde, R., Hodell, D.A., Blum, P., et al., *Proc. ODP, Init. Repts.,* 177, 1–57 [CD-ROM]. Available from: Ocean Drilling Program, Texas A&M University, College Station, TX 77845-9547, U.S.A.

Shipboard Scientific Party, 1999b. Site 1092. *In* Gersonde, R., Hodell, D.A., Blum, P., et al., *Proc. ODP, Init. Repts.,* 177, 1–82 [CD-ROM]. Available from: Ocean Drilling Program, Texas A&M University, College Station, TX 77845-9547, U.S.A.

Spiegler, D., 1991. Occurrence of *Bolboforma* (algae, Chrysophyta) in the subantarctic (Atlantic) Paleogene. *In* Ciesielski, P.F., Kristoffersen, Y., et al., *Proc. ODP, Sci. Results,* 114: College Station, TX (Ocean Drilling Program), 325–334.

Spiegler, D., and von Daniels, C.H., 1991. A stratigraphic and taxonomic atlas of *Bolboforma* (Protophytes, incertae sedis, Tertiary). *J. Foraminiferal Res.,* 21:126–158.

Stow, D.A.V., Faugeres, J., and Gonthier, E., 1986. Facies distribution and textural variation in Faro Drift contourites: velocity fluctuation and drift growth. *Mar. Geol.,* 72:71–100.

Stow, D.A.V., and Piper, D.J.W., 1984. Deep-water fine-grained sediments: facies models. *In* Stow, D.A.V., and Piper, D.J.W. (Eds.), *Fine-Grained Sediments: Deep-Water Processes and Facies*. Geol. Soc. Spec. Publ. London, 15:611–645.

Stow, D.A.V., and Wetzel, A., 1990. Hemiturbidite: a new type of deep-water sediment. *In* Cochran, J.R., Stow, D.A.V., et al., *Proc. ODP, Sci. Results,* 116: College Station, TX (Ocean Drilling Program), 25–34.

Thierstein, H.R., Geitzenauer, K., Molfino, B., and Shackleton, N.J., 1977. Global synchroneity of late Quaternary coccolith datum levels: validation by oxygen isotopes. *Geology,* 5:400–404.

Thomas, E., Barrera, E., Hamilton, N., Huber, B.T., Kennett, J.P., O'Connell, S.B., Pospichal, J.J., Speiß, V., Stott, L.D., Wei, W., and Wise, S.W., Jr., 1990. Upper Cretaceous–Paleogene stratigraphy of Sites 689 and 690, Maud Rise (Antarctica). *In* Barker, P.F., Kennett, J.P., et al., *Proc. ODP, Sci. Results,* 113: College Station, TX (Ocean Drilling Program), 901–914.

Tiedemann, R., Sarnthein, M., and Shackleton, N.J., 1994. Astronomic timescale for the Pliocene Atlantic $\delta^{18}O$ and dust flux records of Ocean Drilling Program Site 659. *Paleoceanography,* 9:619–638.

Timur, A., and Toksöz, M.N., 1985. Downhole geophysical logging. *Ann. Rev. Earth Planet. Sci.,* 13:315–344.

Vail, P.R., Mitchum, R.M. Jr., Todd, R.G., Widmier, S., Thompson, S., Sangree, J.B., Bubb, J.N., Hatlelid, 1977. Seismic stratigraphy and global changes of sea level. *In* Payton, C. (Ed.), *Seismic stratigraphy: applications to hydrocarbon exploration*. AAPG Mem, 26:49–213.

Von Herzen, R.P., and Maxwell, A.E., 1959. The measurement of thermal conductivity of deep-sea sediments by a needle-probe method. *J. Geophys. Res.,* 64:1557–1563.

Weaver, F.M., 1976. Antarctic Radiolaria from the southeast Pacific basin, Deep Sea Drilling Project, Leg 35. *In* Hollister, C.D., Craddock, C., et al., *Init. Repts. DSDP,* 35: Washington (U.S. Govt. Printing Office), 569–603.

Weber, M.E., Niessen, F., Kuhn, G., and Wiedicke, M., 1997. Calibration and application of marine sedimentary physical properties using a multi-sensor core logger. *Mar. Geol.,* 136:151–172.

Wei, W., 1993. Calibration of Upper Pliocene–Lower Pleistocene nannofossil events with oxygen isotope stratigraphy. *Paleoceanography,* 8:85–99

Wetzel, A., 1984. Bioturbation in deep-sea fine-grained sediments: influence of sediment texture, turbidite frequency and rates of environmental change. *In* Stow, D.A.V., and Piper D.J.W. (Eds.), *Fine-Grained Sediments: Deep Water Processes and Facies*. Geol. Soc. Spec. Publ. London, 24:595–608.

Figure F1. Lithologic classification scheme used during Leg 178 for sediments that consist of >70% terrigenous components. This classification scheme is used also for sediment that consists of 50%–70% terrigenous components; the terrigenous component name is preceded by a modifier that describes the nonterrigenous component. The general term *mud* is modified by more specific names, such as sand, silt, or clay.

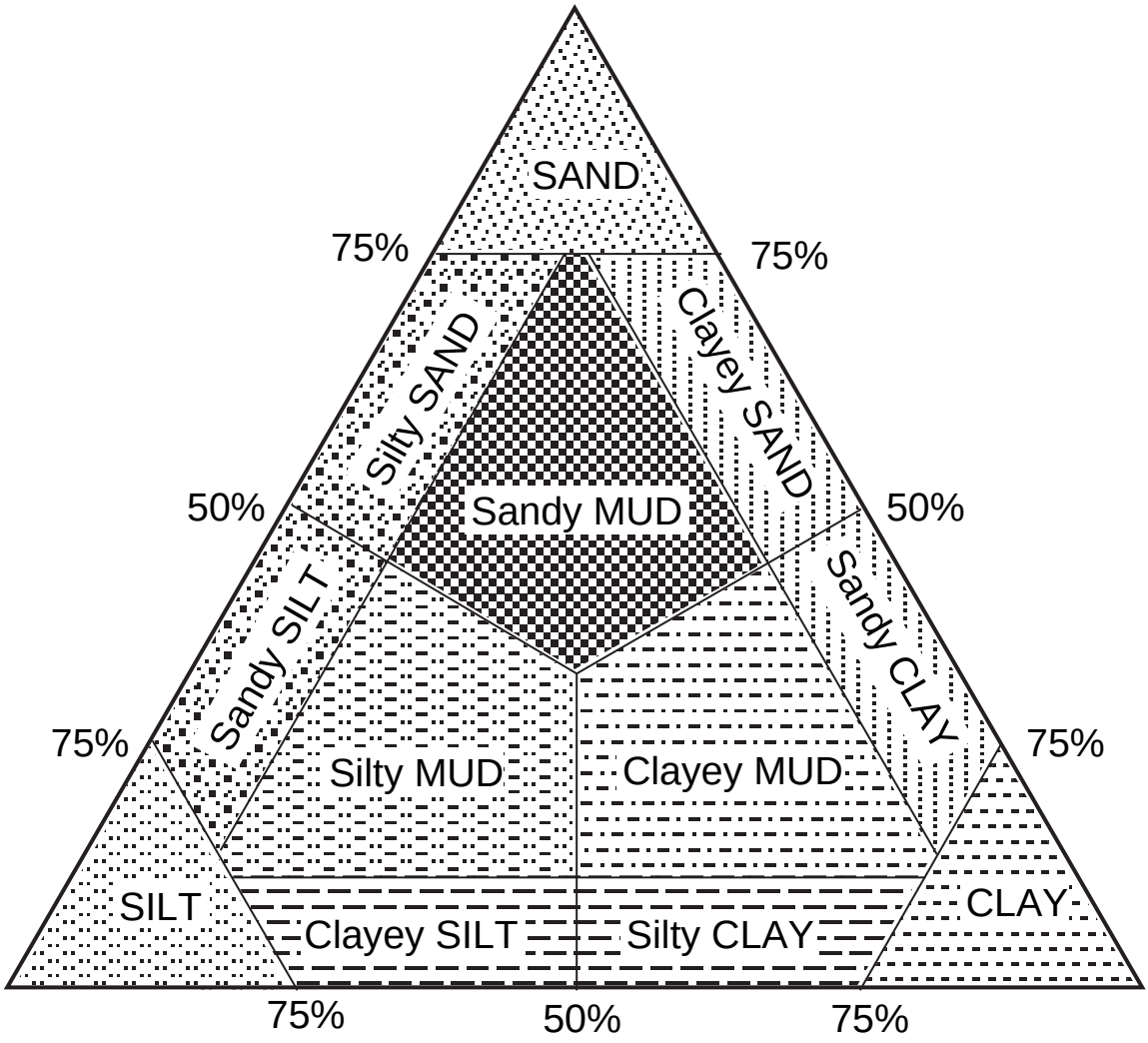

Figure F2. Compositional classification for biogenic and siliciclastic marine sediments.

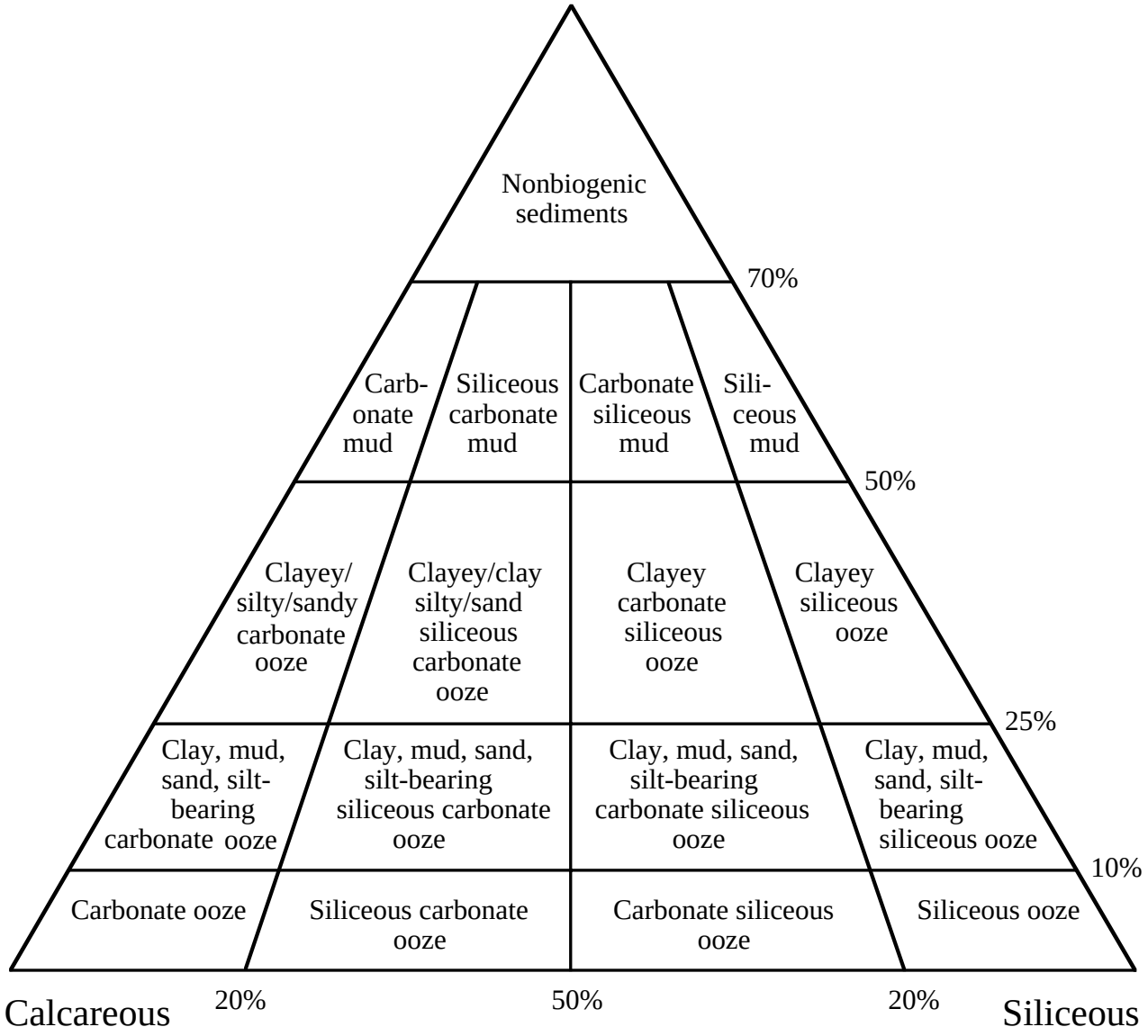

Figure F3. Schematic representation of internal structure of facies within turbidites recovered during Leg 178 compared with Piper's (1978) descriptive scheme for muddy turbidites. The three facies recognized are essentially formed by repetitive turbidite sequences that form relatively thick depositional units. Intensity of bioturbation, amount of ice-rafted debris, and thickness of hemipelagic division at bed tops depends on the recurrence interval of turbidity currents.

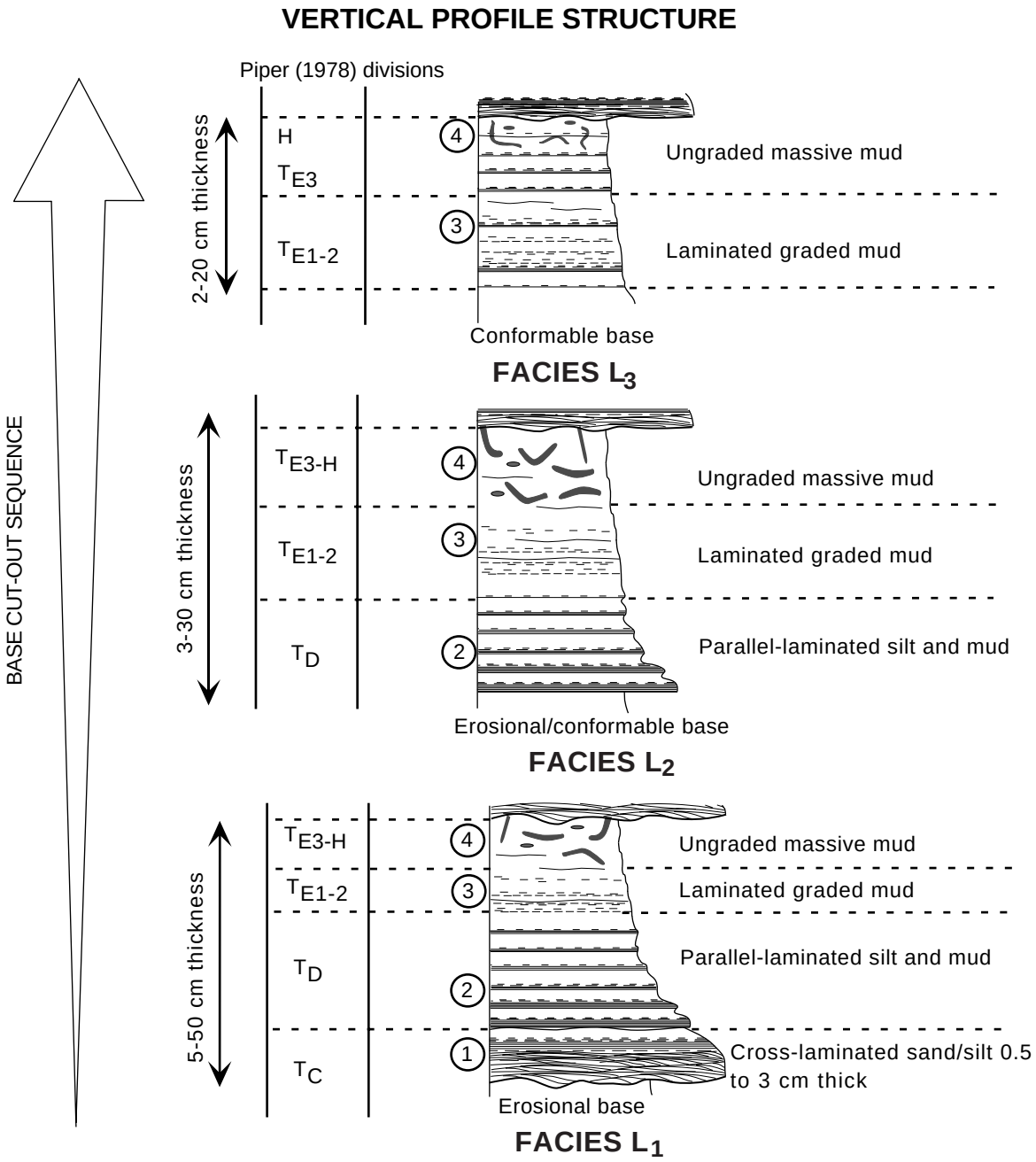

Figure F4. Schematic diagram showing typical downslope and across-slope relationship between turbidite Facies L_1, L_2, and L_3 as proposed by Stow and Piper (1984).

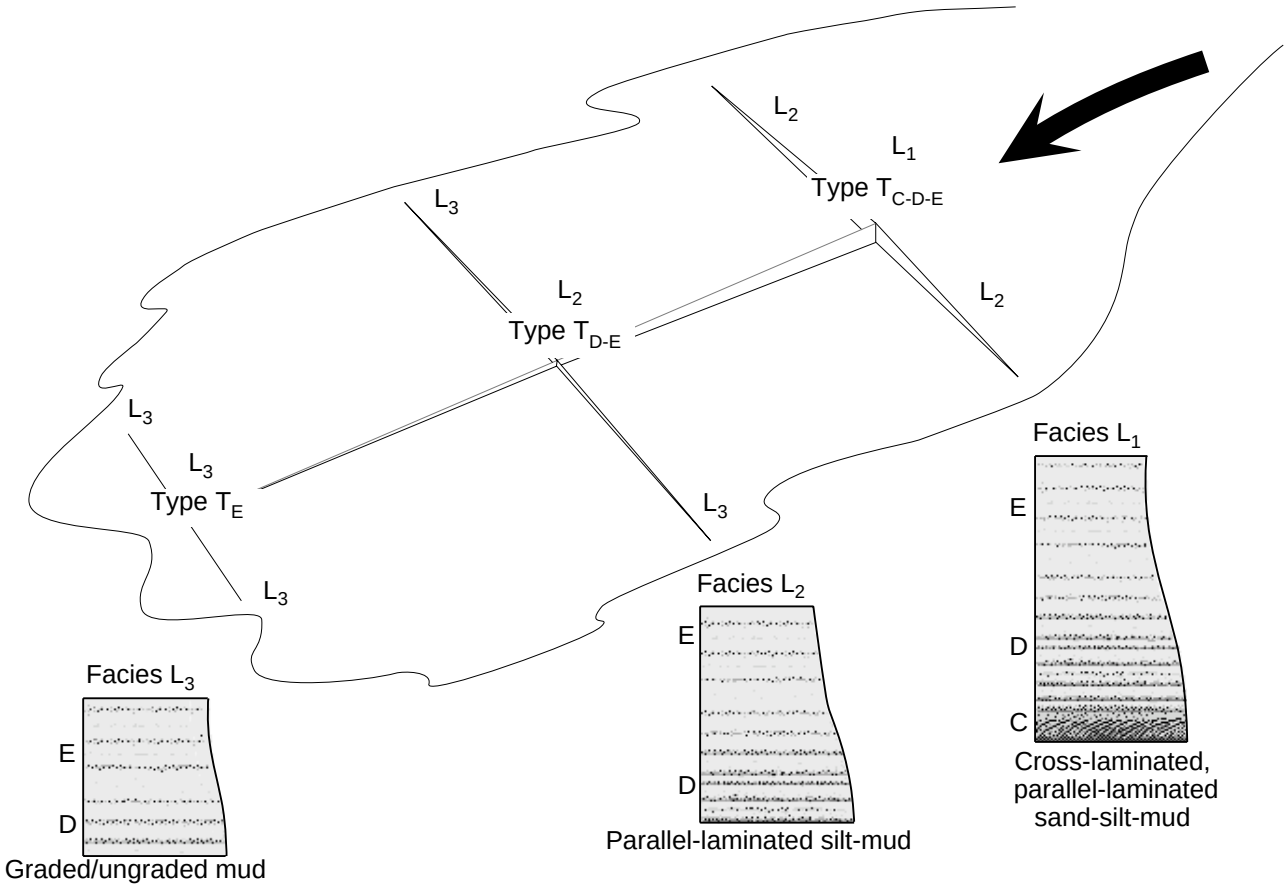

Figure F5. Schematic representation of Facies C (contourite). Modified from Stow and Piper (1984). Such facies can occur in association with the hemipelagic H interval of fine-grained muddy turbidites (Fig. F3, p. 39).

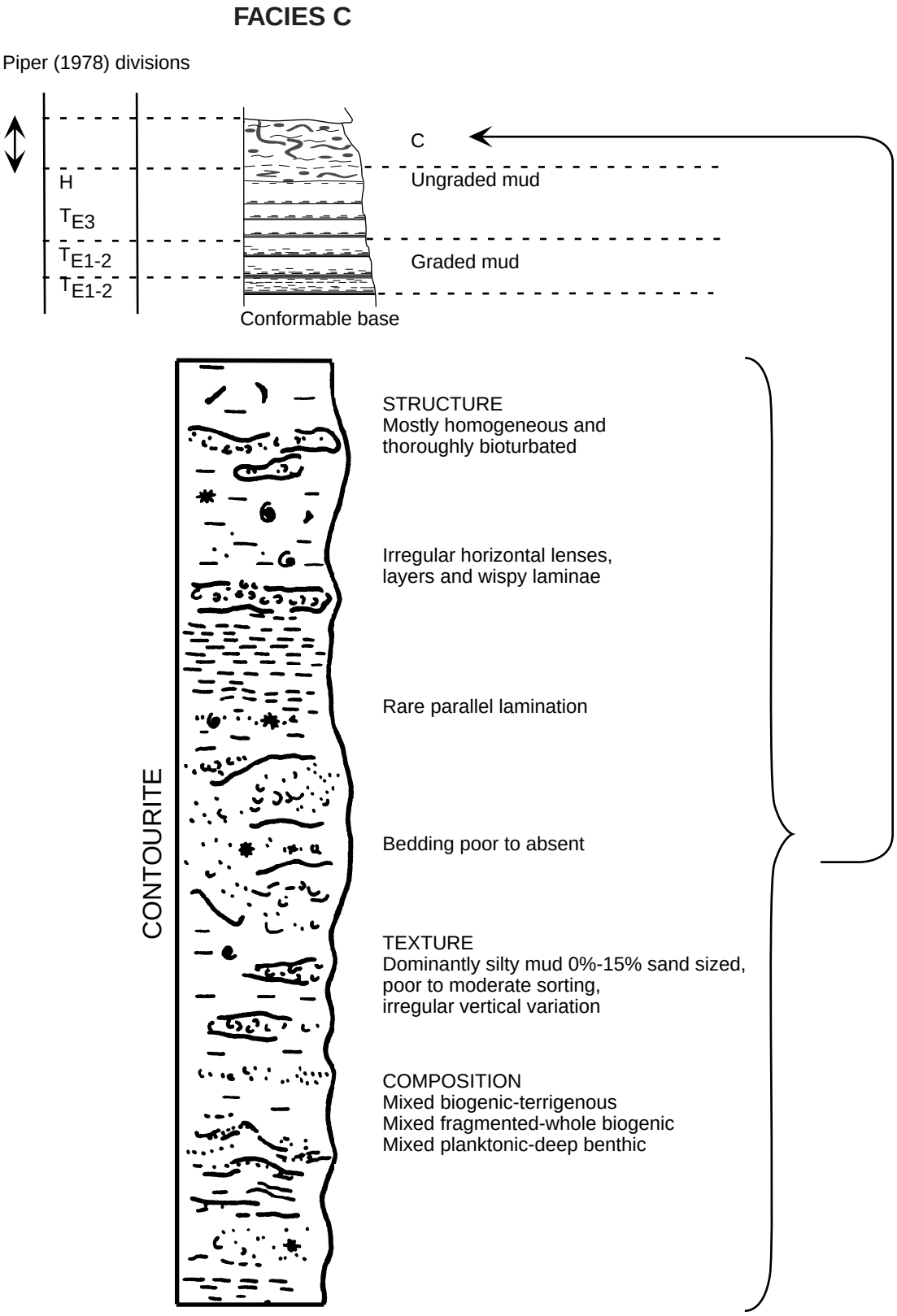

Figure F6. Schematic representation of diamict and other facies and physical structures identified during Leg 178.

Lithofacies code and accompanying symbols for diamicts based upon the scheme of Eyles et al. (1983).
Hyphens show possible combinations; second letter (m and c) indicates matrix or clast support (degree undefined). Third letter gives internal structure (m = massive, s = stratified, g = graded).

DIAMICT, D

Dm	matrix supported
Dc	clast supported
D-m	massive
D-s	stratified
D-g	graded

SANDS, S

Sr	rippled
St	trough cross-bedded
Sh	horizontal lamination
Sm	massive
Sg	graded
Sd	soft sediment deformation

FINE-GRAINED (mud), F

Fl	laminated
Fm	massive
F-d	with dropstones

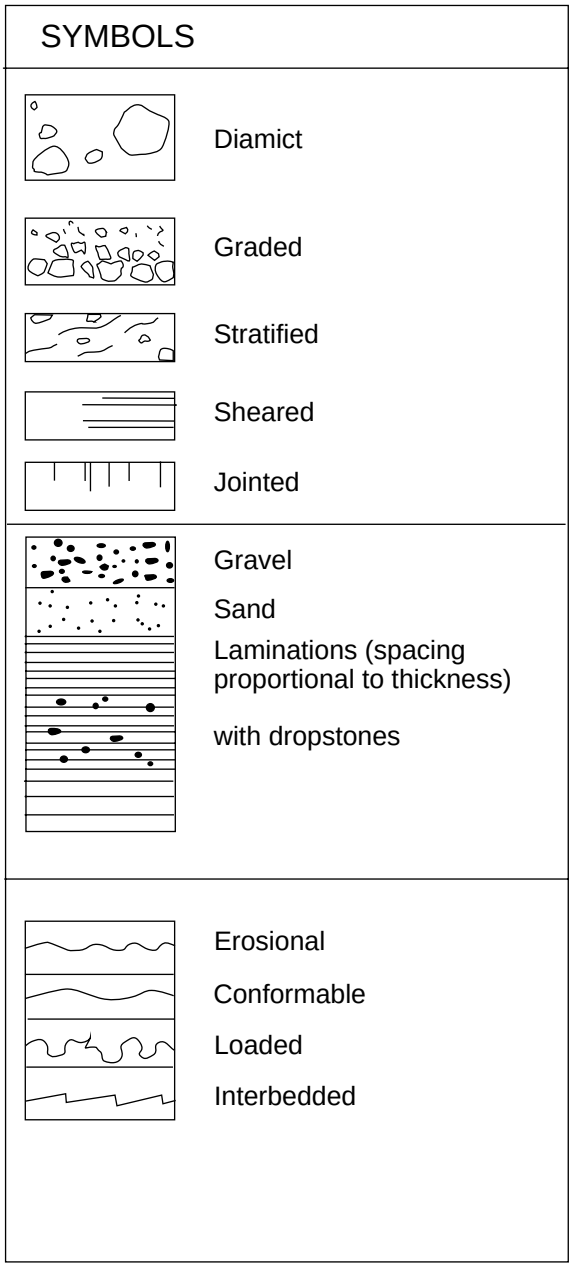

Figure F7. Key symbols used in the "Graphic Lithology," "Bioturbation," "Structure," "Disturbance," and "Sample" columns of the core description forms and barrel sheets.

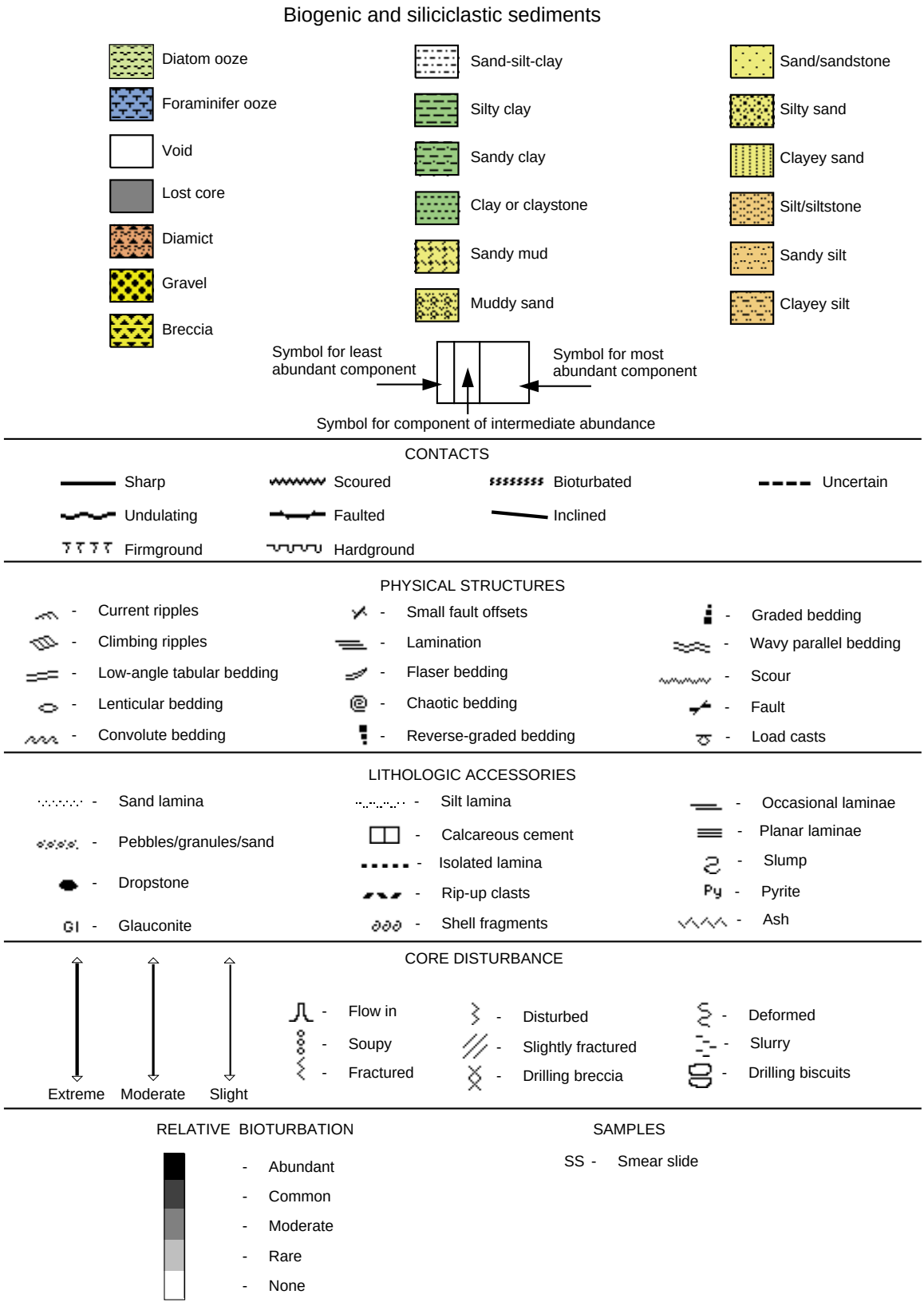

Figure F8. Geomagnetic polarity time scale of Berggren et al. (1985a, 1985b) correlated with Berggren et al. (1995).

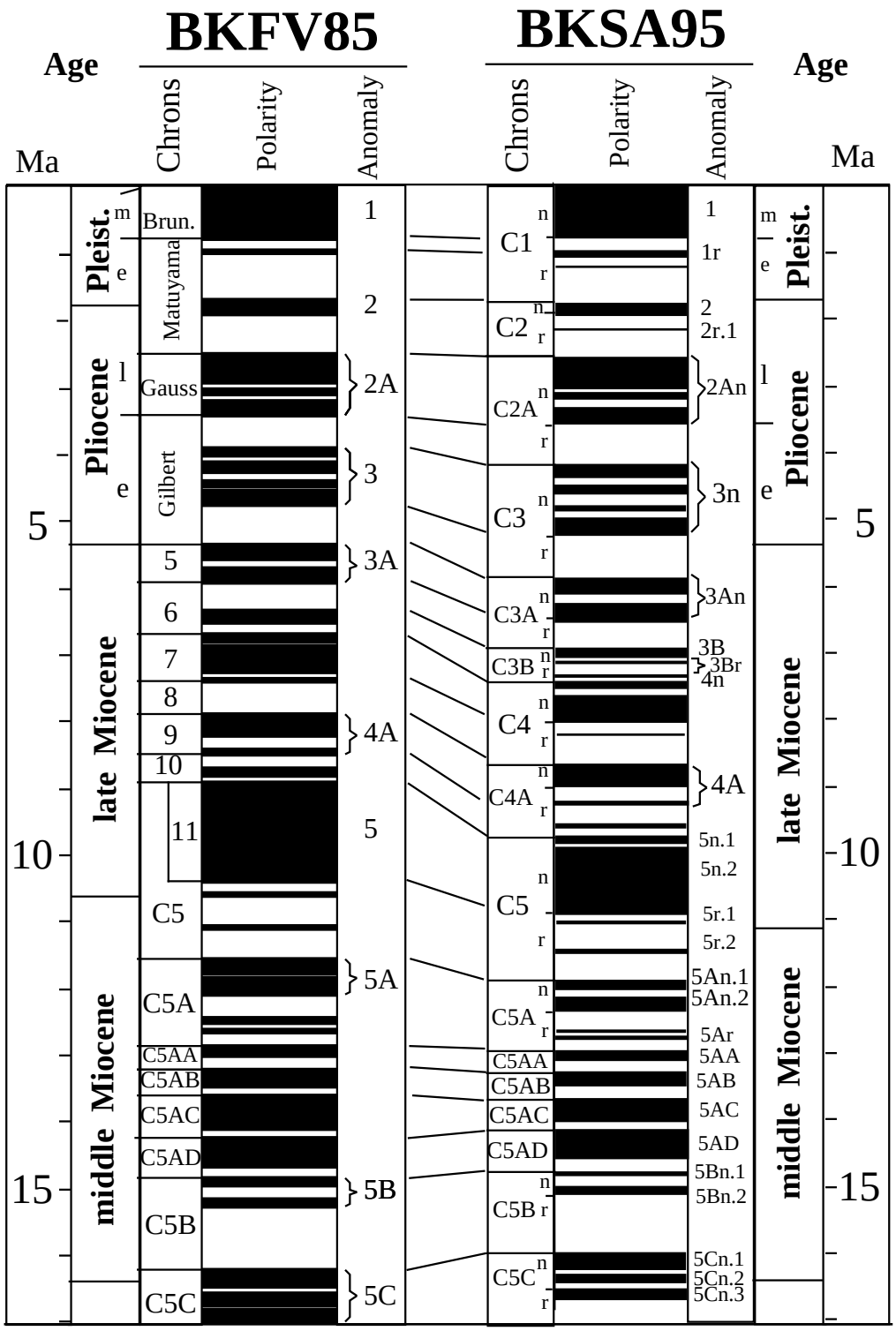

Figure F9. Combined geomagnetic polarity time scales of Berggren et al. (1985a, 1985b) and Berggren et al. (1995) with the biostratigraphic zones used during Leg 178. The diatom zonation is based mainly on Harwood and Maruyama (1992), as well as Leg 177 results. Standard calcareous nannofossil zonations are from Martini (1971) and Okada and Bukry (1980). Radiolarian zonation is from Lazarus (1992).

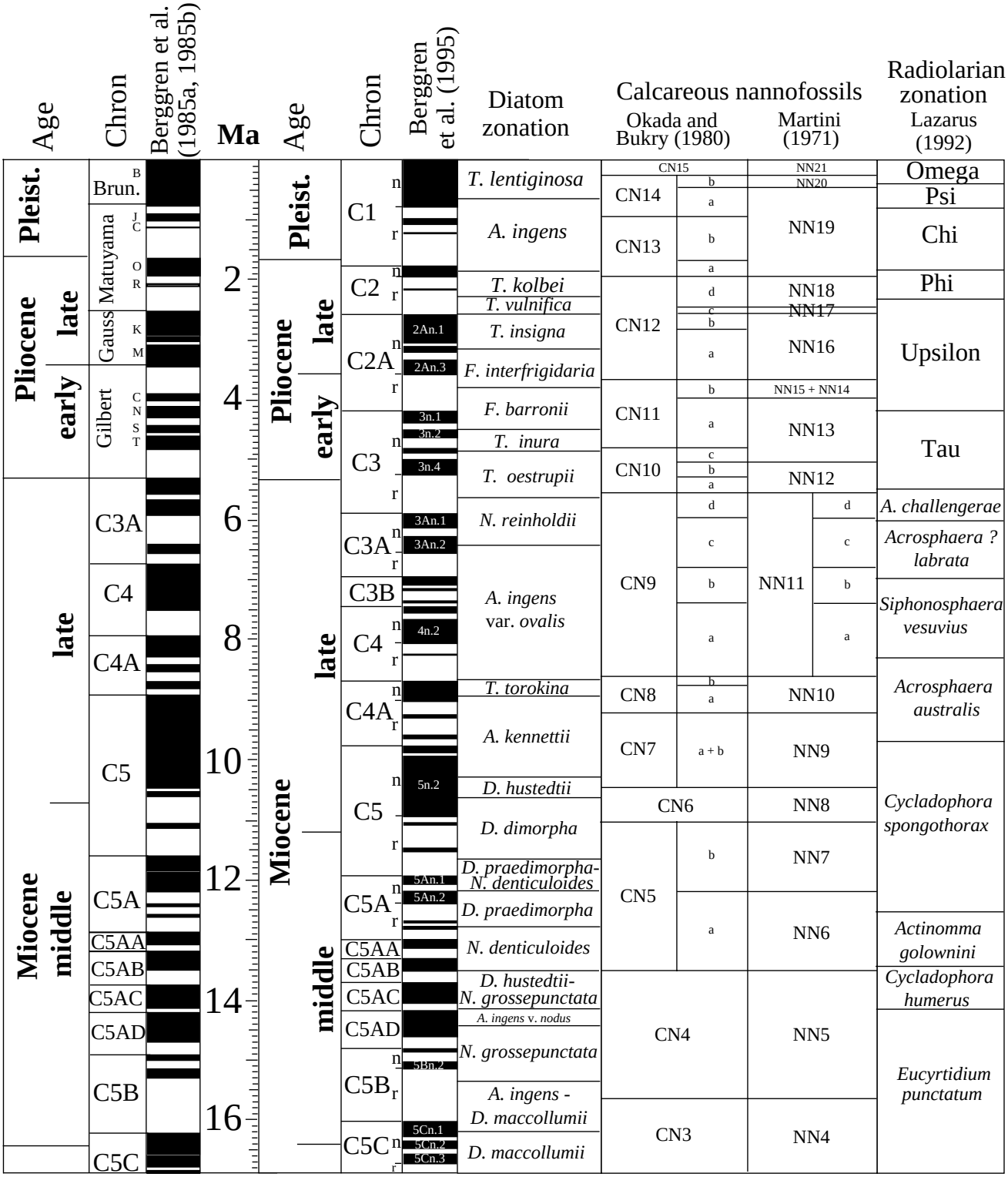

Figure F10. Diatom zones and datums used during Leg 178. Geomagnetic time scale of Berggren et al. (1995). T = top/last occurrence, B = base/first occurrence. Age references are from Harwood and Maruyama (1992).

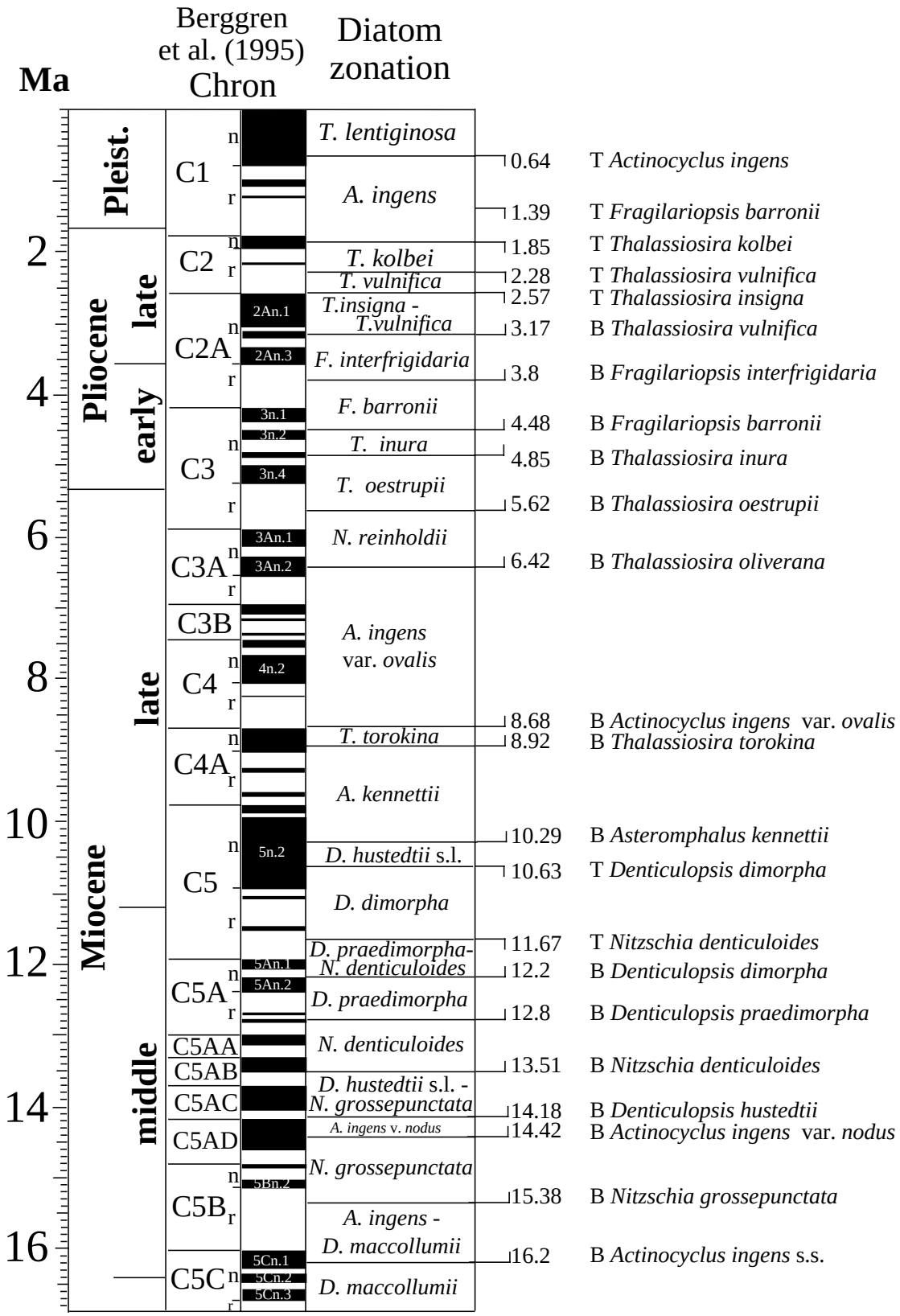

Figure F11. Radiolarian zonation used for Leg 178 and the magnetostratigraphy of Berggren et al. (1995). Preceding each event is its age in Ma; events defining zonal boundaries are in bold. T = top occurrence, B = bottom occurrence, ET = evolutionary transition. Numbers in parentheses are the sources of the ages: (1) Lazarus (1990); (2) Caulet (1991); (3) Hayes and Opdyke (1967); (4) Lazarus (1992); (5) Abelmann (1992).

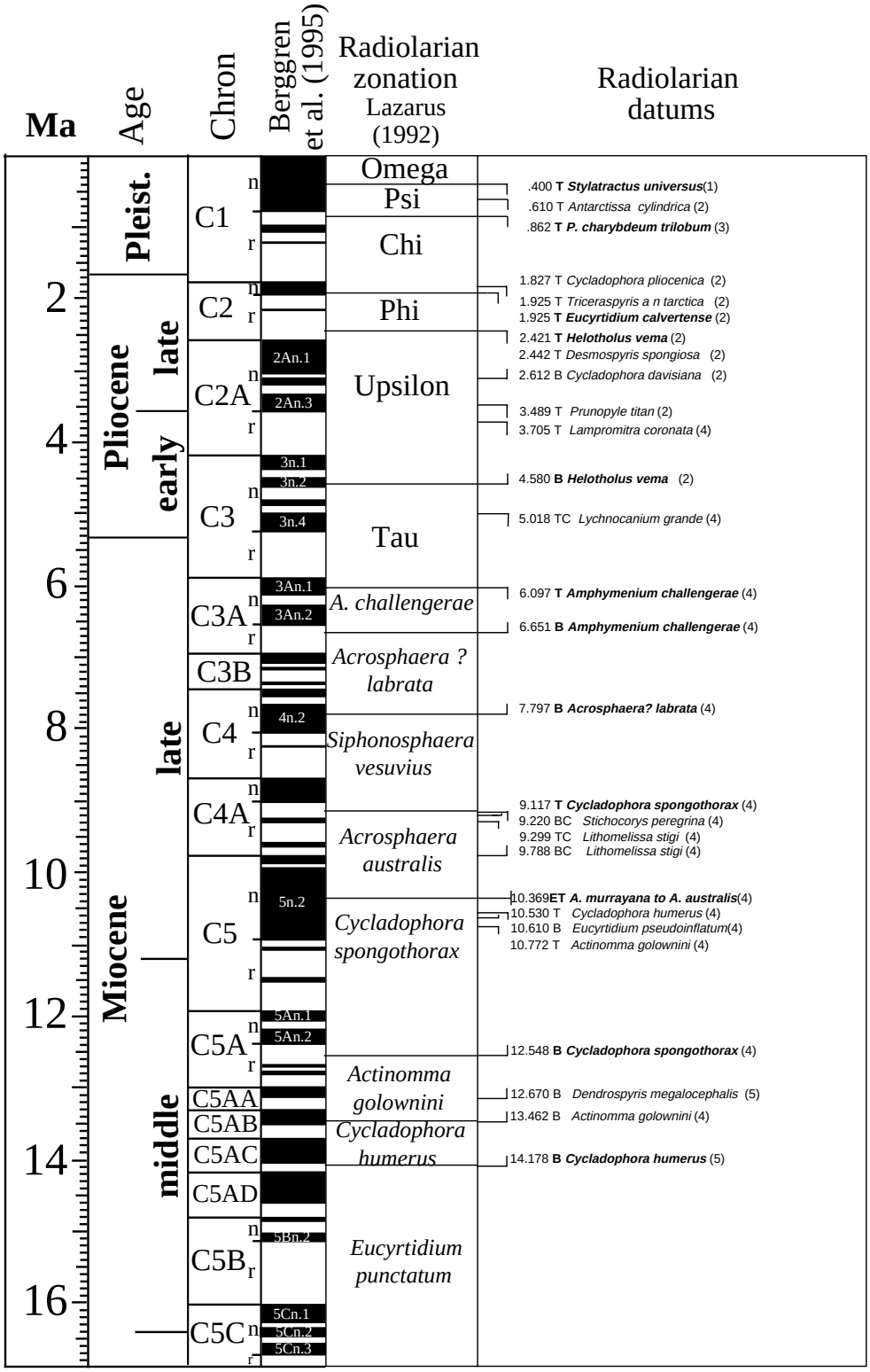

Figure F12. Geomagnetic polarity time scale of Berggren et al. (1995), correlation of the Martini (1971) and Okada and Bukry (1980) calcareous nannofossil biostratigraphic zonations, and selected events used during Leg 178. FCO = first common occurrence. Age references: (1) Thierstein et al. (1977); (2) Raffi et al. (1993); (3) Lourens et al. (1996); (4) Tiedemann et al. (1994); (5) Raffi and Flores (1995); (6) Gartner (1990); (7) Backman and Raffi (1997); and (8) Berggren et al. (1995).

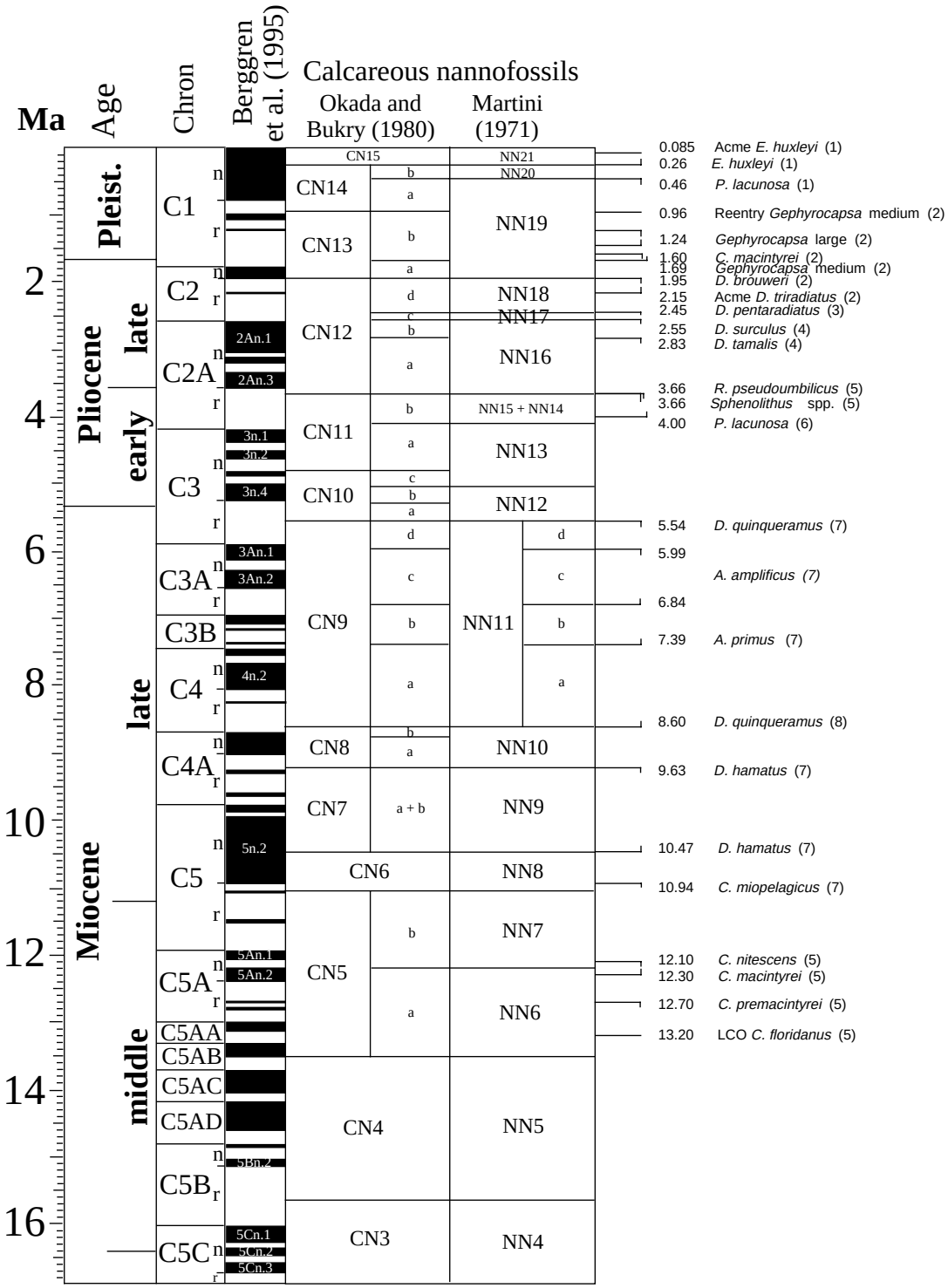

Figure F13. A. ODP paleomagnetic coordinate system for archive halves. **B.** Coordinate system for discrete samples collected with the extruder. **C.** Coordinate system for discrete push-in samples.

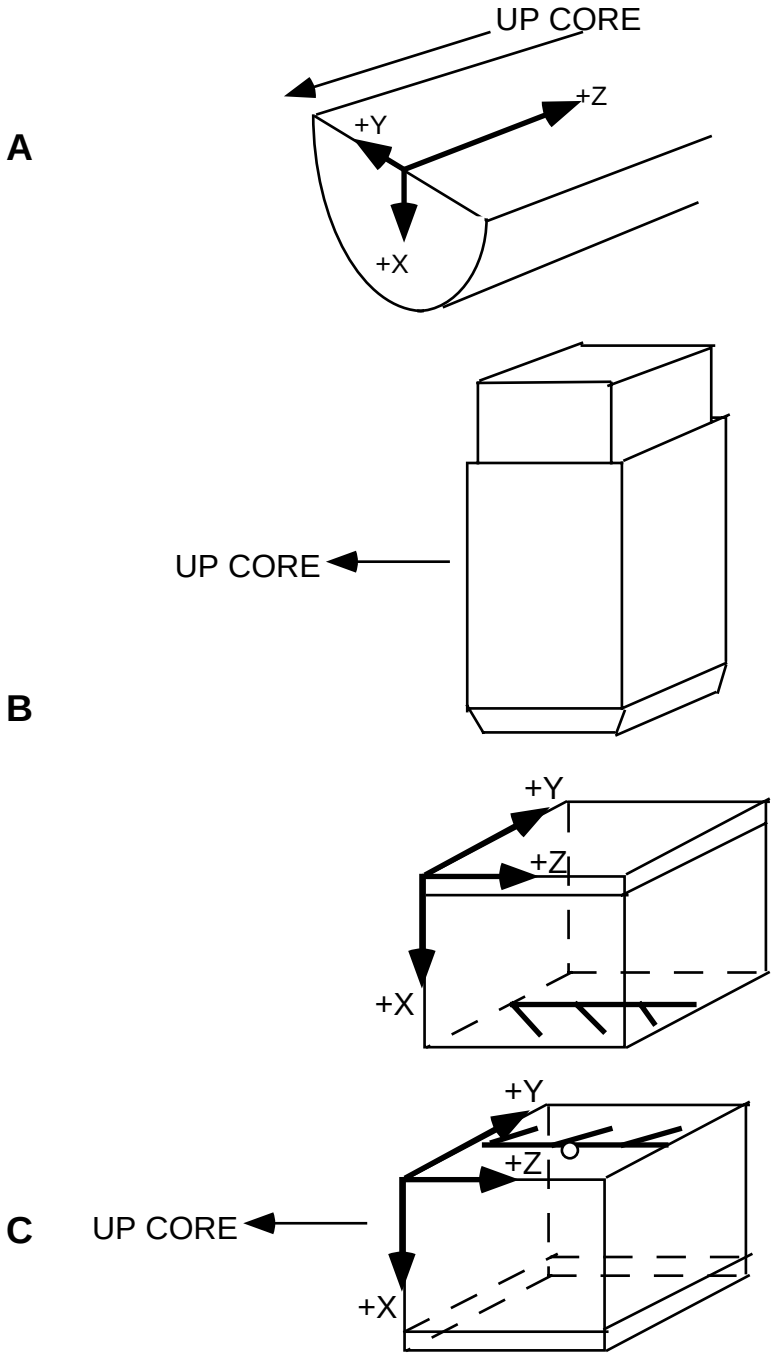

Figure F14. Example of the magnetic susceptibility records (5–30 mbsl) from Site 1096. **A.** Cores plotted on the mbsf depth scale. Data from Hole 1096B have a horizontal offset by a constant factor. **B.** The same cores on the mcd scale. The composite depth section has the advantage that features common to all holes are in relative alignment. **C.** Provisional spliced section of Holes 1096A and 1096B.

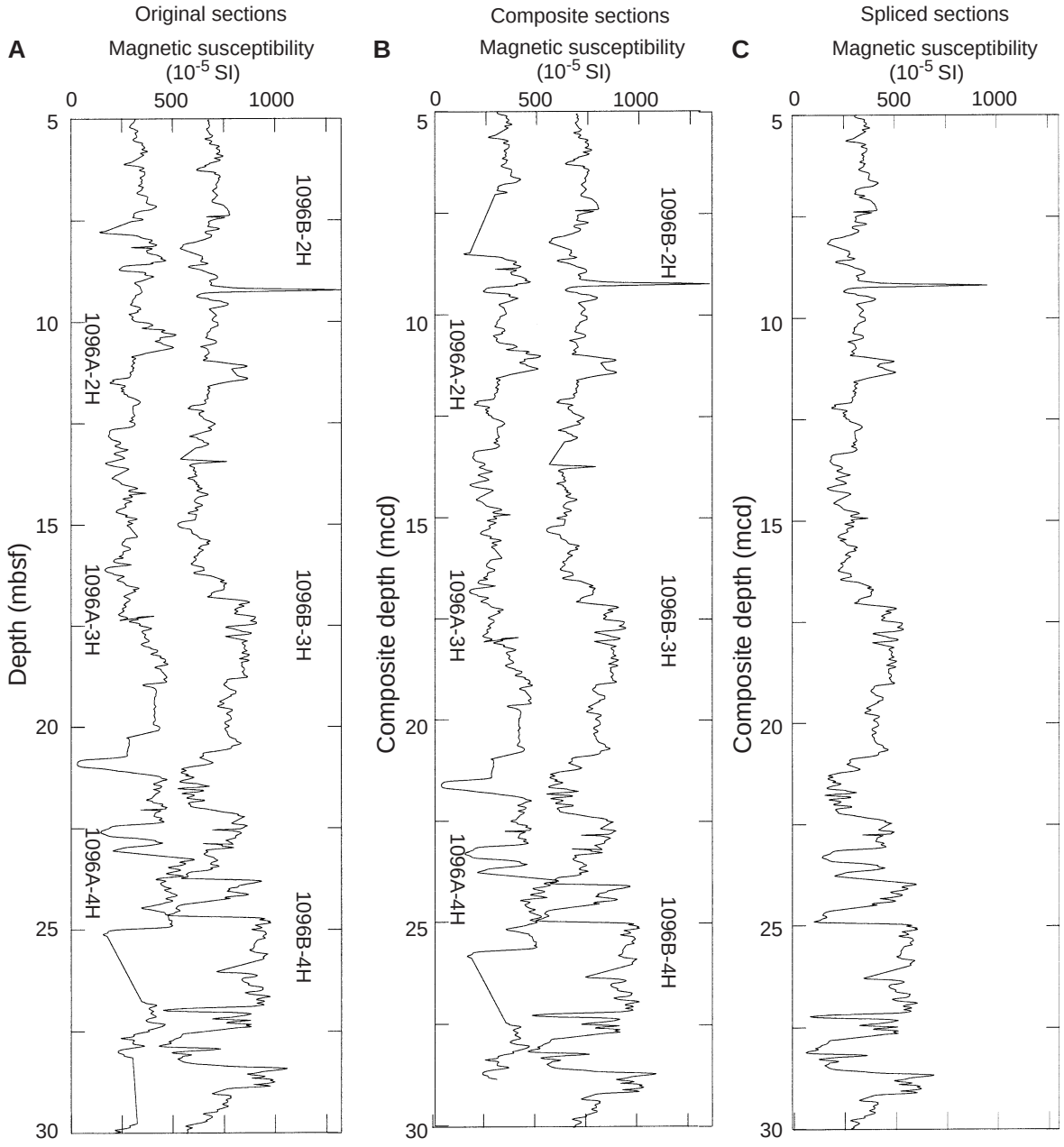

Figure F15. Example of a synthetic seismogram calculated from an oversimplified density and velocity model.

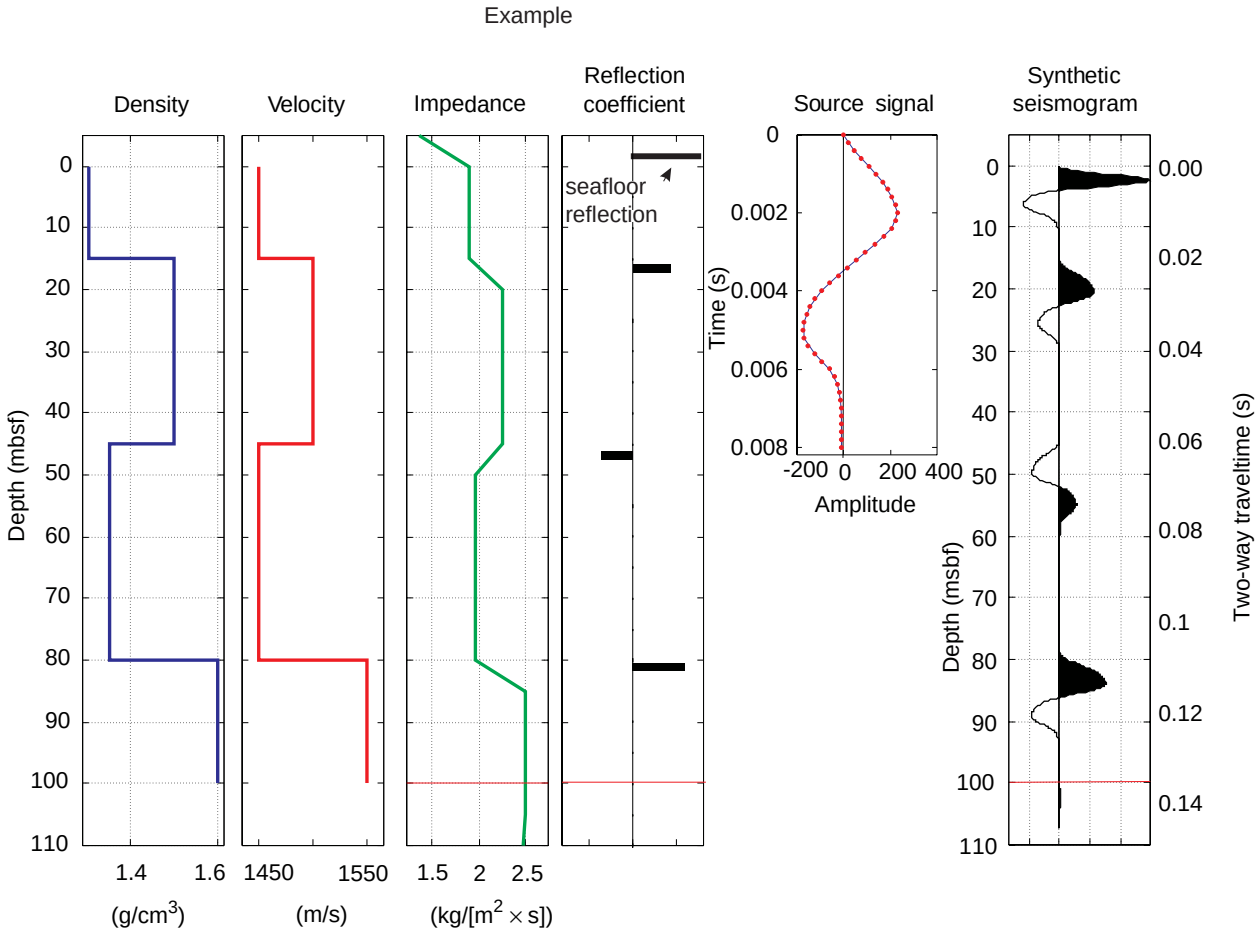

Figure F16. Example of the data "cleaning" process used to remove extreme values and artifacts from raw data sets before constructing a synthetic seismogram.

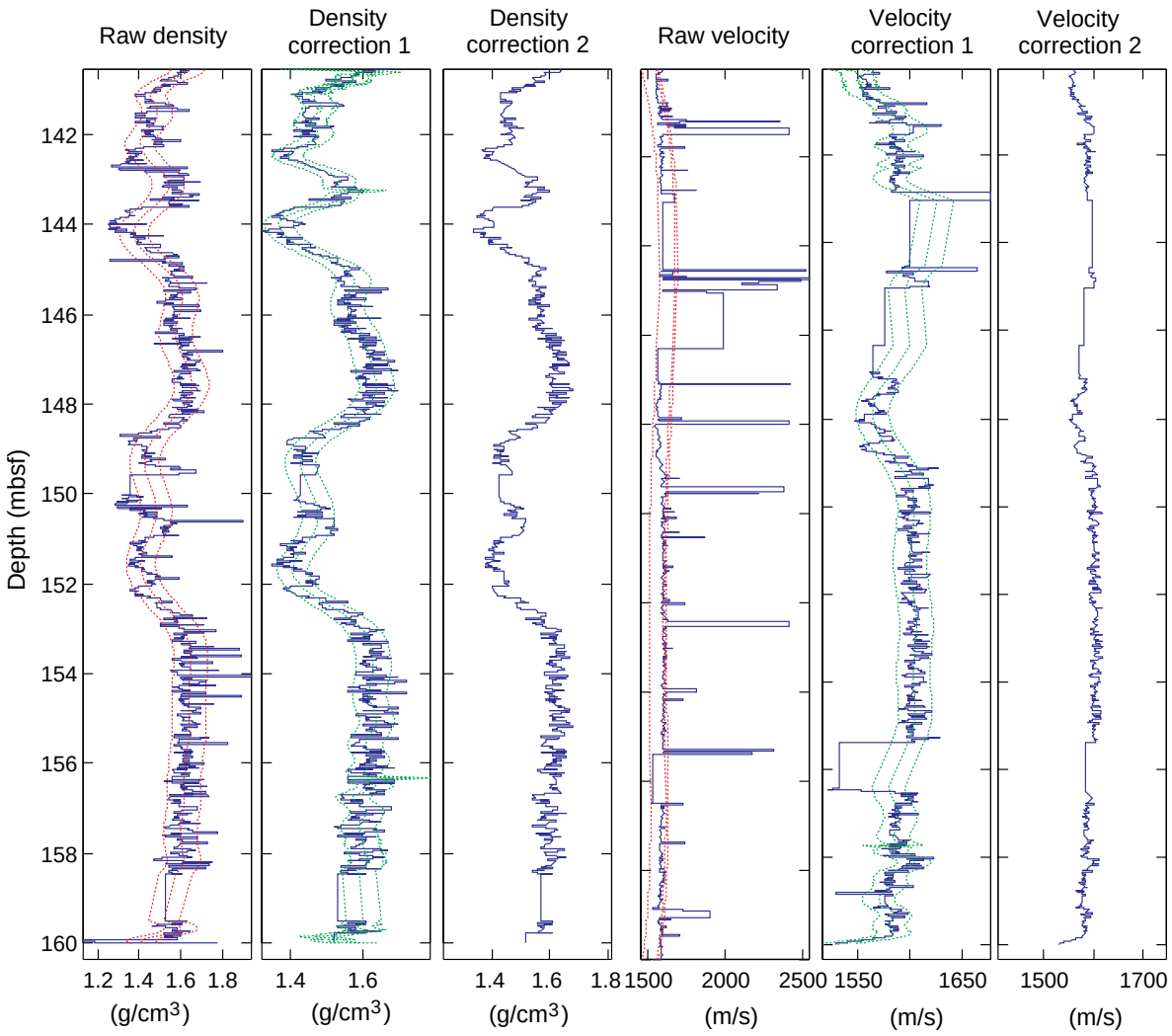

Table T1. Neogene geomagnetic polarity time scale and magnetostratigraphic nomenclature used during Leg 178. (Continued on next page.)

Events	Sense	BKSA95 (Ma)	Original data source
C1n (o); "Brunhes/Matuyama"	R->N	0.780	SBP90
C1r.1n "Jaramillo" (t)	N->R	0.990	SBP90
C1r.1n "Jaramillo" (o)	R->N	1.070	SBP90
C2n "Olduvai" (t)	N->R	1.770	SBP90
C2n "Olduvai" (o)	R->N	1.950	SBP90
C2r.1n (t)	N->R	2.140	CK95
C2r.1n (o)	R->N	2.150	CK95
C2An.1n (t); "Matuyama/Gauss"	N->R	2.581	H91
C2An.1n (o); "Kaena" (t)	R->N	3.040	H91
C2An.2n (t); "Kaena" (o)	N->R	3.110	H91
C2An.2n (o); "Mammoth" (t)	R->N	3.220	H91
C2An.3n (t); "Mammoth" (o)	N->R	3.330	H91
C2An.3n (o); "Gauss/Gilbert"	R->N	3.580	H91
C3n.1n "Cochiti" (t)	N->R	4.180	H91
C3n.1n "Cochiti" (o)	R->N	4.290	H91
C3n.2n "Nunivak" (t)	N->R	4.480	H91
C3n.2n "Nunivak" (o)	R->N	4.620	H91
C3n.3n "Sidufjall" (t)	N->R	4.800	H91
C3n.3n "Sidufjall" (o)	R->N	4.890	H91
C3n.4n "Thvera" (t)	N->R	4.980	H91
C3n.4n "Thvera" (o)	R->N	5.230	H91/SCHPS95
C3An.1n (t)	N->R	5.894	CK95
C3An.1n (o)	R->N	6.137	CK95
C3An.2n (t)	N->R	6.269	CK95
C3An.2n (o)	R->N	6.567	CK95
C3Bn (t)	N->R	6.935	CK95
C3Bn (o)	R->N	7.091	CK95
C3Br.1n (t)	N->R	7.135	CK95
C3Br.1n (o)	R->N	7.170	CK95
C3Br.2n (t)	N->R	7.341	CK95
C3Br.2n (o)	R->N	7.375	CK95
C4n.1n (t)	N->R	7.432	CK95
C4n.1n (o)	R->N	7.562	CK95
C4n.2n (t)	N->R	7.650	CK95
C4n.2n (o)	R->N	8.072	CK95
C4r.In (t)	N->R	8.225	CK95
C4r.1n (o)	R->N	8.257	CK95
C4An (t)	N->R	8.699	CK95
C4An (o)	R->N	9.025	CK95
C4Ar.1n (t)	N->R	9.230	CK95
C4Ar.1n (o)	R->N	9.308	CK95
C4Ar.2n (t)	N->R	9.580	CK95
C4Ar.2n (o)	R->N	9.642	CK95
C5n.1n (t)	N->R	9.740	CK95
C5n.1n (o)	R->N	9.880	CK95
C5n.2n (t)	N->R	9.920	CK95
C5n.2n (o)	R->N	10.949	CK95
C5r.1n (t)	N->R	11.052	CK95
C5r.1n (o)	R->N	11.099	CK95
C5r.2n (t)	N->R	11.476	CK95
C5r.2n (o)	R->N	11.531	CK95
C5An.1n (t)	N->R	11.935	CK95
C5An.1n (o)	R->N	12.078	CK95
C5An.2n (t)	N->R	12.184	CK95
C5An.2n (o)	R->N	12.401	CK95
C5Ar.1n (t)	N->R	12.678	CK95
C5Ar.1n (o)	R->N	12.708	CK95
C5Ar.2n (t)	N->R	12.775	CK95
C5Ar.2n (o)	R->N	12.819	CK95
C5AAn (t)	N->R	12.991	CK95
C5AAn (o)	R->N	13.139	CK95
C5ABn (t)	N->R	13.302	CK95
C5ABn (o)	R->N	13.510	CK95
C5ACn (t)	N->R	13.703	CK95
C5ACn (o)	R->N	14.076	CK95
C5ADn (t)	N->R	14.178	CK95

Table T1 (continued).

Events	Sense	BKSA95 (Ma)	Original data source
C5ADn (o)	R->N	14.612	CK95
C5Bn.1n (t)	N->R	14.800	CK95
C5Bn.1n (o)	R->N	14.888	CK95
C5Bn.2n (t)	N->R	15.034	CK95
C5Bn.2n (o)	R->N	15.155	CK95
C5Cn.1n (t)	N->R	16.014	CK95
C5Cn.1n (o)	R->N	16.293	CK95
C5Cn.2n (t)	N->R	16.327	CK95
C5Cn.2n (o)	R->N	16.488	CK95
C5Cn.3n (t)	N->R	16.556	CK95
C5Cn.3n (o)	R->N	16.726	CK95
C5Dn (t)	N->R	17.277	CK95
C5Dn (o)	R->N	17.615	CK95

Notes: (t) = termination, (o) = onset. SBP90 = Shackleton et al. (1990), H91 = Hilgen (1991a, 1991b), SCHPS95 = Shackleton et al. (1995), CK95 = Cande and Kent (1995).

Table T2. Correlation among the published Neogene geomagnetic polarity time scales and magnetostratigraphic nomenclature. (Continued on next page.)

Events	Sense	BKSA95/CK95 (Ma)	SSP95 (Leg 154)	SCHPS95 (Leg 138)	CK92	BKFV85	Age (Ma)	BKSA95/ CK95-BKFV85	BKSA95/ CK95-SSP95	BKSA95/ CK95-SCHPS95
C1n (o)	R->N	0.780	0.780	0.780	0.780	Brunhes/Matuyama	0.73	0.050		
C1r.1n (t)	N->R	0.990	0.990	0.990	0.984	Jaramillo (t)	0.91	0.080		
C1r.1n (o)	R->N	1.070	1.070	1.070	1.049	Jaramillo (o)	0.98	0.090		
C2n (t)	N->R	1.770	1.770	1.770	1.757	Olduvai (t)	1.66	0.110		
C2n (o)	R->N	1.950	1.950	1.950	1.983	Olduvai (o)	1.88	0.070		
C2r.1n (t)	N->R	2.140	ND	ND	2.197		ND			
C2r.1n (o)	R->N	2.150	ND	ND	2.229		ND			
C2An.1n (t)	N->R	2.581	2.581	2.600	2.600	Matuyama/Gauss	2.47	0.111		–0.019
C2An.1n (o)	R->N	3.040	3.040	3.046	3.054	Kaena (t)	2.92	0.120		–0.006
C2An.2n (t)	N->R	3.110	3.110	3.131	3.127	Kaena (o)	2.99	0.120		–0.021
C2An.2n (o)	R->N	3.220	3.220	3.233	3.221	Mammoth (t)	3.00	0.220		–0.013
C2An.3n (t)	N->R	3.330	3.330	3.331	3.325	Mammoth (o)	3.18	0.150		–0.001
C2An.3n (o)	R->N	3.580	3.580	3.594	3.553	Gauss/Gilbert	3.40	0.180		–0.014
C3n.1n (t)	N->R	4.180	4.180	4.199	4.033	Cochiti (t)	3.88	0.300		–0.019
C3n.1n (o)	R->N	4.290	4.290	4.316	4.134	Cochiti (o)	3.97	0.320		–0.026
C3n.2n (t)	N->R	4.480	4.480	4.479	4.265	Nunivak (t)	4.10	0.380		0.001
C3n.2n (o)	R->N	4.620	4.620	4.623	4.432	Nunivak (o)	4.24	0.380		–0.003
C3n.3n (t)	N->R	4.800	4.800	4.781	4.611	Sidufjall (t)	4.40	0.400		0.019
C3n.3n (o)	R->N	4.890	4.890	4.878	4.691	Sidufjall (o)	4.47	0.420		0.012
C3n.4n (t)	N->R	4.980	4.980	4.977	4.812	Thvera (t)	4.57	0.410		0.003
C3n.4n (o)	R->N	5.230	5.230	5.232	5.046	Thvera (o)	4.77	0.460		–0.002
C3An.1n (t)	N->R	5.894	5.875	5.875	5.705	C3An1 (t)	5.35	0.544	0.019	0.019
C3An.1n (o)	R->N	6.137	6.122	6.122	5.946	C3An1 (o)	5.53	0.607	0.015	0.015
C3An.2n (t)	N->R	6.269	6.256	6.256	6.078	C3An2 (t)	5.68	0.589	0.013	0.013
C3An.2n (o)	R->N	6.567	6.555	6.555	6.376	C3An2 (o)	5.89	0.677	0.012	0.012
C3Bn (t)	N->7.091	7.072	7.072	6.901		C3An3 (o)	6.50	0.591	0.019	0.019
C3Br.1n (t)	N->R	7.135	ND	ND	ND		ND			
C3Br.1n (o)	R->N	7.170	ND	ND	ND		ND			
C3Br.2n (t)	N->R	7.341	ND	ND	ND		ND			
C3Br.2n (o)	R->N	7.375	ND	ND	ND		ND			
C4n.1n (t)	N->R	7.432	7.406	7.406	7.245	C4n1 (t)	6.70	0.435	0.026	0.026
C4n.1n (o)	R->N	7.562	7.533	7.533	7.376	C4n1 (o)	6.78	0.390	0.029	0.029
C4n.2n (t)	N->R	7.650	7.618	7.618	7.464	C4n2 (t)	6.85	0.491	0.032	0.032
C4n.2n (o)	R->N	8.072	8.027	8.027	7.892	C4n2 (o)	7.28	0.095	0.045	0.045
C4r.1n (t)	N->R	8.225	8.174	8.174	8.047	C4n3 (t)	7.35	0.082	0.051	0.051
C4r.1n (o)	R->N	8.257	8.205	8.205	8.079	C4n3 (o)	7.41	0.152	0.052	0.052
C4An (t)	N->R	8.699	8.631	8.631	8.529	C4An1 (t)	7.90	–0.250	0.068	0.068
C4An (o)	R->N	9.025	8.945	8.945	8.861	C4An1 (o)	8.21	–0.138	0.080	0.080
C4Ar.1n (t)	N->R	9.230	9.142	9.142	9.069	C4An2 (t)	8.41	–0.185	0.088	0.088
C4Ar.1n (o)	R->N	9.308	9.218	9.218	9.149	C4An2 (o)	8.50	–0.243	0.090	0.090
C4Ar.2n (t)	N->R	9.580	9.482	9.482	9.428	C4An3 (t)	8.71	–0.011	0.098	0.098
C4Ar.2n (o)	R->N	9.642	9.543	9.543	9.491	C4An3 (o)	8.80	0.225	0.099	0.099
C5n.1n (t)	N->R	9.740	9.639	9.639	9.592	C5n1 (t)	8.92	0.310	0.101	0.101
C5n.1n (o)	R->N	9.880	9.775	9.775	9.735		ND		0.105	0.105
C5n.2n (t)	N->R	9.920	9.815	9.815	9.777		ND		0.105	0.105
C5n.2n (o)	R->N	10.949	10.839	10.839	10.834	C5n1 (o)	10.42	–0.778	0.110	0.110
C5r.1n (t)	N->R	11.052	10.943	10.943	10.940	C5n2 (t)	10.54	–0.800	0.109	0.109
C5r.1n (o)	R->N	11.099	10.991	10.991	10.989	C5n2 (o)	10.59	–0.710	0.108	0.108
C5r.2n (t)	N->R	11.476	11.373	11.373	11.378	C5n3 (t)	11.03	–1.110	0.103	0.103
C5r.2n (o)	R->N	11.531	11.428	11.428	11.434	C5n3 (o)	11.09	–0.141	0.103	0.103
C5An.1n (t)	N->R	11.935	11.841	11.841	11.852	C5An1 (t)	11.55	–0.498	0.094	0.094
C5An.1n (o)	R->N	12.078	11.988	11.988	12.000	C5An1 (o)	11.73	–0.631	0.090	0.090
C5An.2n (t)	N->R	12.184	12.096	12.096	12.108	C5An2 (t				
C5An.2n (o)	R->N	12.401	12.320	12.320	12.333	C5An2 (o)	12.12	–0.589	0.081	0.081
C5Ar.1n (t)	N->R	12.678	12.605	12.605	12.618	C5An3 (t)	12.46	–0.525	0.073	0.073
C5Ar.1n (o)	R->N	12.708	12.637	12.637	12.649	C5An3 (o)	12.49	–0.412	0.071	0.071
C5Ar.2n (t)	N->R	12.775	12.705	12.705	12.718	C5An4 (t)	12.58	–0.396	0.070	0.070
C5Ar.2n (o)	R->N	12.819	12.752	12.752	12.764	C5An4 (o)	12.62	–0.219	0.067	0.067
C5AAn (t)	N->R	12.991	12.929	12.929	12.941	C5AAn (t)	12.83	–0.152	0.062	0.062
C5AAn (o)	R->N	13.139	13.083	13.083	13.094	C5AAn (o)	13.01	–0.302	0.056	0.056
C5ABn (t)	N->R	13.302	13.252	13.252	13.263	C5ABn (t)	13.20	–0.425	0.050	0.050
C5ABn (o)	R->N	13.510	13.466	13.466	13.476	C5ABn (o)	13.46	–0.641	0.044	0.044
C5ACn (t)	N->R	13.703	13.666	13.666	13.674	C5ACn (t)	13.69	–0.699	0.037	0.037
C5ACn (o)	R->N	14.076	14.053	14.053	14.059	C5ACn (o)	14.08	–0.941	0.023	0.023
C5ADn (t)	N->R	14.178	14.159	14.159	14.164	C5ADn (t)	14.20	–0.898	0.019	0.019
C5ADn (o)	R->N	14.612	14.607	14.607	14.608	C5ADn (o)	14.66	–1.150	0.005	0.005
C5Bn.1n (t)	N->R	14.800	14.800	14.800	14.800	C5Bn.1n (t)	14.87	–1.167		
C5Bn.1n (o)	R->N	14.888	14.890	ND	14.890	C5Bn.1n (o)	14.96	–0.884	–0.002	

Table T2 (continued).

Events	Sense	BKSA95/CK95 (Ma)	SSP95 (Leg 154)	SCHPS95 (Leg 138)	CK92	BKFV85	Age (Ma)	BKSA95/ CK95-BKFV85	BKSA95/ CK95-SSP95	BKSA95/ CK95-SCHPS95
C5Bn.2n (t)	N->R	15.034	15.038	ND	15.038	C5Bn.2n (t)	15.13	–0.952	–0.004	
C5Bn.2n (o)	R->N	15.155	15.162	ND	15.162	C5Bn.2n (o)	15.27	–0.658	–0.007	
C5Cn.1n (t)	N->R	16.014	16.035	ND	16.035	C5Cn.1n (t)	16.22	–1.420	–0.021	
C5Cn.1n (o)	R->N	16.293	16.318	ND	16.318	C5Cn.1n (o)	16.52	–1.632	–0.025	
C5Cn.2n (t)	N->R	16.327	16.352	ND	16.352	C5Cn.2n (t)	16.56	–1.526	–0.025	
C5Cn.2n (o)	R->N	16.488	16.515	ND	16.515	C5Cn.2n (o)	16.73	–1.575	–0.027	
C5Cn.3n (t)	N->R	16.556	16.583	ND	16.583	C5Cn.3n (t)	16.80	–0.786	–0.027	
C5Cn.3n (o)	R->N	16.726	16.755	ND	16.755	C5Cn.3n (o)	16.98	–0.687	–0.029	
C5Dn (t)	N->R	17.277	17.310	ND	17.310	C5Dn(t)	17.57	–1.243	–0.033	
C5Dn (o)	R->N	17.615	17.650	ND	17.650	C5Dn(o)	17.90	–1.412	–0.035	

Notes: ND = not determined, (t) = termination, (o) = onset. SCHPS95 = Shackleton et al. (1995), CK92 = Cande and Kent (1992), CK95 = Cande and Kent (1995), SSP95 = Shipboard Scientific Party (1995), BKFV85 = Berggren et al. (1985a), BKSA95 = Berggren et al. (1995).

Table T3. Age assignments of standard epoch/stage boundaries.

Age	Date (Ma)	Chron	Reference
Pliocene/Pleistocene	1.77	C2n–C1r	Cande and Kent, 1995
early/late Pliocene	3.58	C2Ar–C2An.3n	Berggren et al., 1995
Miocene/Pliocene	5.23	C3r–C3n.4n	Berggren et al., 1995
middle/late Miocene	11.2	C5r.2r	Berggren et al., 1995
early/middle Miocene	16.4	C5Cn.2n	Berggren et al., 1985a, 1985b, 1995

Table T4. Combined published ages referenced for Leg 178. (Continued on next two pages.)

		Diatom datums published ages	Using Berggren et al. (1985a); Gersonde and Burckle (1990)	Using Berggren et al. (1985a); Harwood and Maruyama (1992)	Using Berggren et al. (1995); Harwood and Maruyama (1992)	Berggren (1985a) (Chrons)	Using Berggren et al. (1995); Shipboard Scientific Party (1999a)	Using Berggren et al. (1995); Gersonde and Bárcena (1998)
T. lentiginosa	T	*Actinocyclus tabularis group*	2.5				0	
T. lentiginosa	T	*Fragilariopsis doliolus*					0	
T. lentiginosa	T	*Fragilariopsis kerguelensis*					0	
T. lentiginosa	T	*Thalassiosira oestrupii*	~2.5				0	
T. lentiginosa	**TC**	***Hemidiscus karstenii***		**0.195**		**C1n1**		0.19
T. lentiginosa	BC	*Hemidiscus karstenii*						0.42
	T	***Actinocyclus ingens***	**0.6**	**0.62**	0.64	**C1n1**	**0.64**	0.65
A. ingens	T	*Fragilariopsis reinholdii*		3.2		C2An3	0.65	
A. ingens	T	*Thalassiosira elliptipora*		0.65	0.68	C1n1	0.7	1.04-1.11*
A. ingens	T	*Thalassiosira fasciculata*		1.6	1.7	C1r.1r	0.7	
A. ingens	T	*Fragilariopsis fossilis*					0.9	
A. ingens	**T**	***Fragilariopsis barronii***	**1.5**	**1.25**	1.39	**C1r2**	**1.4**	1.3
A. ingens	T	*T. tetraoestrupii* var. *reimerii*					1.5	
A. ingens	B	*Thalassiosira elliptipora*		1.6	1.7	C1r2	1.77	
A. ingens	T	*Proboscia barboi*		3.1		C2An2	1.8	1.8
A. ingens	T	*Thalassiosira torokina*		1.8	1.85	C2n1	1.8	
A. ingens	B	*Fragilariopsis doliolus*					1.9	
	T	***Thalassiosira kolbei***		**1.8**	1.85	**C2n1**	**2**	2
T. kolbei	T	*Fragilariopsis matuyamae*					2.1	2.0-2.1
T. kolbei	T	*Thalassiosira convexa*					2.18	
T. kolbei	T	*Thalassiosira convexa* var. *aspinosa*	3.9				2.18	
T. kolbei	B	*T. tetraoestrupii* var. *reimerii*					2.2	
T. kolbei	B	*Fragilariopsis matuyamae*					2.5	2.3
T. kolbei	T	*Thalassiosira complicata*	~2.5	3.1-3.3	3.4		2.5	
T. kolbei	T	*Actinocyclus karstenii*		1.7-2.8	1.7 8-2.9			
T. kolbei	T	*Thalassiosira inura*	1.7?	1.8	1.85	C2n1	2.5	
	T	***Thalassiosira vulnifica***		**2.2**	2.28	**C2r3**	**2.5**	2.3
T. vulnifica	B	*Thalassiosira gracilis*		2.2	2.28	C2r3		
T. vulnifica	T	*Rouxia diploneis*		2.4	2.48	C2r3		
T. vulnifica	T	*Fragilariopsis interfrigidaria*	2.1-2.5	2.6	2.67	C2An1	2.63	
	T	***Thalassiosira insigna***		**2.5**	2.57	**C2r3**	**2.63**	2.6
T. insigna/vul.	T	*Fragilariopsis weaverii*		2.64	2.7	C2n1	2.65	
T. insigna/vul.	B	*Fragilariopsis kerguelensis*		3.1	3.33	C2An3	2.7	
T. insigna/vul.	T	*Fragilariopsis lacrima*	~2.8	4.3	4.61	C3n2.r	2.9	
T. insigna/vul.	T	*Rouxia heteropolara*	~2.5	2.5	2.58	C2An1	2.9	
T. insigna/vul.	T	*Thalassiosira striata*		2.8-3.2	2.92-3.4			
	B	***Thalassiosira vulnifica***		**3.1**	3.17	**C2An2**	**3.26**	
F. interfrigidaria	B	*Fragilariopsis weaveri*		3.2	3.4	C2An3	3.4	
F. interfrigidaria	B	*Thalassiosira insigna*		3.2	3.4	C2An3	3.4	
F. interfrigidaria	T	*Thalassiosira webbi*		3.25	3.45	C2An3		
F. interfrigidaria	B	*Fragilariopsis ritscherii*		3.4	3.53	C2An3		
F. interfrigidaria	B	*Fragilariopsis curta*		3.5	3.64	C2Ar3		
F. interfrigidaria	B	*Thalassiosira convexa*					3.7	
F. interfrigidaria	B	*Thalassiosira kolbei*		3.8	4.07	C2Ar3	3.75	
	B	***Fragilariopsis interfrigidaria***	**3.6**	**3.6**	3.8	**C2Ar3**	**3.8**	
F. barronii	T	*Fragilariopsis praeinterfrigidaria*	3.6	3.5	3.64	C2Ar3	3.8	
F. barronii	T	*Fragilariopsis praecurta*	3.8	3.6	3.8	C2Ar3	4.15	
F. barronii	T	*Fragilariopsis aurica*	3.8	3.8	4.07	C2Ar3	4.18	
F. barronii	T	*Fragilariopsis cylindrica*					4.3	
F. barronii	B	*Thalassiosira lentiginosa*		3.9	4.2	C3n1		
F. barronii	T	*Thalassionema nitzschiodes* var. *parva*		3.9	4.2	C3n1		
F. barronii	B	*Asteromphalus parvulus*		4.1	4.48	C3n2		
F. barronii	B	*Rouxia diploneis*		4.1	4.48	C3n2		
F. barronii	B	*Thalassiosira striata*		4.1	4.48	C3n2		
	B	***Fragilariopsis barronii***	**4.1-4.2**	**4.1**	4.48	**C3n2**	**4.44**	
T. inura	B	*Thalassiosira complicata*	4.3	4.3	4.62	C3n.2r	4.44	
T. inura	T	*Fragilariopsis arcula*	3.6	3.6	3.8	C2Ar3	4.48	
T. inura	B	*Thalassiosira fasciculata*		4.1	4.48	C3n2	4.5	
T. inura	B	*Fragilariopsis lacrima*	4.3	4.3	4.62	C3n.2r	4.62	
T. inura	B	*Rouxia heteropolara*	4.3	4.3	4.62	C3n.2r	4.7	

Table T4 (continued).

		Diatom datums published ages	Using Berggren et al. (1985a); Gersonde and Burckle (1990)	Using Berggren et al. (1985a); Harwood and Maruyama (1992)	Using Berggren et al. (1995); Harwood and Maruyama (1992)	Berggren (1985a) (Chrons)	Using Berggren et al. (1995); Shipboard Scientific Party (1999a)	Using Berggren et al. (1995); Gersonde and Bárcena (1998)
T. inura	T	*Cosmiodiscus intersectus*	4.5				4.89	
T. inura	T	*Thalassiosira oliverana* var. *sparsa*		4.5	4.85	C3n.3r		
	B	***Thalassiosira inura***	**4.47**	**4.5(4.8)**	4.85	**C3n.3r**	**4.92**	
T. oestrupii	T	*Denticulopsis hustedtii*	4.5	5.6-5.7*	6.28		5.3	
T. oestrupii	B	*Fragilariopsis praeinterfrigidari*	4.5?	4.5	4.85	C3n.3r	5.3	
	B	***Thalassiosira oestrupii***	**4.9**	**5.1**	5.62	**C3r4**	**5.56**	
N. reinholdii	T	*Nitzschia donahuensis*		5.3	5.89	C3An1		
N. reinholdii	T	*Asteromphalus kennettii*	7.1	5.7	6.32	C3An2	6	
N. reinholdii	T	*Actinocyclus ingens* var. *ovalis*	7.2				6.27	
N. reinholdii	T	*Hemidiscus ovalis*		5.7	6.32	C4An1		
N. reinholdii	T	*Thalassiosira miocenica*		5.1	5.62	C3r4	6.27	
N. reinholdii	B	*Thalassiosira miocenica*		5.8	6.42	C3An2	6.3	
	B	***Thalassiosira oliverana***		**5.8**	6.42	**C3An2**	**6.42**	
H. ovalis	T	*Actinocyclus fryxellae*					6.7	
H. ovalis	B	*Thalassiosira convexa* var. *aspinosa*	4.85				6.7	
H. ovalis	B	*Fragilariopsis cylindrica*					7.55	
H. ovalis	B	*Fragilariopsis reinholdii*		5.8	6.42	C3An2	8.1	
H. ovalis	B	*Fragilariopsis arcula*	7.8				8.6	
	B	***Actinocyclus ingens* var. *ovalis***	**7.8-7.9**				**8.68**	
	B	***Hemidiscus ovalis***		**7.9**	8.68	**C4An1**		
T. torokina	B	*Cosmiodiscus intersectus*	7.9				8.68	
T. torokina	B	*Thalassiosira oliverana* var. *sparsa*		7.9	8.68	C4An1		
T. torokina	B	*Fragilariopsis aurica*	7.9*				8.75	
T. torokina	B	*Fragilariopsis fossilis*					9	
	B	***Thalassiosira torokina***		**8.2(8.6)***	8.92		**9.01**	
A. kennettii	T	*Denticulopsis lauta*					9.8	
A. kennettii	T	*Nitzschia claviceps*					9.8	
A. kennettii	B	*Hemidiscus karstenii*		8.7	9.59	C4An3		
A. kennettii	B	*Nitzschia donahuensis*		8.8	9.63	C4An3		
	B	***Asteromphalus kennettii***	**9.6**	**9.6***	10.29	**C5n1**	**10.23**	
D. hustedtii								
	T	***Denticulopsis dimorpha***	**4.3**	**10.1***	10.63	**C5n1**	**10.7**	
D. dimorpha	B	*Actinocyclus fryxellae*					11.05	
D. dimorpha	B	*Fragilariopsis praecurta*	10.5				11.05	
D. dimorpha	T	*Denticulopsis praedimorpha*	10.4	11.1*	11.5	C5n3	11.53	
	T	***Nitzschia denticuloides***	**11.5**	**11.3***	11.67	**C5n3**	**11.7**	
D. praedi./N. dent.	B	*Actinocyclus karstenii*		11.7	11.98	C5An1		
	B	***Denticulopsis dimorpha ****	**12.4**	**11.9/12.2**	12.2		12.2	
D. praedimorpha								
	B	***Denticulopsis praedimorpha***	**12.6**	**12.6***	12.8	**C5Ar4**	**12.4**	
N. denticuloides	B	*Proboscia barboi*		12.5	12.73	C5Ar3	12.5	
N. denticuloides	T	*Actinocyclus ingens* var. *nodus*	12.3	12.3	12.54	C5Ar2	12.71	
N. denticuloides	T	*Coscinodiscus lewisianus*		13.2	13.32	C5ABn	13.2	
	B	***Nitzschia denticuloides***	**13.5**	**13.5***	13.51	**C5ABr**	**13.51**	
D. hust./N. gross.	T	*Nitzschia grossepunctata*	13.5	12.6	12.8	C5Ar4	13.51	
D. hust./N. gross.	B	*Nitzschia claviceps*					13.9	
	B	***Denticulopsis hustedtii* s.l.**	**14.2**	**14.2***	14.18	**C5ADn**	**14.17**	
A. ingens var. *nodus*								
	B	***Actinocyclus ingens* var. *nodus***	**14.9**	**14.5***	14.42	**C5ADn**	**14.38**	
N. grossepunctata	T	*Cavitatus jouseanus* (Synedra)	14.6	14.7	14.58	C5ADr	14.61	
N. grossepunctata	T	*Nitzschia maleinterpretaria*	14.6	14.1	14.01	C5ACr	14.61	
N. grossepunctata	T	*Denticulopsis macculumii*	14.4	14.4	14.38	C5ADn	14.7	
N. grossepunctata	T	*Cavitatus linearis*					15.2	
	B	***Nitzschia grossepunctata***	**15.3**	**15.5***	15.38	**C5Bn.2r**	**15.38**	

Table T4 (continued).

		Diatom datums published ages	Using Berggren et al. (1985a); Gersonde and Burckle (1990)	Using Berggren et al. (1985a); Harwood and Maruyama (1992)	Using Berggren et al. (1995); Harwood and Maruyama (1992)	Berggren (1985a) (Chrons)	Using Berggren et al. (1995); Shipboard Scientific Party (1999a)	Using Berggren et al. (1995); Gersonde and Bárcena (1998)
A. ingens/D. macc.								
	B	***Actinocyclus ingens***	**15.2**	**16.4***	16.2	**C5Cn.1n**	**16.2**	
D. maccollumii	B	*Denticulopsis lauta*		16	15.81	C5Bn.2r	16.2	
D. maccollumii	T	*Crucidenticulopsis kanayae*					16.56	
D. maccollumii	B	*Denticulopsis macculumii*	17.6/15.4	17*	16.6	C5Cn.3r	16.75	

Notes: Harwood and Maruyama (1992) ages have been adapted to Berggren et al. (1995) to allow direct application to the paleomagnetic time scale used on this leg. Species with two names currently used in the literature have both names listed with a box around them, and the ages from each reference are given in the appropriate column. Zone names used during this leg are listed in the far left column. T = top/last occurrence, B = bottom/first occurrence, TC = last common occurrence, BC = first common occurrence. * = zonal datums based on increased abundance of species.

Table T5. XRF operating conditions for sediment trace elements.

Element	Line	Crystal	Detector	Collimator	Peak angle (°)	Background offset (°2θ)	Total count time	
							Peak (s)	Background (s)
Rh	Kα-Compton	LIF(200)	Scint	Fine	18.20	0.00	60	0
Nb	Kα	LIF(200)	Scint	Fine	21.40	–0.35	200	200
Zr	Kα	LIF(200)	Scint	Fine	22.55	–0.35	100	100
Y	Kα	LIF(200)	Scint	Fine	23.80	–0.40	100	100
Sr	Kα	LIF(200)	Scint	Fine	25.15	–0.40	100	100
Rb	Kα	LIF(200)	Scint	Fine	26.62	–0.60	100	100
Zn	Kα	LIF(200)	Scint	Medium	41.81	–0.40	100	100
Cu	Kα	LIF(200)	Scint	Fine	45.03	–0.40	100	100
Ni	Kα	LIF(200)	Scint	Medium	48.67	–0.60	100	100
Fe	Kα	LIF(200)	FPC	Fine	85.65	0.00	100	0
Cr	Kα	LIF(200)	FPC	Fine	69.35	–0.50	100	100
Ti	Kα	LIF(200)	FPC	Fine	86.18	0.00	40	0
V	Kα	LIF(200)	FPC	Fine	123.06	–0.50	100	100
Ce	Kα	LIF(200)	FPC	Medium	128.13	1.50	100	100
Ba	Lβ	LIF(200)	FPC	Medium	128.78	1.50	100	100

Note: Detectors: Scint = NaI scintillation counter, FPC = flow proportional counter using P10 gas. Trace elements analyzed under vacuum using generator setting of 50 kV and 50 mA.

Table T6. Precision and accuracy of 12 replicate trace-element analyses on sediment reference standard MAG-1

Element	Concentration (ppm)	Standard deviation	Recommended (ppm)
Nb	18	1.17	12
Zr	132	1.42	126
Y	40	0.67	28
Sr	142	1.15	146
Rb	159	1.32	149
Zn	135	1.25	130
Cu	30	1.20	30
Ni	57	0.97	53
Cr	94	3.57	91
V	158	3.45	140
Ce	80	4.24	88
Ba	442	9.92	479

Note: From Govindaraju (1989).

Table T7. Specifications of downhole tools deployed during Leg 178.

Tool string	Tool	Measurement	Sample interval (cm)	Approximate vertical resolution (cm)
Triple combination (TC)	HNGS	Natural gamma	15	45
	APS	Porosity	5 and 15	30
	HLDS	Bulk density, PEF	2.5 and 15	15/45
	DIT	Resistivity	2.5 and 15	200/150/75
	Temperature tool	Temperature	1 per second	—
FMS-sonic	NGT	Natural gamma	15	45
	GPIT	Tool orientation and acceleration	15	—
	SDT	Sonic velocity	15	120
	FMS	Resistivity image	0.25	0.5
GHMT	NGT	Natural gamma	15	45
	SUMS	Susceptibility	5 and 15	35
	NMRS	Total magnetic field	5 and 15	45
WST	WST	Sonic traveltime	—	—

Notes: Other acronyms defined in Table **T8,** p. 64. — = not applicable.

Table T8. Schlumberger tool and measurement acronyms.

Tool	Tool name and output	Explanation	Units
HNGS	Hostile environment natural gamma sonde		
	HSGR	Standard (total) gamma ray	gAPI
	HCGR	Computed gamma ray (HSGR minus uranium contribution)	gAPI
	HFK	Formation potassium	Fraction
	HTHO	Thorium	ppm
	HURA	Uranium	ppm
NGT	Natural gamma tool		
	SGR	Standard (total) gamma ray	gAPI
	CGR	Computed gamma ray (SGR minus uranium contribution)	gAPI
	POTA	Potassium	Percent
	THOR	Thorium	ppm
	URAN	Uranium	ppm
APS	Accelerator porosity sonde		
	APLC	Near/array porosity (limestone corrected)	Fraction
	FPLC	Near/far porosity (limestone corrected)	Fraction
	SIGF	Neutron capture cross section of the formation (S_f)	Capture units
	STOF	Tool standoff (computed distance from borehole wall)	Inches
HLDS	Hostile environment lithodensity sonde		
	RHOM	Bulk density (corrected)	g/cm^3
	PEFL	Photoelectric effect	Barns/e$^-$
	LCAL	Caliper (borehole diameter)	Inches
	DRH	Bulk density correction	g/cm^3
DIT	Dual induction tool		
	IDPH	Deep induction phasor-processed resistivity	Wm
	IMPH	Medium induction phasor-processed resistivity	Wm
	SFLU	Spherically focused resistivity	Wm
SUMS	Susceptibility magnetic sonde		
	MAGS	Magnetic susceptibility (limited range)	ppm
	RMGS	Low-resolution magnetic susceptibility (wider range)	ppm
	MAGC	Earth conductivity	ppm
NMRS	Nuclear magnetic resonance sonde		
	MAGB	Earth total magnetic field	nT
SDT	Digital sonic tool		
	LTT1-4	Transit times (10-, 8-, 12-, 10-ft transmitter-receiver spacings)	µs
	DTLF	Slowness (12 minus 10-ft traveltimes)	µs/ft
	DTLN	Slowness (10 minus 8-ft traveltimes)	µs/ft
FMS	Formation MicroScanner		
GPIT	General purpose inclinometry tool		
WST	Well seismic tool		

Note: The IPLT (integrated porosity-lithology tool) is composed of the HNGS, APS, and HLDS.

Table T9. Multichannel seismic surveys associated with the continental shelf and rise sites.

	British Antarctic Survey (*Discovery*)	Brazilian Antarctic Program (*Almirante Câmara*)	Osservatorio Geofisico Sperimentale (*OGS-Explora*)			Univ. Granada-CSIC (*Hesperides*)	Japanese National Oil Co. (*Hakurei Maru*)
Depositional environment:	Shelf	Shelf	Shelf	Rise	Rise and Shelf	Shelf	Shelf
Survey/profile:	1984-85/AMG 845-08, -10	1986-87, 1987-88/BRAZ5-28	1995/I95-152	1995/I95-130-135A-137	1989, 1992/IT89-47 IT92-109-114;	1997/AISM02-06 - 11-12	1996/HM-96
Leg 178 sites:	1100-1102, 1103	1100-1102, 1103	1100-1102, 1103	1095, 1096	1096, 1097, 1101	1097	1101-1103, 1103
Source							
Gun types:	Bolt array	Bolt array	GI	GI	Bolt array	Bolt air gun	GI
Number of guns:	4	8	2	2	2 × 20	5	4
Total volume:	15.8 L (964 in^3)	8.8 L (536 in^3)	6.8 L (420 in^3)	6.8 L (420 in^3)	72 L (4390 in^3)	22.4 L (1365 in^3)	9.83 L (600 in^3)
Tow depth (m):	10	7	6	7	6	7	15
Shot interval (m):	50	50	25	25	50	25	50
Sensors							
Number of traces:	48	72	120	120	120	96	192
Length of streamer (m):	2400	1800	1500	3000	3000	2400	2400
Trace interval (m):	50	25	12.5	25	25	25	12.5
Tow depth (m):	10	10-11	8	12	50	7-9	15
Recording							
Coverage:	24-fold	18-fold	30-fold	60-fold	30-fold	24-fold	24-fold
Sampling rate (ms):	4	4	2	2	4	2	4
Record length:	8 s	8 s	8 s	8 s	14 s	5 s	10 ms

Notes: Acquisition parameters are indicated. GI = Generator Injector.

Table T10. Single-channel and deep-tow boomer surveys across the Antarctic Peninsula continental shelf.

	Deep-tow boomer		Single-channel boomer			
	British Antarctic Survey (*James Clark Ross*)	Hamilton College (USAP) (*Polar Duke*)	Osservatorio Geofisico Sperimentale (PNRA) (*OGS-Explora*)			Rice University (USAP) (*Polar Duke*)
Depositional environment	Shelf	Palmer Deep	Palmer Deep	Palmer Deep	Shelf	Shelf
Survey/profile	1992/DTB-01A to O6A	PD92, DTB Survey	1997/I97H-218 to 223	I97-224 to 230	I97-233, -234	1988/PD88-04, -B
Leg 178 Sites	1100, 1102, 1103	1098, 1099	1098, 1099	1098, 1099	1100, 1102, 1103	1097
Source						
Gun types	Piezoelectric transducer	Piezoelectric transducer	GI	Air gun	GI	Air gun
Number of guns	NA	NA	1, true GI mode	1	1, true GI mode	1 or 2
Volume	NA	NA	2.5 L (150 in^3)	0.25 L (15 in^3)	2.5 L (150 in^3)	1.6 L (150 in^3)
Firing depth (m)	NA	NA	4	2	4	1-3
Shot interval (m)	NA	NA	12.5	9	12.5	20
Tow depth	100 m from seafloor	50-100 m from seafloor				
Sensors						
Type	1-m long, 6-element hydrophone	10-element hydrophone streamer		10-hydrophone array, spacing 1.6 m		Hydrophone array
Tow depth	Trailed from tow vehicle	Trailed from tow vehicle	1 m	1 m	1 m	1-3 m
Recording						
Sampling interval	100 µs	100 µs	1 ms (1000 Hz)	0.5 ms (2000 Hz)	1 ms (1000 Hz)	1 ms (1000 Hz)
Record length	400 ms	250 ms	4 s	2.5 s	3 s	2 s

Notes: Acquisition parameters are indicated. NA = not applicable, GI = Generator Injector. Palmer Deep = Sites 1098 and 1099.